

CHAPTER 4

RESULTS AND DISCUSSION

4.1. Introduction

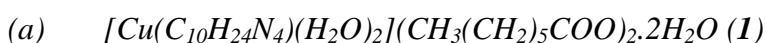
The main objectives of this research were to synthesize thermally stable and magnetic complexes made up of copper(II) ion, 1,4,8,11-tetraazacyclotetradecane (cyclam) and alkylcarboxylate ion or arylcarboxylate ion, and then to correlate their structures and properties (magnetic and/or liquid crystal) with the alkyl chain length and the electronic effect of a substituent on the aromatic ring.

A total of 14 complexes were obtained in good yields from a facile synthesis involving copper(II) carboxylates ($[\text{Cu}_2(\text{RCOO})_4]$) and cyclam, where R is either linear $\text{C}_n\text{H}_{2n+1}$ ($n = 6, 7, 9, 11, 13, 15$), $\text{CH}_3(\text{CH}_2)_7\text{CH}((\text{CH}_2)_5\text{CH}_3)$, $p\text{-XC}_6\text{H}_4$ ($X = \text{NH}_2, \text{OH}, \text{OCH}_3, \text{CH}_3, \text{CN}, \text{H}$), or C_6F_5 .

Complexes **1** ($n = 6$), **3-6** ($n = 9-15$), and **8-14** (arylcarboxylates) were obtained as single crystals and their respective structures were successfully deduced by X-ray crystallography. On the other hand, **2** ($n = 7$) and **7** ($\text{CH}_3(\text{CH}_2)_7\text{CH}((\text{CH}_2)_5\text{CH}_3)$) were obtained as viscous liquids and their chemical formulae were proposed based on microelemental analyses and comparison of FTIR and UV-visible spectral results with those recorded for the crystalline analogs.

4.2. Copper(II)-cyclam-alkylcarboxylate complexes

4.2.1. Structural elucidation



Diaqua(1,4,8,11-tetraazacyclotetradecane- $\kappa^4\text{N}^1, \text{N}^4, \text{N}^8, \text{N}^{11}$)copper(II) heptanoate dihydrate (**1**) was obtained as purple crystals from the reaction of $[\text{Cu}_2(\text{CH}_3(\text{CH}_2)_5\text{COO})_4]$ with cyclam (mole ratio 1:2) in ethanol. The yield was 78%.

Based on single-crystal XRD, the molecular structure of **1** (**Figure 4.1**) shows that it is made up of a $[\text{Cu}(\text{C}_{10}\text{H}_{24}\text{N}_4)(\text{H}_2\text{O})_2]^{2+}$ cation, two $\text{CH}_3(\text{CH}_2)_5\text{COO}^-$ anions, and two lattice H_2O molecules. The Cu^{II} atom is located in a special position, $(1, \frac{1}{2}, 0)$, of a crystallographic inversion centre. The geometry of the Cu^{II} atom is based on an axially-distorted octahedron, in which it is coordinated to cyclam through the four *aza*-N atoms that form the basal plane and the apical positions are occupied by H_2O molecules. Two lattice H_2O molecules present interconnect the cationic entity and $\text{CH}_3(\text{CH}_2)_5\text{COO}^-$ anions through $\text{O}-\text{H}\cdots\text{O}$ hydrogen bonding. The relatively long $\text{Cu1}-\text{O1W}$ distance (2.507(3) Å) when compared to $\text{Cu1}-\text{N1}$ (2.019(2) Å) and $\text{Cu1}-\text{N2}$ (2.027(3) Å), is a consequence of the Jahn–Teller distortion that causes the cationic complex to exhibit axial elongation.

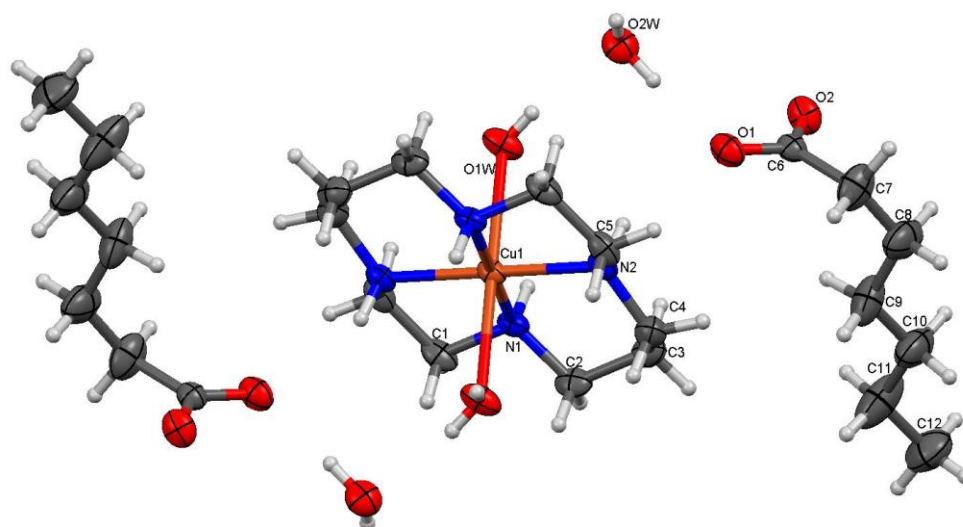


Figure 4.1 Molecular structure of **1**, showing displacement ellipsoids at 50% probability level; operator used to generate symmetry equivalent elements: $x, \frac{1}{2}-y, -\frac{1}{2}+z$

The four aza-N atoms that define the basal plane are in *R,R,S,S* chirality, which attributes the *trans*-III isomerism of the cyclam ring. It is noted that this is the most stable configuration, where the six-membered chelate ring (A) adopts the least-strained

chair conformation and the five-membered chelate ring (B) in gauche conformation [1,2] (**Figure 4.2**).

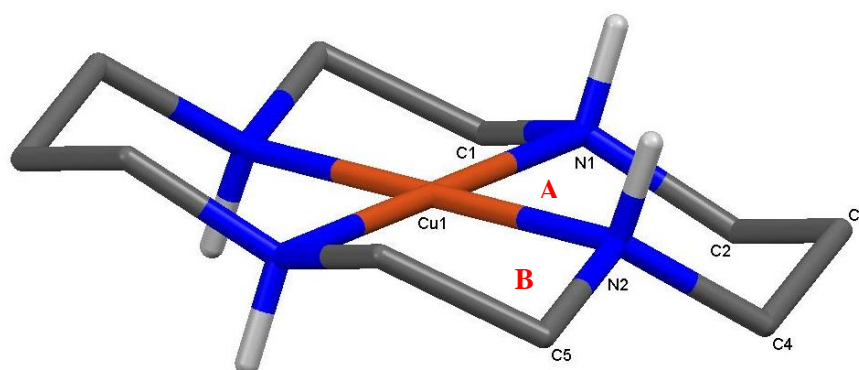


Figure 4.2 Representation of the chair conformation of the six-membered (A) and gauche five-membered chelate ring (B) of cyclam group of **1**; carbon bound H-atoms were not shown

The intermolecular N–H···O and O–H···O bifurcated hydrogen bondings between the carboxylate-O atoms and the cationic complex build up a two-dimensional network forming a layer structure parallel to (001) plane (**Figure 4.3**).

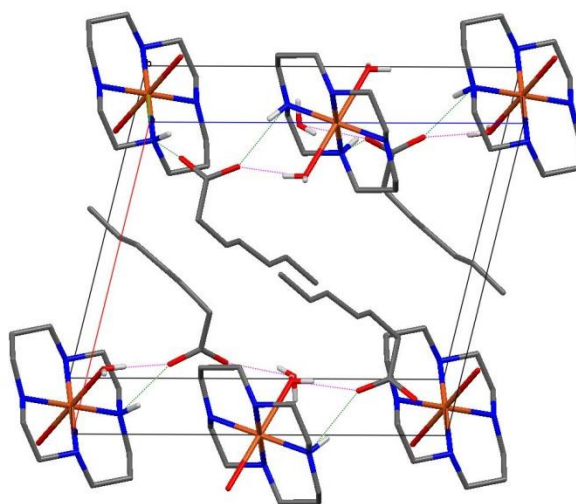


Figure 4.3 Unit cell of **1**, viewed along crystallographic *b*-axis, N–H···O and O–H···O bond is indicated as green and pink dashes respectively (some hydrogen atoms were not shown)

It is interesting to note that **1** was formed from copper(II) heptanoate ($[\text{Cu}_2(\text{CH}_3(\text{CH}_2)_5\text{COO}]_4$), the crystals of which show dimeric paddlewheel structure [3]

(**Figure 4.4**). From this, it may be inferred that the dimer dissociated in ethanol in the presence of cyclam, and the freed Cu(II) ion, $\text{CH}_3(\text{CH}_2)_5\text{COO}^-$ ion and cyclam molecule then self-assembled to form **1**, a mononuclear ionic complex [4].

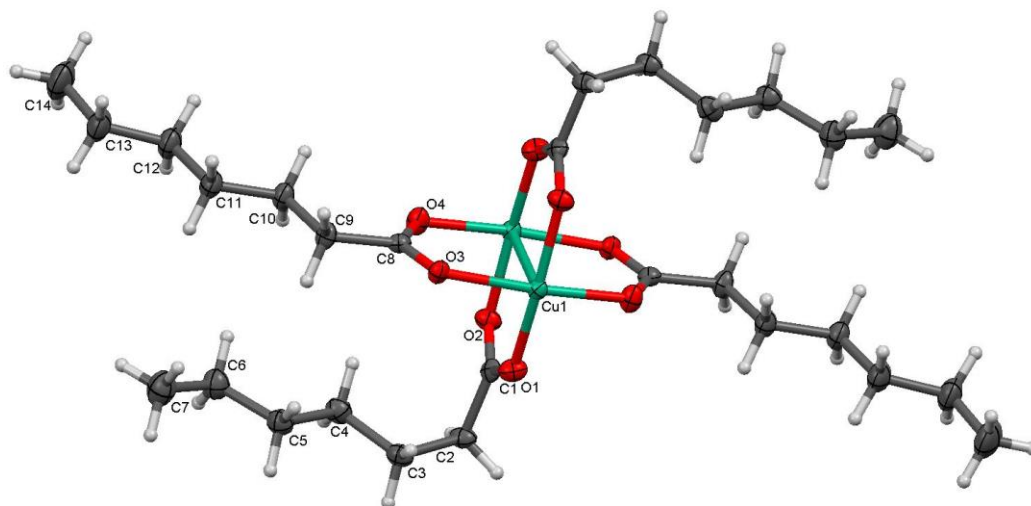


Figure 4.4 Molecular view of the dimeric paddlewheel structure of $[\text{Cu}_2(\text{CH}_3(\text{CH}_2)_5\text{COO})_4]$ [3], drawn at 70% probability level; symmetry elements are related by operator $-x, 2-y, -z$

The FTIR spectrum of **1** (**Figure 4.5**) shows the presence of the expected functional groups and bonds (**Table 4.1**). The Δ_{COO} value ($\bar{\nu}_{\text{as,COO}} - \bar{\nu}_{\text{s,COO}}$) is 155 cm^{-1} , in agreement with the ionic (non-coordinated) $\text{CH}_3(\text{CH}_2)_5\text{COO}^-$ ion [5,6] found from its crystal structure.

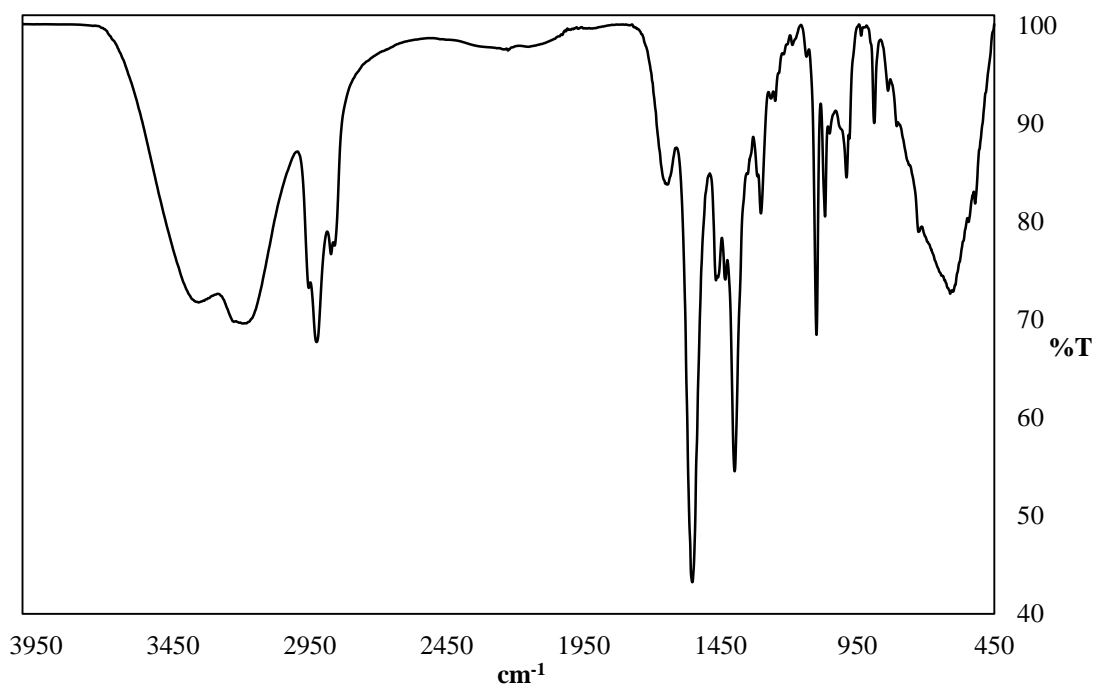


Figure 4.5 The FTIR spectrum of **1**

Table 4.1 FTIR data and assignments of **1**

Wavenumber (cm ⁻¹)	Assignment
3356, 3233	Coordinated and lattice H ₂ O (H-bonded)
2925	$\bar{\nu}_{\text{asym}}$ CH ₂
2872	$\bar{\nu}_{\text{sym}}$ CH ₂
1553	$\bar{\nu}_{\text{asym}}$ COO
1398	$\bar{\nu}_{\text{sym}}$ COO

The electronic spectrum of **1** in acetone (**Figure 4.6**) shows a broad *d-d* band at $\lambda_{\text{max}} = 550 \text{ nm}$ ($\epsilon_{\text{max}} = 108 \text{ M}^{-1} \text{ cm}^{-1}$). The peak position suggests a square planar geometry at Cu(II) centre [7]. The result implied that the octahedral geometry noted from the crystal structure was not maintained in solution. This is likely due to the dissociation of the weakly coordinated H₂O molecules at the axial positions, as a result of four strong Cu–N_{cyclam} equatorial bonds.

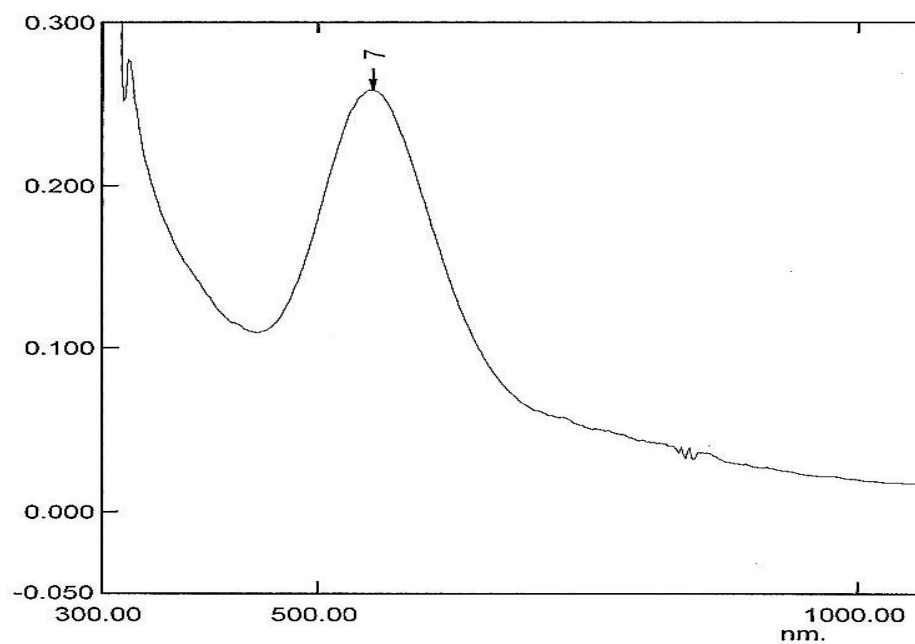
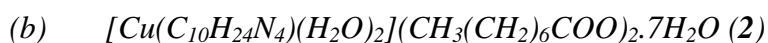


Figure 4.6 The UV-vis spectrum of **1**



Diaqua(1,4,8,11-tetraazacyclotetradecane-κ⁴N¹,N⁴,N⁸,N¹¹)copper(II) octanoate heptahydrate (**2**) was obtained as a maroon viscous liquid from the reaction of $[Cu_2(CH_3(CH_2)_6COO)_4]$ with cyclam (mole ratio 1:2) in ethanol. The yield was 81%. Its chemical formula, based on the results of elemental analyses (**Table 4.2**) is $CuC_{26}H_{86}N_4O_{13}$ (FW = 712.30 g mol⁻¹).

Table 4.2 Elemental analytical data of **2**

Element	Calculated (%)	Found (%)
C	43.8	43.7
H	10.2	10.1
N	7.9	7.8

Its FTIR spectrum (**Figure 4.7**) is similar to that of **1** (**Figure 4.5**), and may be similarly assigned. The Δ_{COO} value of 165 cm^{-1} suggests non-coordinated $\text{CH}_3(\text{CH}_2)_6\text{COO}^-$ ion.

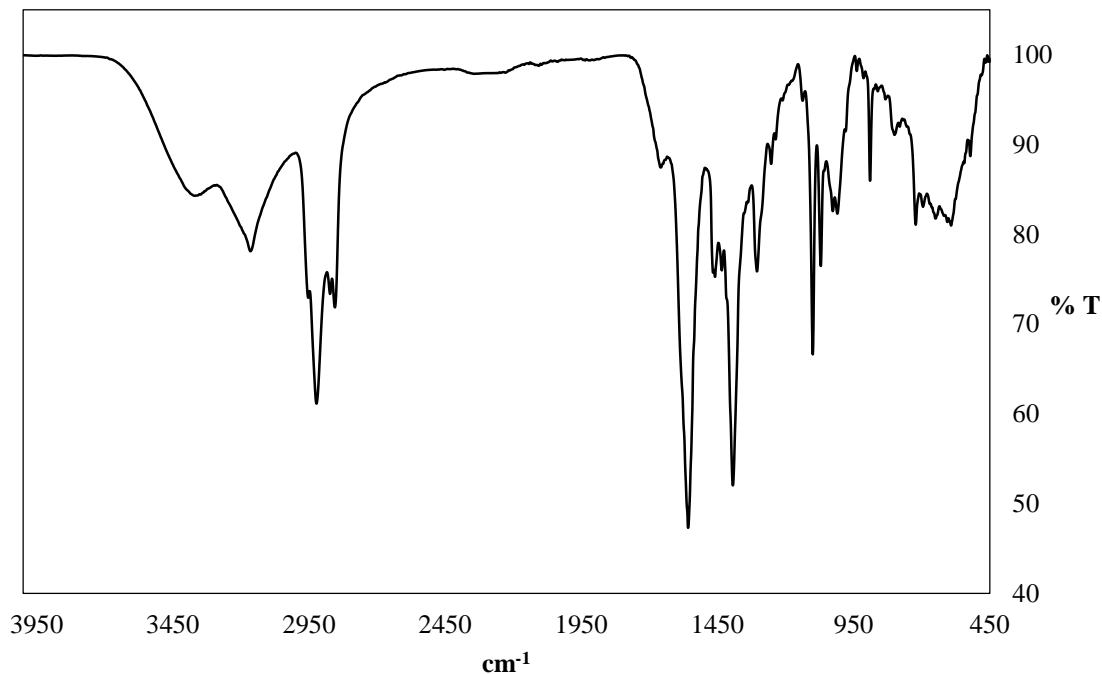


Figure 4.7 The FTIR spectrum of **2**

The electronic spectrum of **2** in ethanol (**Figure 4.8**) shows a broad *d-d* band at $\lambda_{\text{max}} = 538\text{ nm}$ ($\epsilon_{\text{max}} = 120\text{ M}^{-1}\text{ cm}^{-1}$). The value is similar to that of **1** ($\lambda_{\text{max}} = 550\text{ nm}$; $\epsilon_{\text{max}} = 108\text{ M}^{-1}\text{ cm}^{-1}$), suggesting similar square planar geometry at Cu(II) in solution.

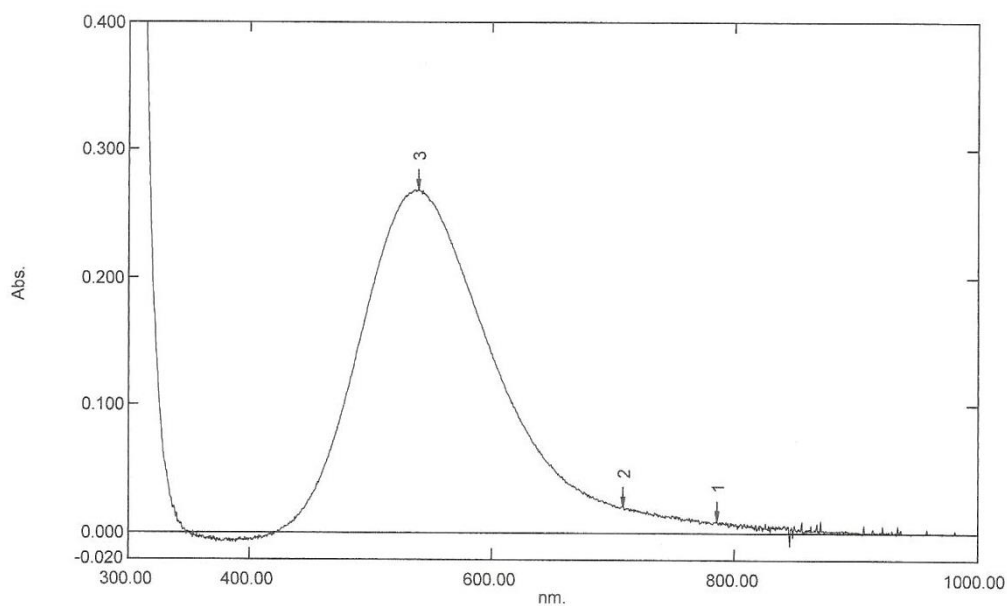


Figure 4.8 The UV-vis spectrum of **2**

Based on the above instrumental data, it is proposed that the structure of **2** is similar to that of **1**, and is shown in **Figure 4.9**. The complex is mainly made up of a $[\text{Cu}(\text{C}_{10}\text{H}_{24}\text{N}_4)(\text{H}_2\text{O})_2]^{2+}$ cation, two $\text{CH}_3(\text{CH}_2)_6\text{COO}^-$ anions, and seven solvated H_2O molecules. The coordination geometry of Cu atom is distorted octahedral, where the Cu(II) metal centre is chelated by the four aza-N of cyclam ligand and its axial positions are occupied by H_2O molecules. The cation, anions and solvated H_2O molecules are linked by hydrogen bonds.

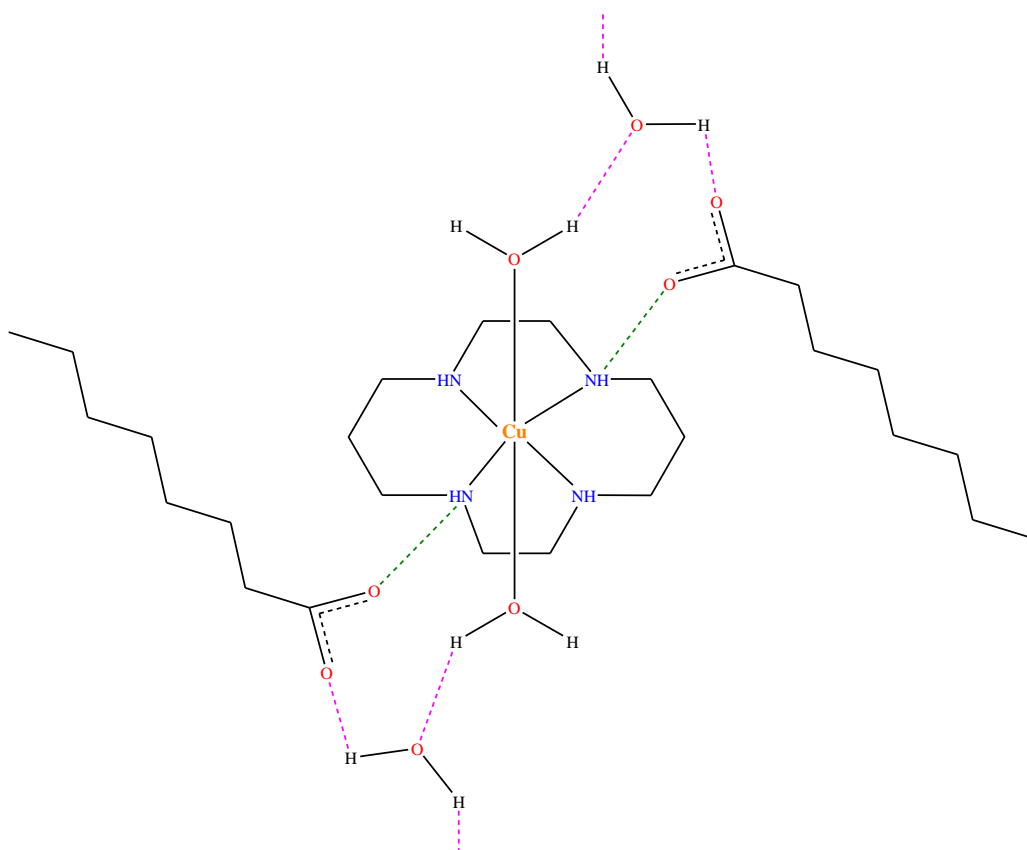
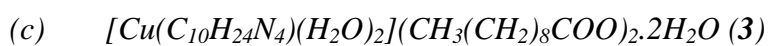


Figure 4.9 Schematic representation of the proposed structure of **2**; N–H···O and O–H···O bond is indicated as green and pink dashes respectively; the remaining five solvated H₂O molecules are not shown.



Diaqua(1,4,8,11-tetraazacyclotetradecane- $\kappa^4 N^1, N^4, N^8, N^{11}$)copper(II) decanoate dihydrate (**3**) was obtained as purple crystals from the reaction of $[Cu_2(CH_3(CH_2)_8COO)_4]$ with cyclam (mole ratio 1:2) in ethanol. The yield was 53%.

The single-crystal XRD result shows that **3** exhibits analogous coordination propensities as **1**. A perspective view of the molecular structure of **3** is shown in **Figure 4.10**.

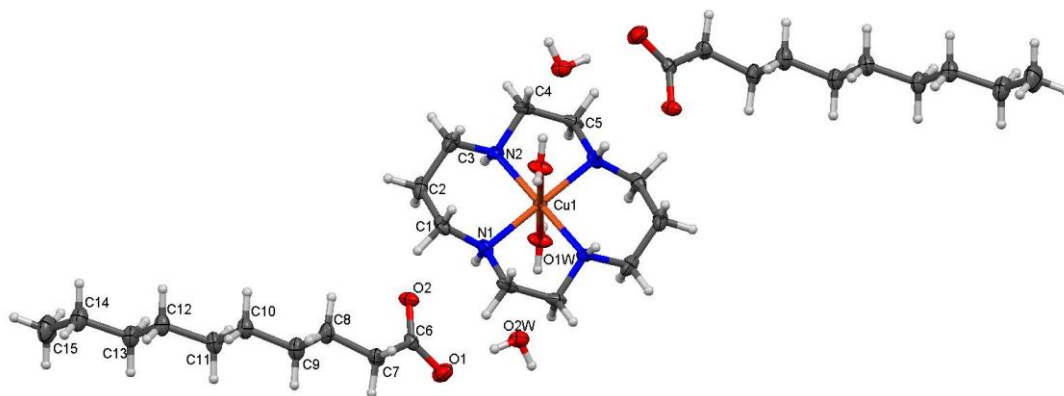


Figure 4.10 Molecular structures of **3**, showing displacement ellipsoids at 70% probability level; operator used to generate symmetry equivalent elements: $1-x, 1-y, 1-z$

The cations, anions and lattice H_2O molecules are linked by intermolecular $\text{N}-\text{H}\cdots\text{O}$ and $\text{O}-\text{H}\cdots\text{O}$ hydrogen bonds, forming a successive chain along the crystallographic a -axis (**Figure 4.11**).

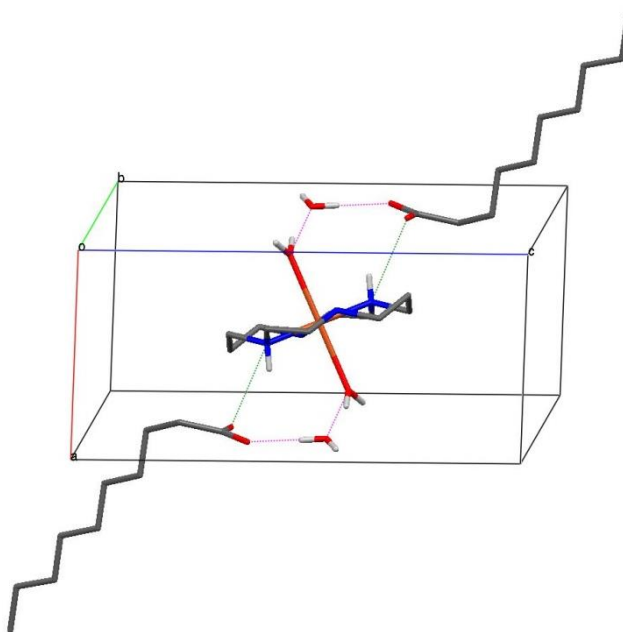


Figure 4.11 Unit cell of **3**, viewed along crystallographic b -axis, $\text{N}-\text{H}\cdots\text{O}$ and $\text{O}-\text{H}\cdots\text{O}$ bond is indicated as green and pink dashes respectively (some hydrogen atoms were not shown).

The FTIR spectrum of **3** (**Figure 4.12**) and the Δ_{COO} value (162 cm^{-1}) are similar to the previously discussed complexes.

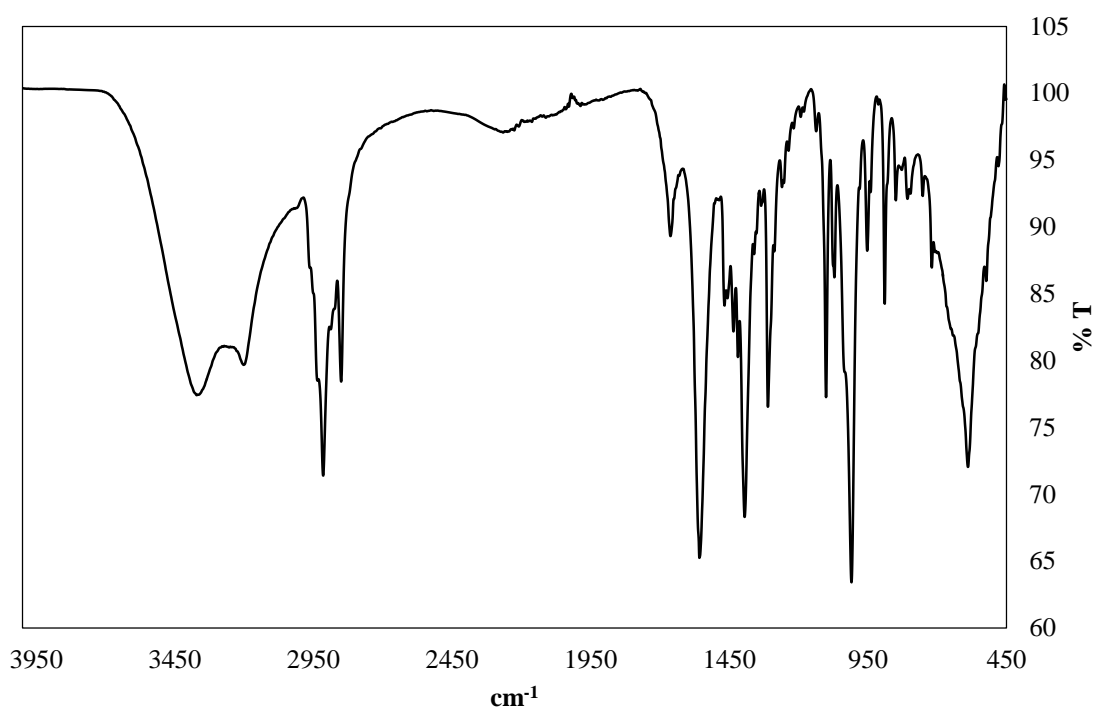


Figure 4.12 The FTIR spectrum of **3**

The electronic spectrum of **3** in ethanol (**Figure 4.13**) and data ($\lambda_{\text{max}} = 530 \text{ nm}$; $\epsilon_{\text{max}} = 96 \text{ M}^{-1} \text{ cm}^{-1}$) are also similar to the above complexes, and may be similarly explained.

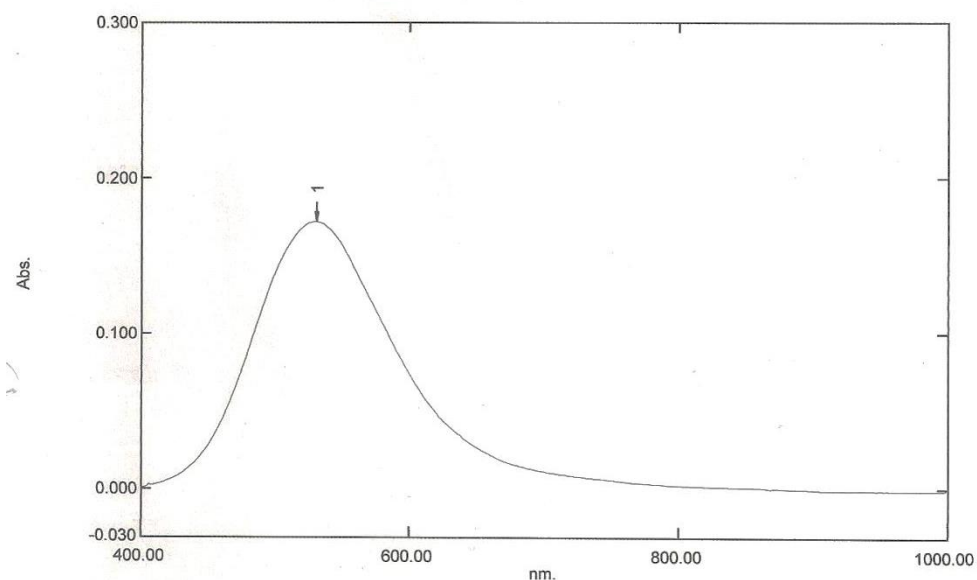
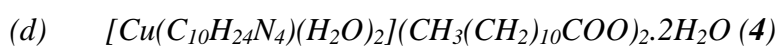


Figure 4.13 The UV-vis spectrum of **3**



Diaqua(1,4,8,11-tetraazacyclotetradecane- $\kappa^4 N^1, N^4, N^8, N^{11}$)copper(II) dodecanoate dihydrate (**4**) was obtained as purple crystals from the reaction of $[Cu_2(CH_3(CH_2)_{10}COO)_4]$ with cyclam (mole ratio 1:2) in ethanol. The yield was 61%.

The single-crystal XRD result shows that **4** exhibits analogous coordination propensities as the previously discussed crystalline complexes. A perspective view of the molecular structure of **4** is shown in **Figure 4.14**.

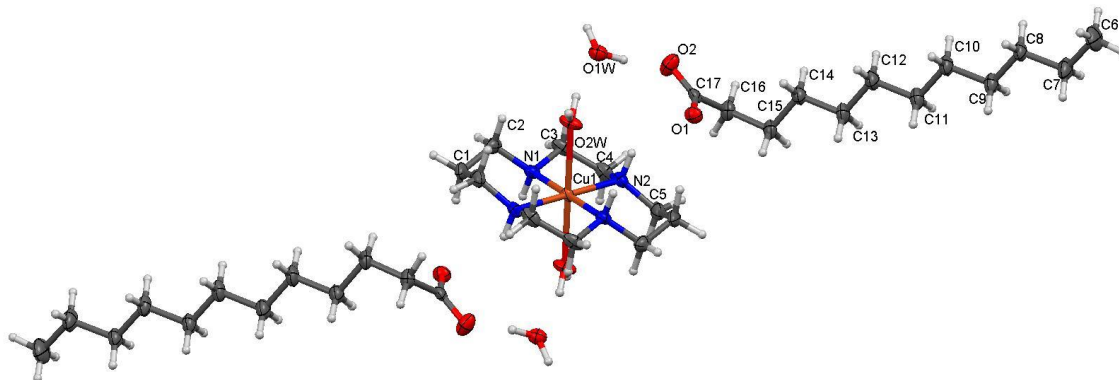


Figure 4.14 Molecular structures of **4**, showing displacement ellipsoids at 70% probability level; operator used to generate symmetry equivalent elements: $2-x$, $-y$, $2-z$

As for the above crystalline complexes, the cation, anions and lattice H_2O molecules in **4** are also linked by intermolecular $\text{N-H}\cdots\text{O}$ and $\text{O-H}\cdots\text{O}$ hydrogen bonds, forming a layered structure parallel to (001) plane (**Figure 4.15**).

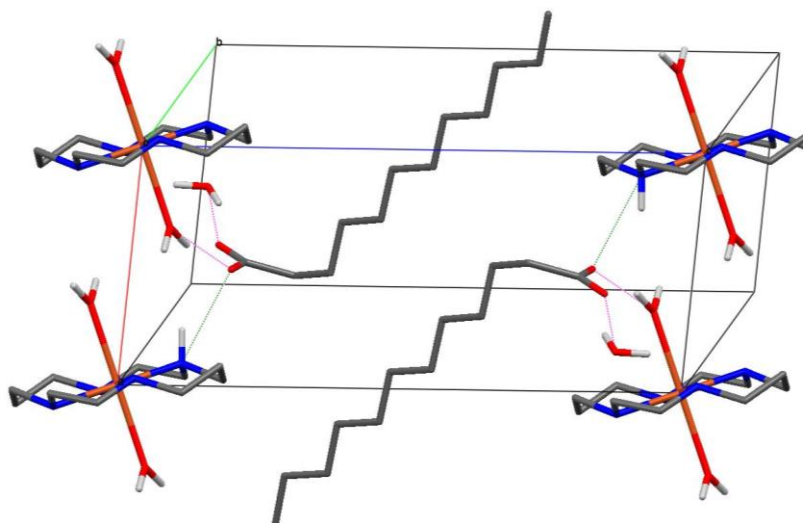


Figure 4.15 Unit cell of **4**, viewed along crystallographic b -axis, $\text{N-H}\cdots\text{O}$ and $\text{O-H}\cdots\text{O}$ bond is indicated as green and pink dashes respectively (some hydrogen atoms were not shown).

The FTIR spectrum of **4** (**Figure 4.16**) and the Δ_{COO} value (162 cm^{-1}) are similar to the above complexes.

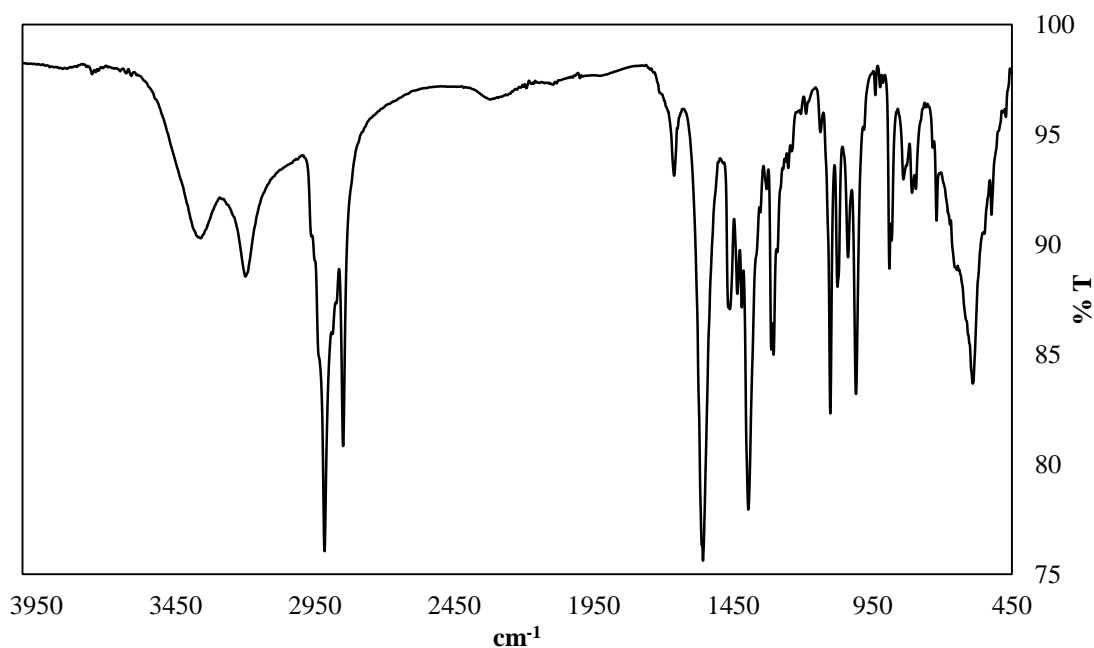


Figure 4.16 The FTIR spectrum of **4**

The electronic spectrum of **4** in ethanol (**Figure 4.17**) and data ($\lambda_{\text{max}} = 541 \text{ nm}$; $\epsilon_{\text{max}} = 121 \text{ M}^{-1} \text{ cm}^{-1}$) are also similar to the above complexes.

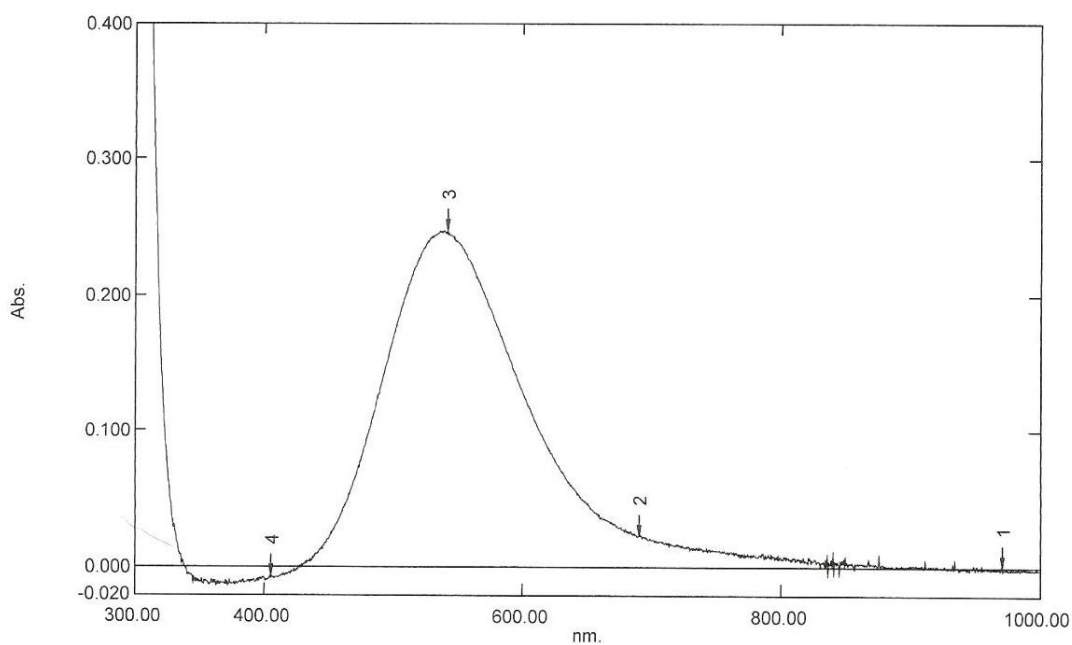
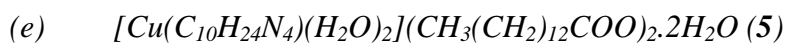


Figure 4.17 The UV-vis spectrum of **4**



Diaqua(1,4,8,11-tetraazacyclotetradecane- $\kappa^4 N^1, N^4, N^8, N^{11}$)copper(II) tetradecanoate dihydrate (**5**) was obtained as purple crystals from the reaction of $[Cu_2(CH_3(CH_2)_{12}COO)_4]$ with cyclam (mole ratio 1:2) in ethanol. The yield was 64%.

The single-crystal XRD result shows that **5** exhibits analogous coordination propensities as the above complexes. A perspective view of the molecular structure of **5** is shown in **Figure 4.18**.

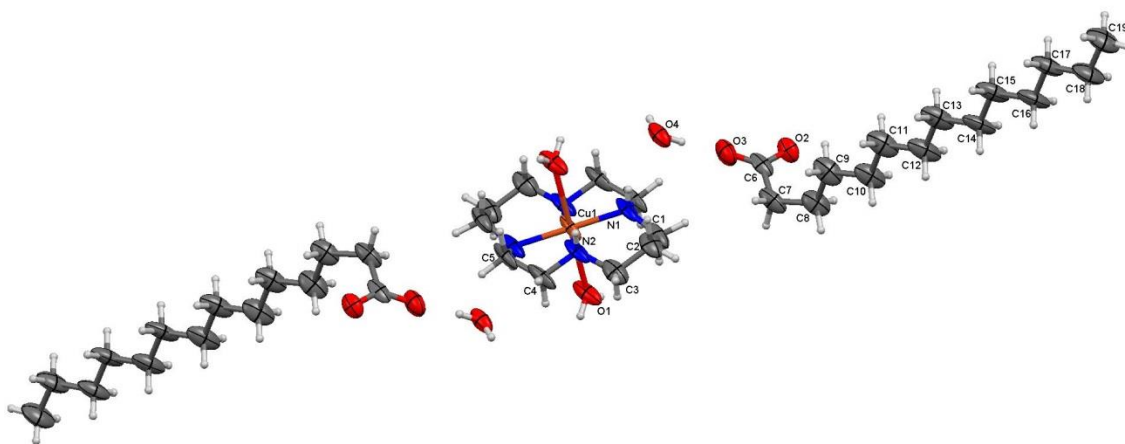


Figure 4.18 Molecular structures of **5**, showing displacement ellipsoids at 70% probability level; operator used to generate symmetry equivalent elements (unlabelled atoms): $2-x, -y, -z$

As found for the above crystalline complexes, the cation, anions and lattice H_2O molecules in **5** are linked by intermolecular $N-H \cdots O$ and $O-H \cdots O$ hydrogen bonds, forming a similar fashion of a layered structure parallel to (001) plane (**Figure 4.19**).

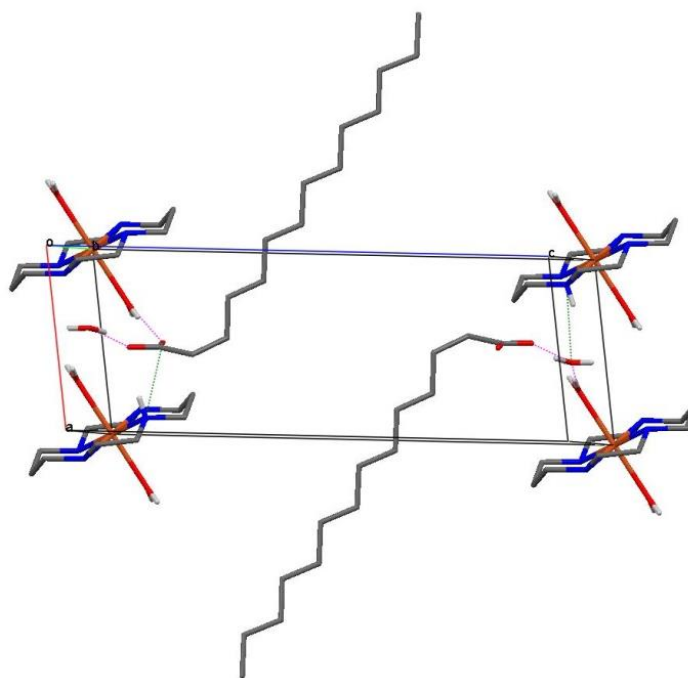


Figure 4.19 Unit cell of **5**, viewed along crystallographic *b*-axis, N–H···O and O–H···O bond is indicated as green and pink dashes respectively (some hydrogen atoms were not shown).

The FTIR spectrum of **5** (**Figure 4.20**) and the Δ_{COO} value (162 cm^{-1}) are similar to the above complexes.

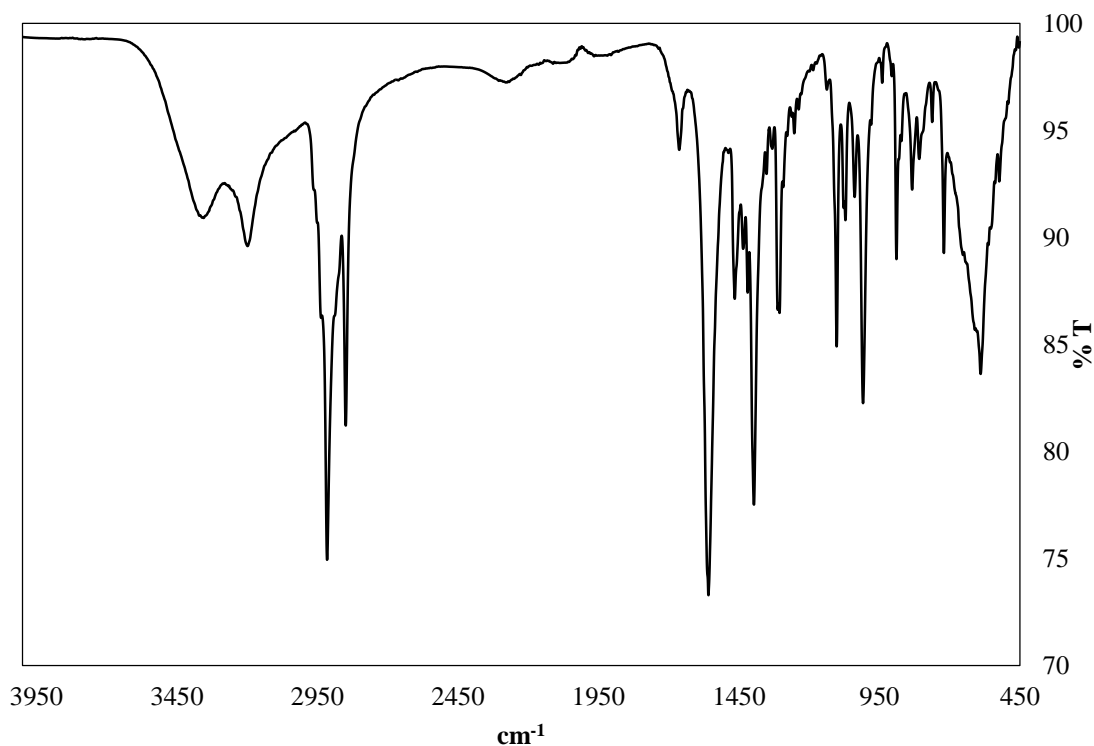


Figure 4.20 The FTIR spectrum of **5**

The electronic spectrum of **5** in ethanol (**Figure 4.21**) and data ($\lambda_{\text{max}} = 538 \text{ nm}$; $\epsilon_{\text{max}} = 121 \text{ M}^{-1} \text{ cm}^{-1}$) are also similar to the above complexes.

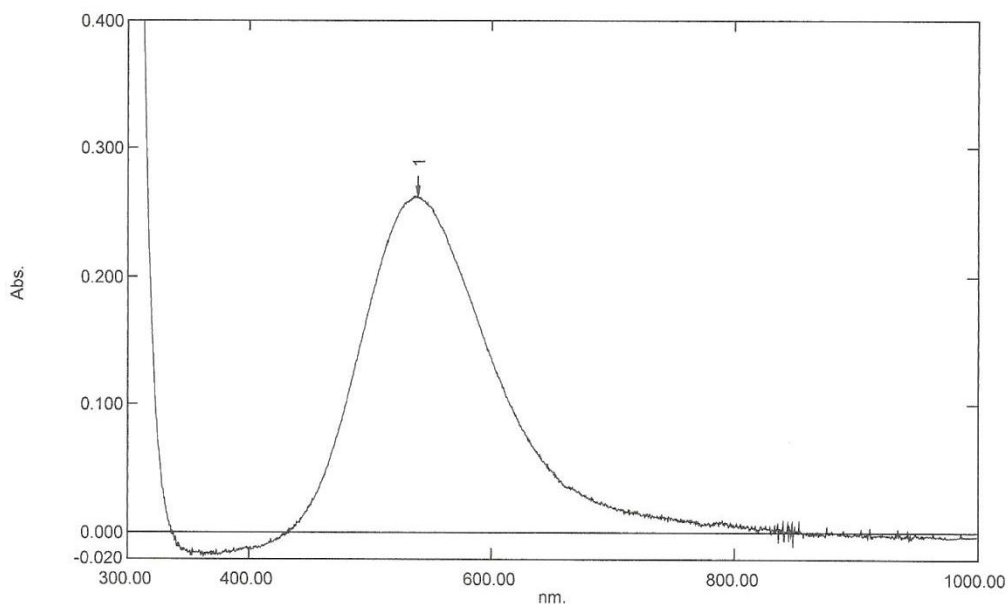
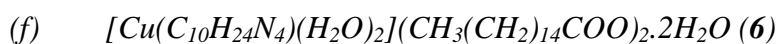


Figure 4.21 The UV-vis spectrum of **5**



Diaqua(1,4,8,11-tetraazacyclotetradecane- $\kappa^4 N^1, N^4, N^8, N^{11}$)copper(II) hexadecanoate dihydrate (**6**) was obtained as purple crystals from the reaction of $[Cu_2(CH_3(CH_2)_{14}COO)_4]$ with cyclam (mole ratio 1:2) in ethanol. The yield was 77%.

The single-crystal XRD result shows that **6** exhibits analogous coordination propensities as the above crystalline complexes. A perspective view of the molecular structure of **6** is shown in **Figure 4.22**.

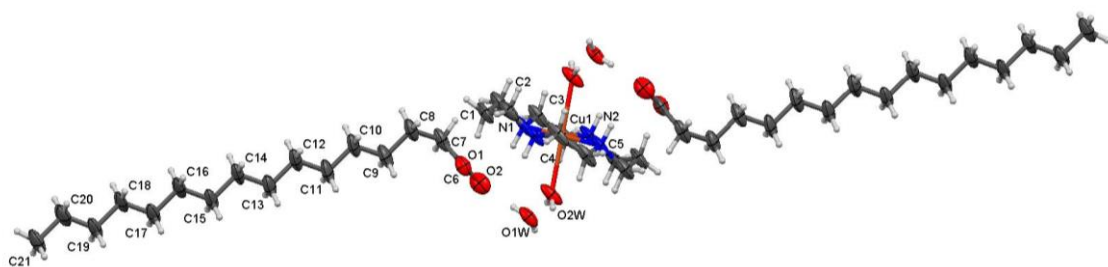


Figure 4.22 Molecular structures of **6**, showing displacement ellipsoids at 50% probability level; operator used to generate symmetry equivalent elements: $-x, -y, 1-z$

The cation, anions and lattice H_2O molecules are similarly linked by intermolecular $\text{N-H}\cdots\text{O}$ and $\text{O-H}\cdots\text{O}$ hydrogen bonds, forming a similar fashion of a layered structure parallel to (001) plane (**Figure 4.23**).

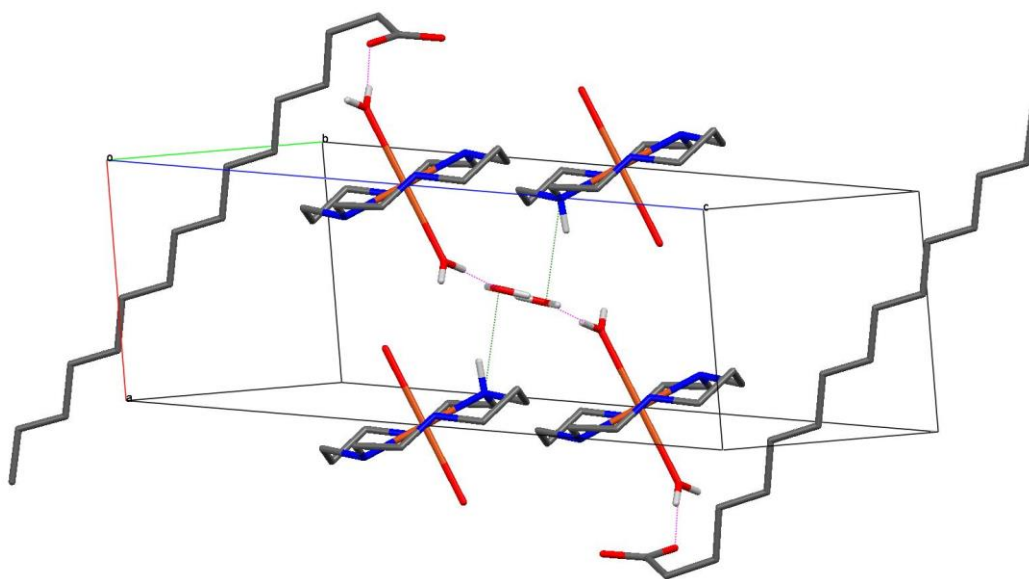


Figure 4.23 Unit cell of **6**, viewed along crystallographic b -axis, $\text{N-H}\cdots\text{O}$ and $\text{O-H}\cdots\text{O}$ bond is indicated as green and pink dashes respectively (some hydrogen atoms were not shown).

The FTIR spectrum of **6** (**Figure 4.24**) and the Δ_{COO} value (162 cm^{-1}) are similar to the above complexes.

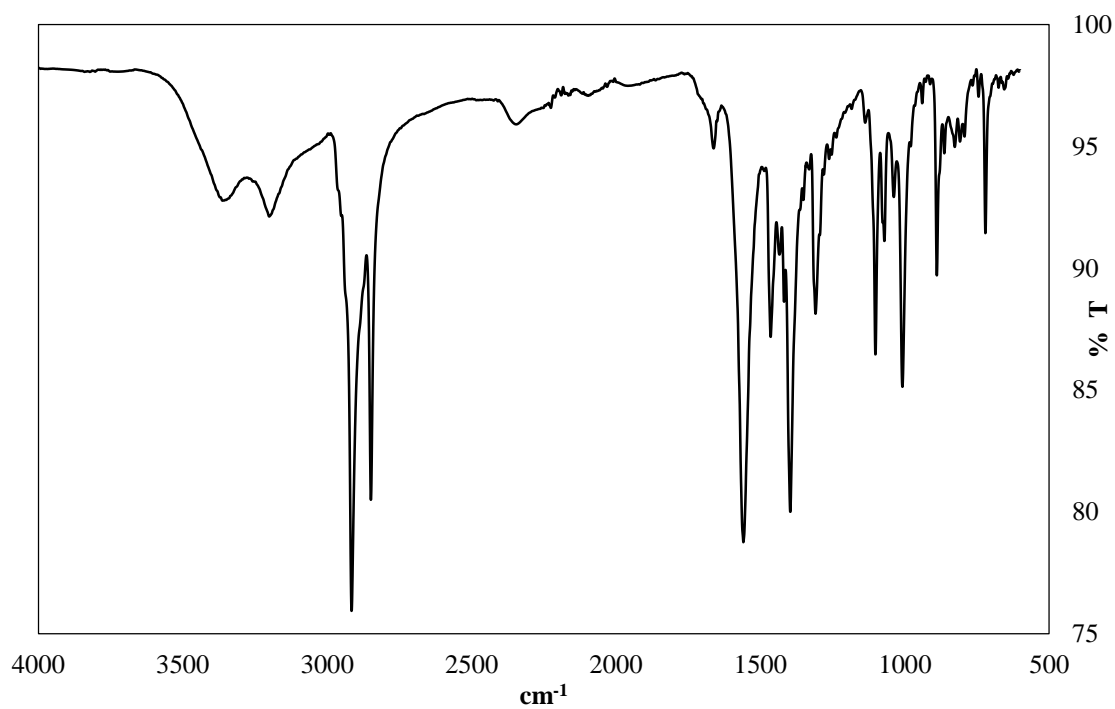


Figure 4.24 The FTIR spectrum of **6**

The electronic spectrum of **6** in acetone (**Figure 4.25**) and data ($\lambda_{\text{max}} = 550 \text{ nm}$; $\epsilon_{\text{max}} = 116 \text{ M}^{-1} \text{ cm}^{-1}$) are also similar to the above complexes.

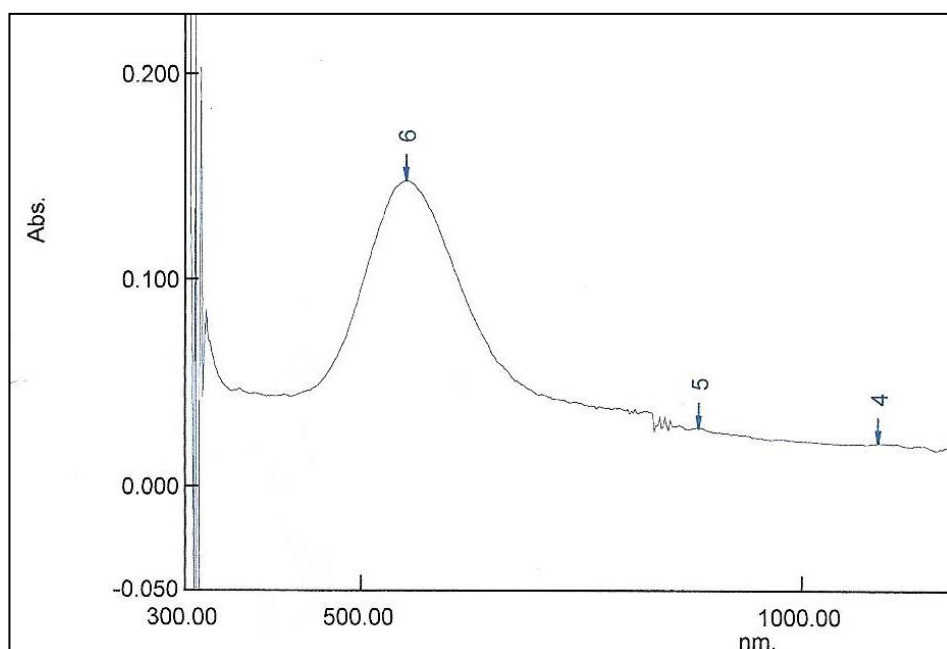
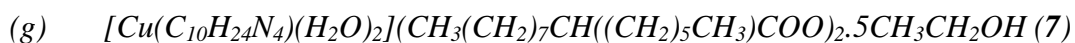


Figure 4.25 The UV-vis spectrum of **6**



Diaqua(1,4,8,11-tetraazacyclotetradecane-κ⁴N¹,N⁴,N⁸,N¹¹)copper(II) 2-hexyldecanoate pentaethanol (**7**) was obtained as a dark-purple viscous liquid from the reaction of $[Cu_2(CH_3(CH_2)_7CH((CH_2)_5CH_3)COO)_4]$ with cyclam (mole ratio 1:2) in ethanol. The yield was 62%. Its chemical formula, based on the results of elemental analyses (**Table 4.3**), is $CuC_{52}H_{120}N_4O_{11}$ (FW = 1041.09 g mol⁻¹).

Table 4.3 Elemental analytical data of **7**

Element	Calculated (%)	Found (%)
C	59.9	59.5
H	11.5	12.0
N	5.4	5.3

The FTIR spectrum of **7** (**Figure 4.26**) and the Δ_{COO} value (155 cm⁻¹) are similar to the above complexes.

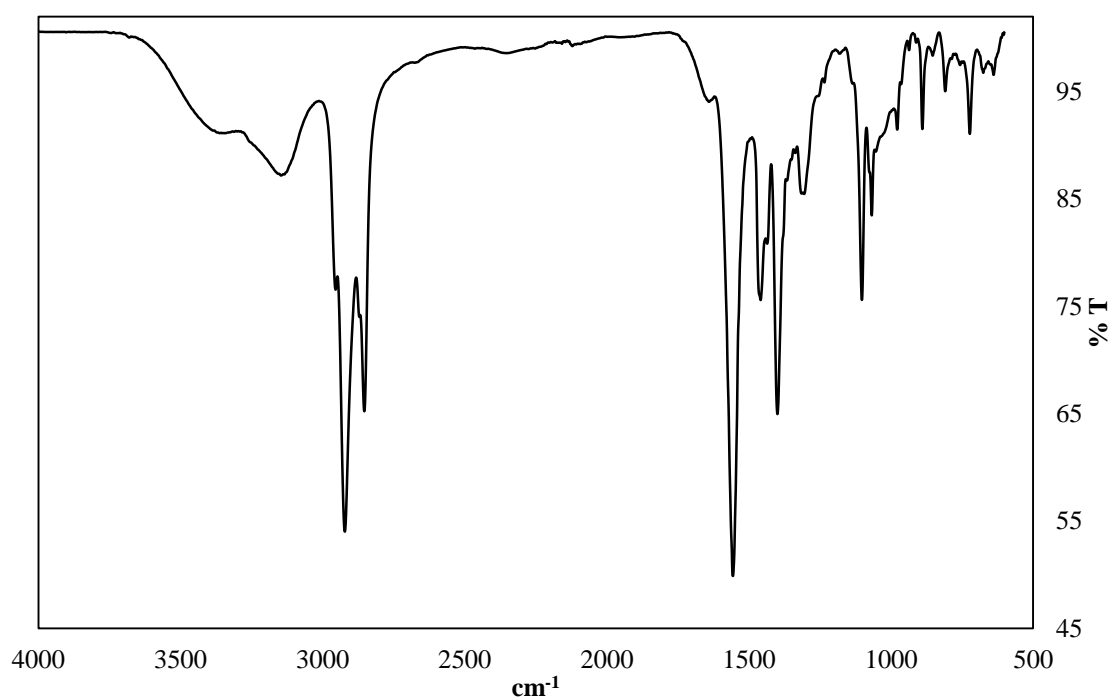


Figure 4.26 The FTIR spectrum of **7**

The electronic spectrum of **7** in ethanol (**Figure 4.27**) and data ($\lambda_{\text{max}} = 532 \text{ nm}$; $\epsilon_{\text{max}} = 117 \text{ M}^{-1} \text{ cm}^{-1}$) are also similar to the above complexes.

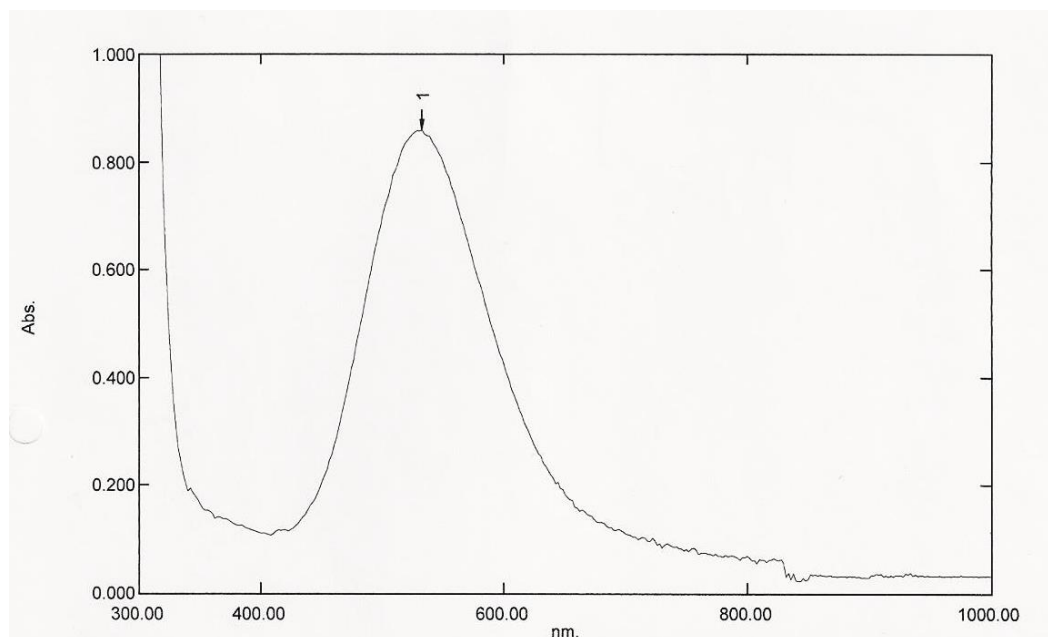


Figure 4.27 The UV-vis spectrum of **7**

Based on the above instrumental data, it is proposed that the structure of **7** is similar to that of the above crystalline complexes, as shown in **Figure 4.28**. The complex is made up of a $[\text{Cu}(\text{C}_{10}\text{H}_{24}\text{N}_4)(\text{H}_2\text{O})_2]^{2+}$ cation and two $\text{CH}_3(\text{CH}_2)_7\text{CH}((\text{CH}_2)_5\text{CH}_3)\text{COO}^-$ anions.

Also present are two solvated H_2O and five solvated $\text{CH}_3\text{CH}_2\text{OH}$ molecules. Similar to the above complexes, the two solvated H_2O molecules are understood to bridge the cationic complex and $\text{CH}_3(\text{CH}_2)_7\text{CH}((\text{CH}_2)_5\text{CH}_3)\text{COO}^-$ ions.

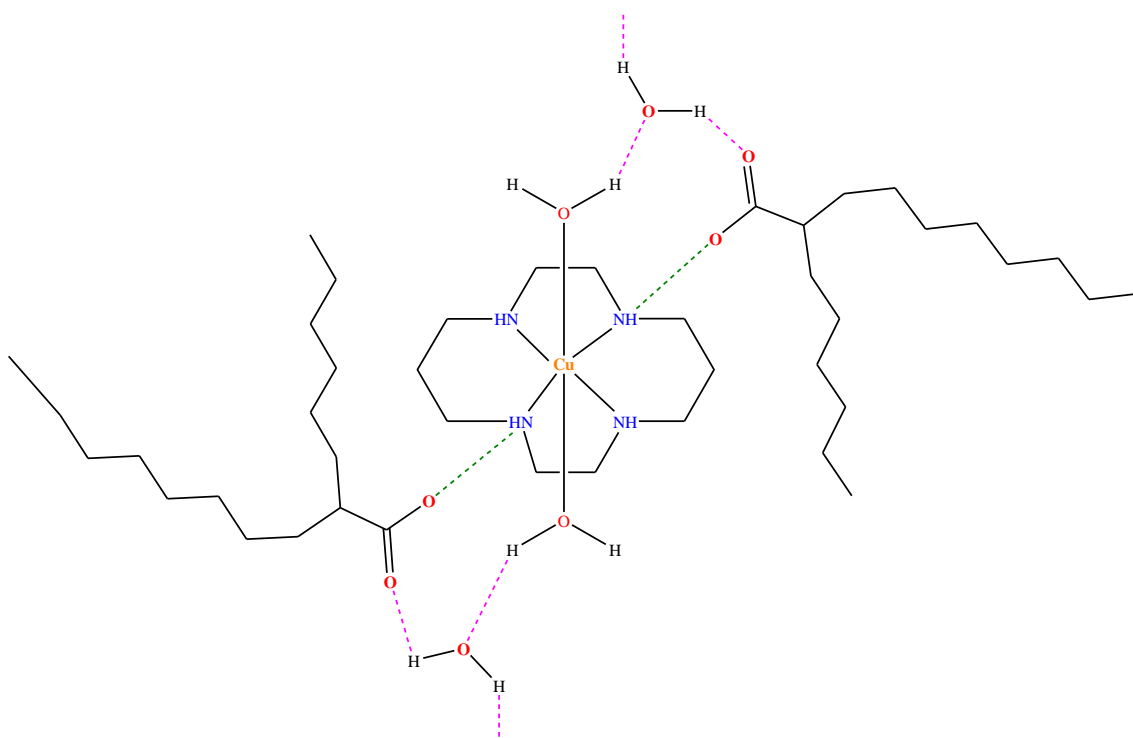


Figure 4.28 Schematic representation of the proposed structure of **7**; N-H...O and O-H...O bond is indicated as green and pink dashes respectively; the five solvated CH₃CH₂OH molecules are not shown.

The selected crystal parameters and refinement details of the crystalline complexes were given in **Table 4.4**.

Table 4.4 Selected crystal parameters and refinement details of aliphatic crystalline complexes

	1	3	4	5	6
Empirical formula	C ₂₄ H ₅₈ CuN ₄ O ₈	C ₃₀ H ₇₀ CuN ₄ O ₈	C ₃₄ H ₇₈ CuN ₄ O ₈	C ₃₈ H ₈₂ CuN ₄ O ₈	C ₄₂ H ₉₄ CuN ₄ O ₈
Formula weight	594.29	678.44	734.54	790.65	846.75
Wavelength (Å)	0.71073	0.71073	0.71073	0.71073	0.71073
Temperature (K)	153(2)	100(2)	150(2)	150(2)	153(2)
Crystal system	Monoclinic	Triclinic	Triclinic	Triclinic	Triclinic
Space group	<i>P</i> 2 ₁ / <i>c</i>	<i>P</i> -1	<i>P</i> -1	<i>P</i> -1	<i>P</i> -1
Volume (Å ³)	1542.5(5)	926.9(10)	1024.13(1)	1109.7(4)	1212.4(4)
<i>a</i> (Å)	11.784(2)	6.986(4)	6.9972(4)	6.9700(14)	6.9873(14)
<i>b</i> (Å)	9.987(2)	8.808(6)	8.8164(5)	8.7954(18)	8.8176(18)
<i>c</i> (Å)	13.464(3)	15.325(8)	17.1495(10)	18.684(4)	20.240(4)
α (°)	90.00	95.07(3)	96.218(3)	79.66(3)	79.09(3)
β (°)	103.23(3)	93.116(18)	8.8164(5)	82.88(3)	88.52(3)
γ (°)	90.00	98.449(2)	17.1495(10)	81.87(3)	81.95(3)
<i>Z</i>	2	1	1	1	1
ρ_{calc} (g cm ⁻³)	1.280	1.215	1.191	1.183	1.16
<i>F</i> (000)	646	371	403	435	467
Measured data	15905	5988	7085	9865	13028
Unique data	2708	3988	4624	4520	4278
Goodness of fit	1.096	0.905	1.079	1.031	0.976
Observed data [<i>I</i> ≥ 2.0σ(<i>I</i>)]	2108	3486	4139	3207	2644
Final R indices [<i>I</i> ≥ 2.0σ(<i>I</i>)]	R ₁ = 0.0451 wR ₂ = 0.1359	R ₁ = 0.0406 wR ₂ = 0.1189	R ₁ = 0.0468 wR ₂ = 0.1257	R ₁ = 0.0488 wR ₂ = 0.1137	R ₁ = 0.0535 wR ₂ = 0.1383
R indices (all data)	R ₁ = 0.0615 wR ₂ = 0.1551	R ₁ = 0.0476 wR ₂ = 0.1301	R ₁ = 0.0517 wR ₂ = 0.1302	R ₁ = 0.0745 wR ₂ = 0.1264	R ₁ = 0.1003 wR ₂ = 0.1805

In overall, the distances between the metal centre and the equatorial cyclam ligand in all complexes are comparable (**Table 4.5**). It is therefore deduced that the cyclam cavity does not significantly differ in presence of anions of variable carbon chain length. The distances between the metal centre and axial H₂O ligand are also similar.

Table 4.5 Distance values between the Cu atom and its ligand

Bond length (Å)	Equatorial		Axial
	Cu–N ₁	Cu–N ₂	Cu–O
1	2.027(3)	2.018(2)	2.499(1)
3	2.029(1)	2.000(1)	2.443(1)
4	2.032(2)	2.005(2)	2.453(1)
5	2.029(3)	2.002(3)	2.440(2)
6	2.022(3)	2.003(3)	2.451(3)

4.2.2. *Physical and chemical properties*

All crystalline complexes had exhibited similar coordination pattern. However, except for **1** ($n = 6$), all of the other crystalline complexes were found to exhibit triclinic polymorphism in $P-1$ space group, whereas **1** was spatially arrayed in monoclinic $P2_1/c$ polymorph. Hence, to understand whether these differences have an effect on the physical and chemical properties of copper(II)-cyclam-alkylcarboxylates, the magnetic and thermal properties of **1** ($n = 6$) and **6** ($n = 15$) were further probed.

(a) *Magnetic studies*

The magnetic susceptibilities of the complexes were measured for solid samples using the Gouy method. The values of the effective magnetic moment, μ_{eff} , (in Bohr Magneton, BM) of **1** and **6** at 298 K were calculated using the values of mass

susceptibility (χ_g), molar susceptibility (χ_m), diamagnetic correction factor (χ_D), and corrected molar susceptibility (χ'_m). The results are shown in **Table 4.6**.

Table 4.6 The magnetic data for **1** and **6**

	1	6
$\chi_g (10^{-6} \text{ cm}^3 \text{ g}^{-1})$	0.82	0.90
$\chi_M (10^{-6} \text{ cm}^3 \text{ mol}^{-1})$	487.32	762.08
$\chi_D (10^{-6} \text{ cm}^3 \text{ mol}^{-1})$	-368.08	-581.56
$\chi_M^{\text{corr}} (10^{-6} \text{ cm}^3 \text{ mol}^{-1})$	855.38	1343.64
$\chi_M^{\text{corr}} T (\text{cm}^3 \text{ K mol}^{-1})$	0.2549	0.4004
$\mu_{\text{eff}} (\text{BM})$	1.43	1.79

It is found that the experimental μ_{eff} value of **1** (1.43 BM) is significantly lower than the spin-only value of a mononuclear Cu(II) complex (1.73 BM). This indicates the presence of antiferromagnetic interactions between the Cu(II) centres. In contrast, the μ_{eff} value of **6** (1.79 BM) is in excellent agreement to the spin-only value, indicating no magnetic communications between the Cu(II) centres.

The contrast in the magnetic interactions in the two complexes may be due to the differences in their extended hydrogen bonding network. For **1**, each $\text{CH}_3(\text{CH}_2)_5\text{COO}^-$ ion showed an additional $\text{N-H}\cdots\text{O}$ bond, where both of its *O*-carboxylate atoms act as the acceptor, bridging the $[\text{Cu}(\text{cyclam})]^{2+}$ ion (**Figure 4.29**). The bridge provides a pathway for an electronic interaction between the Cu(II) centres.

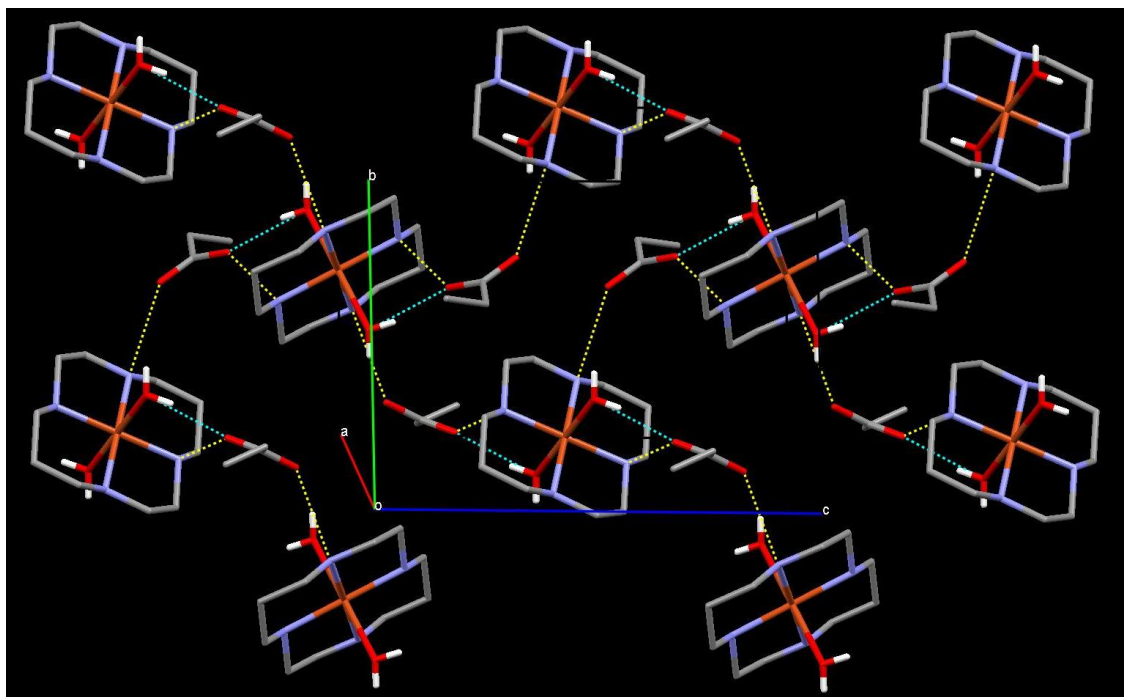


Figure 4.29 The extended hydrogen-bond network of **1** viewed down the *a*-axis, yellow dashed lines indicate N–H···O bond and blue dashed lines indicate O–H···O bond; the $\text{CH}_3(\text{CH}_2)_5\text{COO}^-$ chains were shortened and lattice H_2O molecules were omitted for clarity.

However, the above feature is not observed in **6**. The complex showed only a one-dimensional chain between the $[\text{Cu}(\text{cyclam})]^{2+}$ and $\text{CH}_3(\text{CH}_2)_{14}\text{COO}^-$ ions. In this complex, one of its *O*-carboxylate atoms is hydrogen-bonded to lattice H_2O molecules, preventing its linkage to another $[\text{Cu}(\text{cyclam})]^{2+}$ ion (**Figure 4.30**).

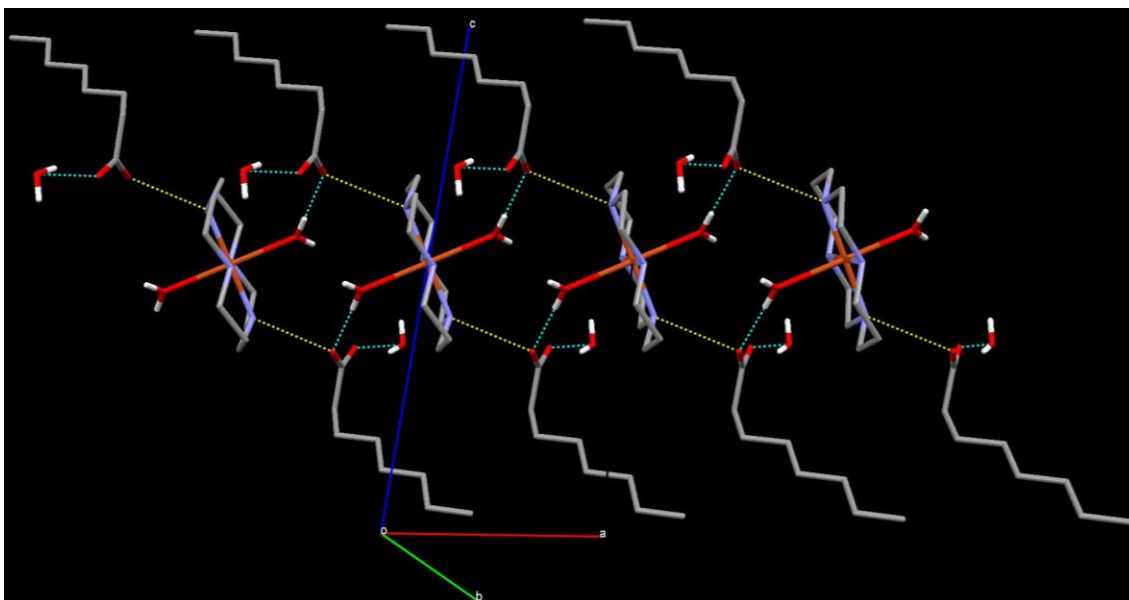


Figure 4.30 The extended hydrogen-bond network of **6** viewed down the *b*-axis, yellow dashed lines indicate N–H···O bond and blue dashed lines indicate O–H···O bond; the $\text{CH}_3(\text{CH}_2)_{14}\text{COO}^-$ chains were shortened.

Therefore, the antiferromagnetism in **1** is proposed to occur through the two-way interchain interactions via the $\text{CH}_3(\text{CH}_2)_5\text{COO}^-$ anions, known as antiferromagnetic long-range ordering properties [8]. From this account, it may be deduced that the presence of additional N–H···O bond is a requisite to promote the magnetic communications in Cu(II)-cyclam-alkylcarboxylate complexes.

(b) Thermal properties

The thermal properties of the complexes were studied by thermogravimetric analyses (TGA), differential scanning calorimetry (DSC) and optical polarised microscopy (OPM).

The TGA trace of **1** (**Figure 4.31**) shows three weight-loss steps. The first two weight losses correspond to evaporation of two lattice H_2O molecules at 103.6 °C and two coordinated H_2O ligands at 139.3 °C (total, 12.1%; expected, 12.2%). The next rapid and major weight loss at 229.8 °C corresponds to the decomposition of cyclam and two $\text{CH}_3(\text{CH}_2)_5\text{COO}^-$ ions (found, 74.3%; expected, 77.2%). The amount of residue

at temperatures above 600 °C was 13.6%. This correlates well with the calculated value of 13.4%, assuming that it is made up of pure CuO [9].

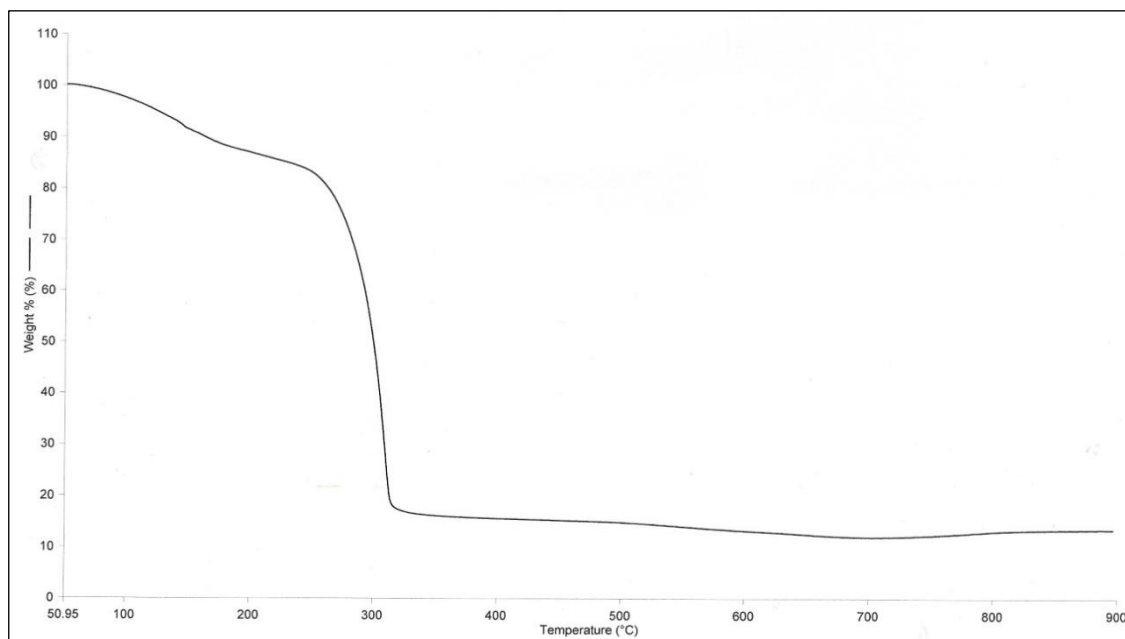


Figure 4.31 TGA trace of **1**

The DSC of **1** was recorded in two successive heating-cooling cycles within the temperature range 30-135 °C. In the first cycle, the scan (**Figure 4.32**) shows one strong endothermic peak at 48.5 °C (onset at 43.9 °C; $\Delta H = -46.51 \text{ kJ mol}^{-1}$), deduced as its melting temperature. However, there were no peaks on first cooling, and subsequent heating-cooling cycle. The results suggest the original structure was either not reformed or formed very slowly from the isotropic liquid.

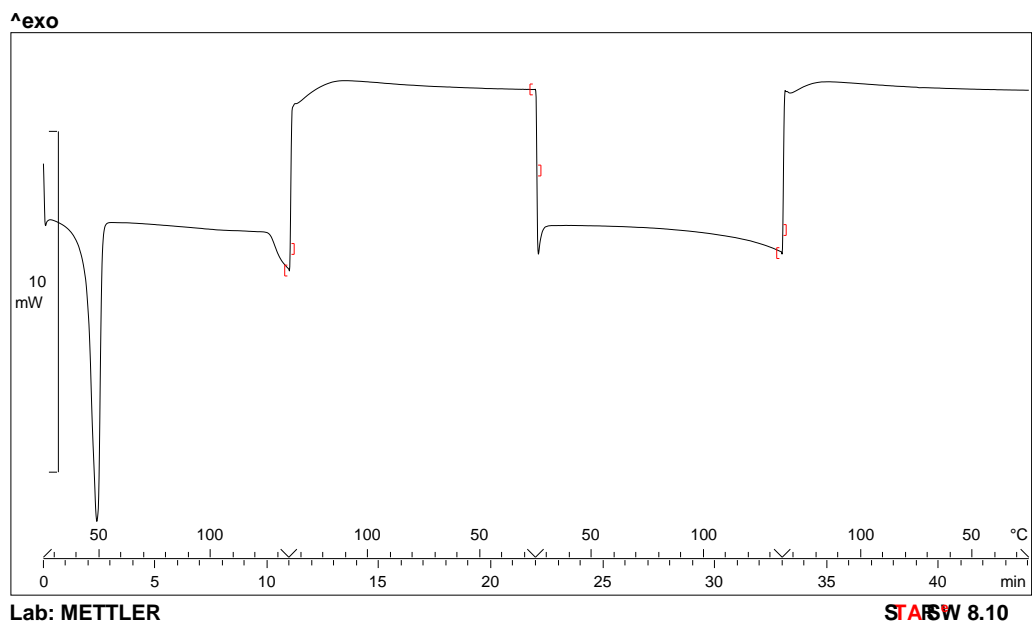


Figure 4.32 DSC traces of **1**

Viewed under OPM (**Figure 4.33**), **1** was observed to melt at 44.2 °C (in agreement with DSC), and then cleared to an isotropic liquid at 135.0 °C. Upon cooling from the isotropic liquid, an optical texture was observed at room temperature. Hence, it may be concluded that **1** was not mesogenic.

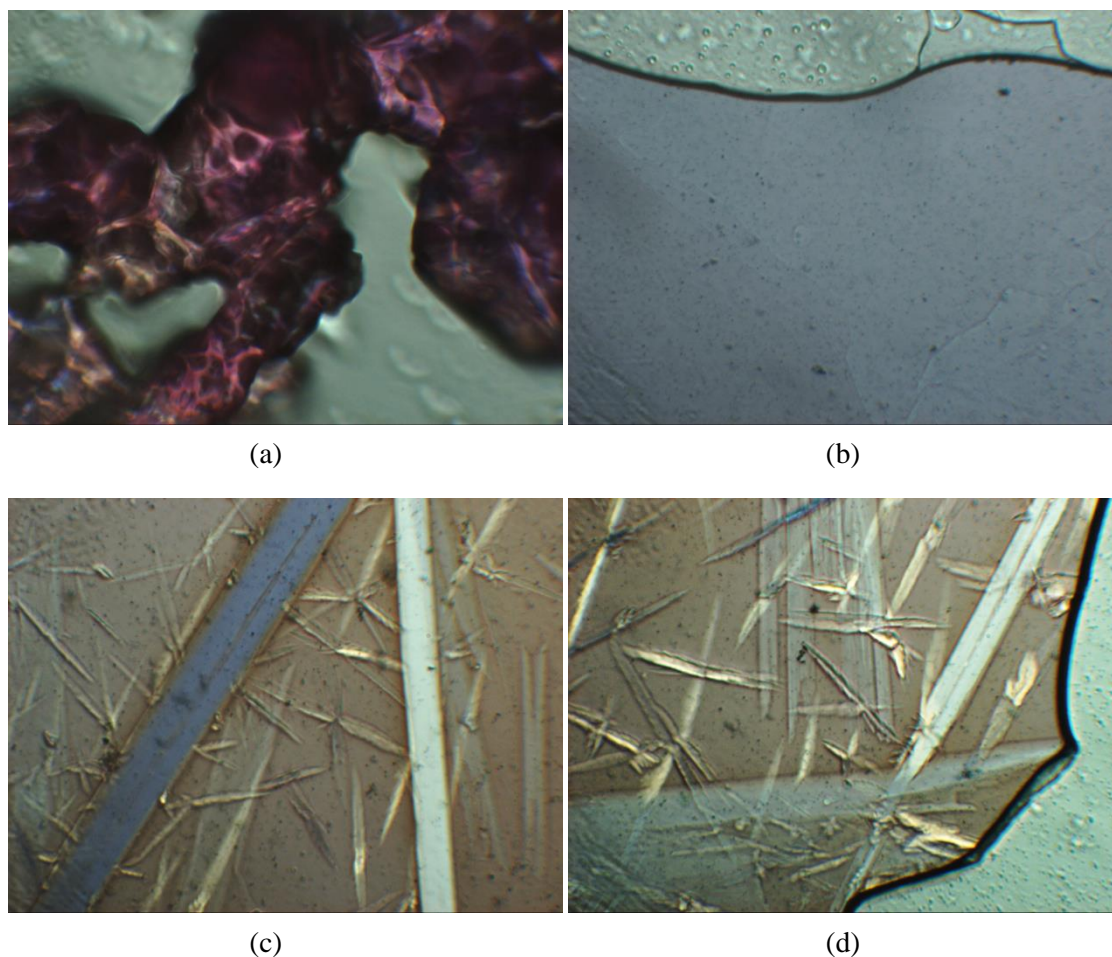


Figure 4.33 Photomicrographs of **1** under crossed polarizers (a) melting at 44.2 °C; (b) clearing to an isotropic liquid at 135.0 °C; (c) and (d) crystals at two different sites upon cooling to room temperature

As for **6**, the TGA trace shows four weight-loss steps (**Figure 4.34**). Similar to **1**, the first two weight losses correspond to the evaporation of two lattice H₂O molecules at 107.7 °C, followed by two coordinated H₂O ligands at 184.7 °C (total, 7.9%, expected 8.5%). The next weight loss at 264.6 °C is assigned to the decomposition of the two CH₃(CH₂)₁₄COO⁻ anions (found, 57.1%; expected, 60.3%), and the final weight loss at 403.9 °C is assigned to the decomposition of cyclam (found, 20.1%; expected, 23.7%). The amount of residue at temperatures above 550 °C was 14.9%. It is assumed to be a mixture of CuO (expected, 9.4%) and Cu₂O (expected, 16.9%). It is inferred that on heating, the Cu(II) ion in the complex was reduced to Cu(I) by cyclam.

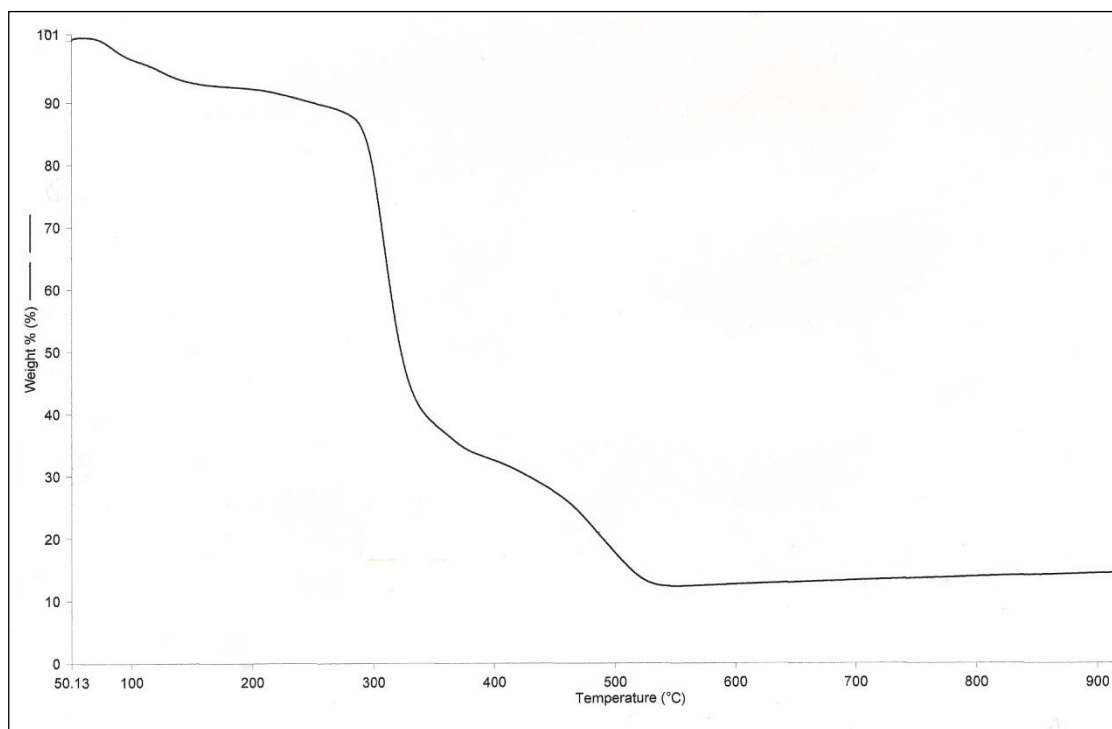


Figure 4.34 TGA trace of **6**

The DSC for **6** was recorded in the temperature range 30-150 °C for two heating-cooling cycles. The scan shows almost repeatable phase transitions during both heating-cooling cycles (**Figure 4.35** and **Figure 4.36**). The calorimetric data is given in **Table 4.7**.

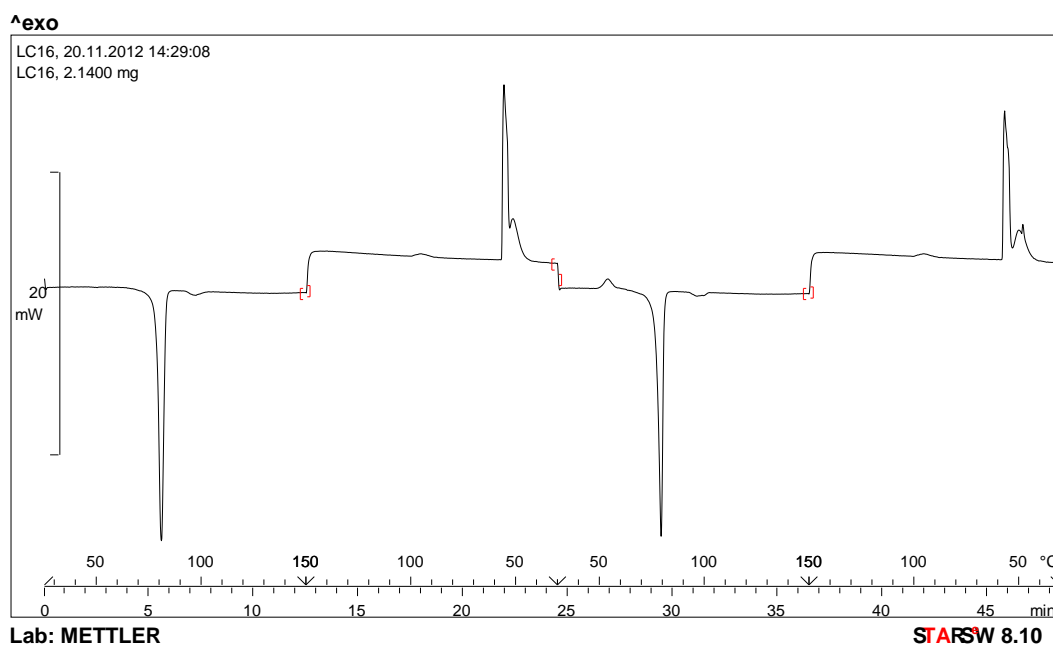
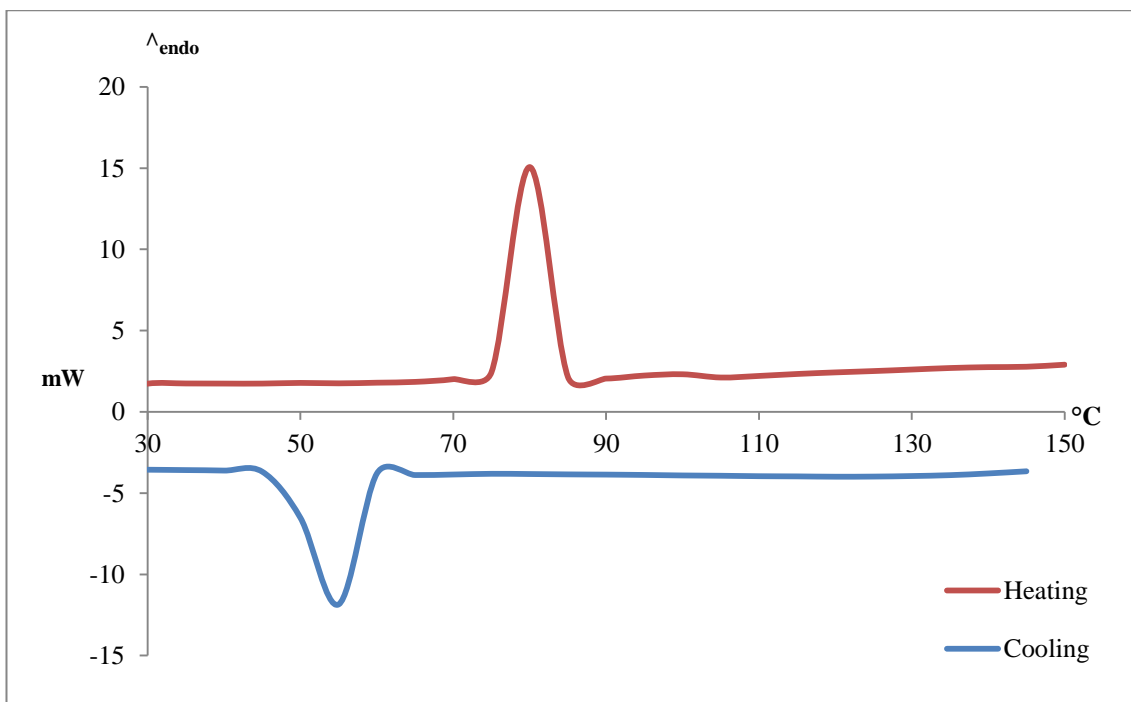
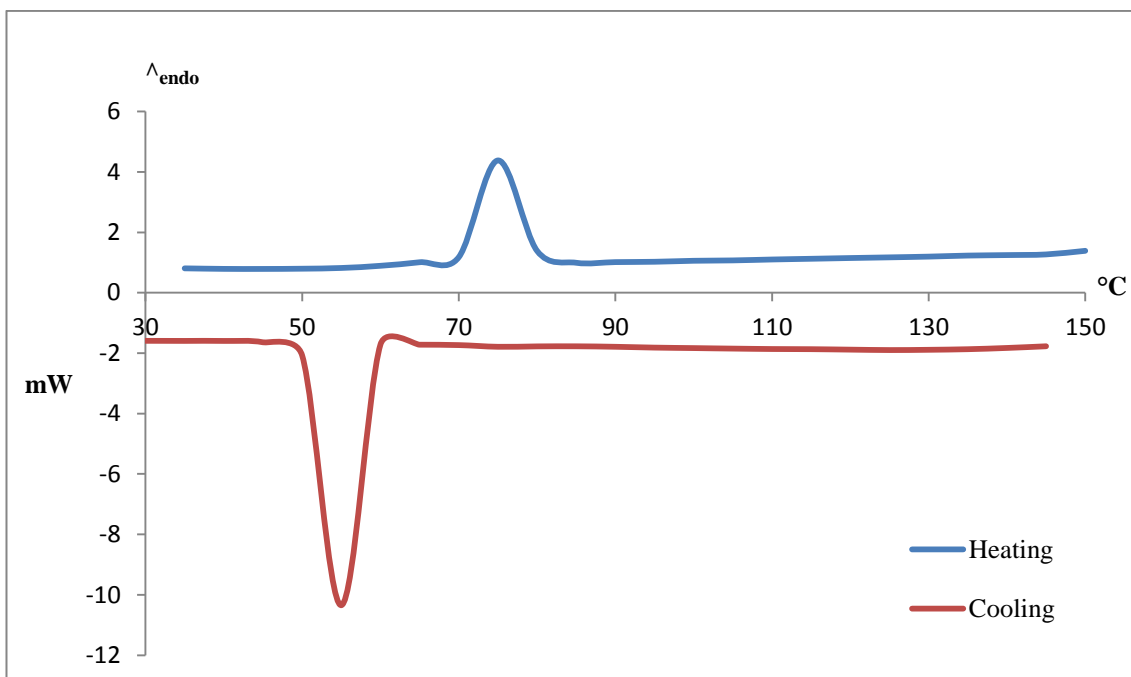


Figure 4.35 DSC traces of **6**



(a)



(b)

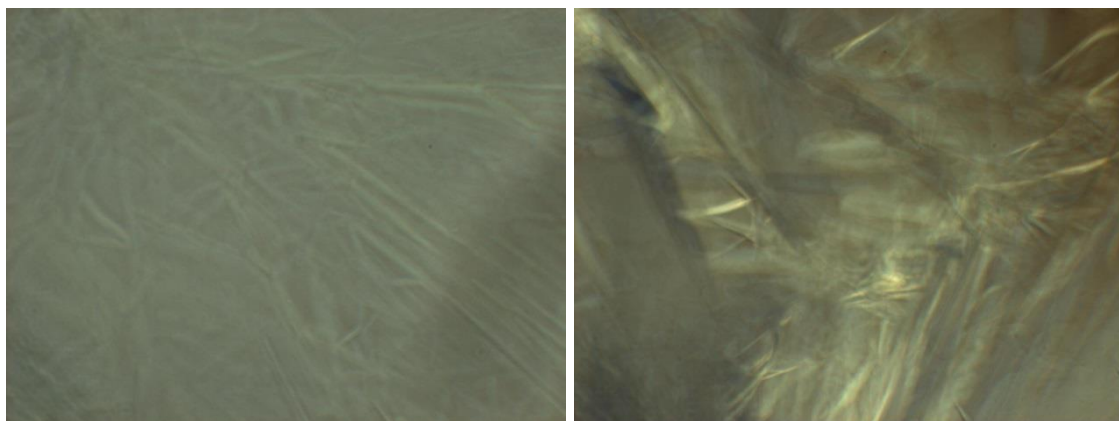
Figure 4.36 DSC traces of **6** separated to: (a) first cycle; and (b) second cycle

Table 4.7 DSC data of **6**

	Temperature (°C)		ΔH (kJ mol ⁻¹)	Phase Transition
Cycle 1	heating	78.3	+130.26	<i>Cr</i> → <i>M</i>
		92.6	+3.40	<i>M</i> → <i>N</i>
	cooling	100.4	-1.53	<i>N</i> → <i>M</i>
		56.9	-59.55	<i>M</i> → <i>Cr</i>
Cycle 2	heating	76.6	+117.65	<i>Cr</i> → <i>M</i>
		92.7	+3.54	<i>M</i> → <i>N</i>
	cooling	99.3	-0.76	<i>N</i> → <i>M</i>
		57.9	-64.63	<i>M</i> → <i>Cr</i>

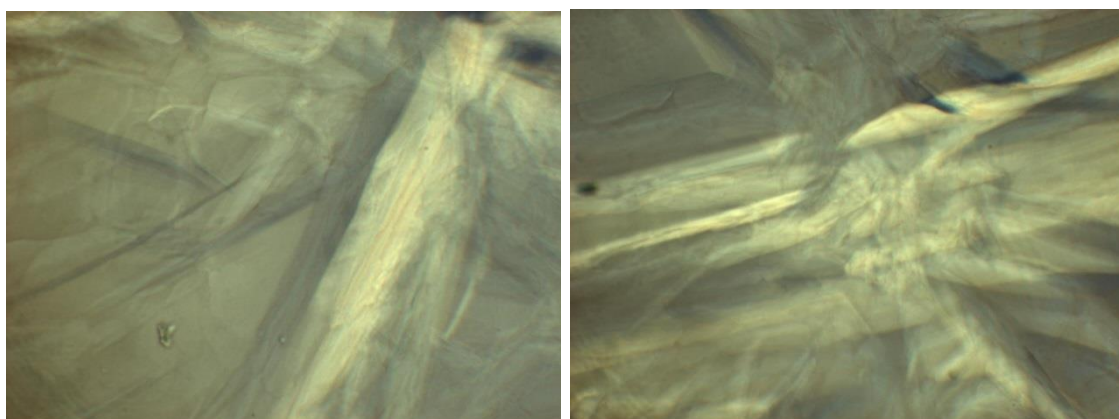
Cr = crystal; *M* = mesophase; *N* = nematic

The phase transition temperatures observed under OPM complement well with those of DSC. Upon cooling from the isotropic liquid, **6** displayed a formation of layers in an aligned orientation at 102 °C. The texture became more prominent with further cooling, and exhibited a stronger birefringence at 88 °C. It is further noted that at the crystallization temperature, the optical texture lost its birefringence (**Figure 4.37**). These results indicate that **6** exhibits mesomorphisms.



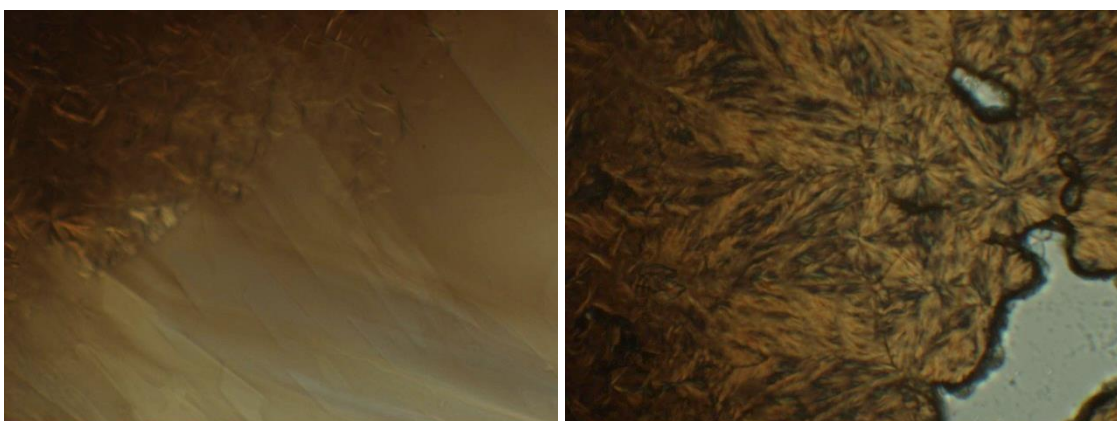
(a)

(b)



(c)

(d)



(e)

(f)

Figure 4.37 Photomicrographs of **6** under crossed polarizers on cooling at: (a) 102 °C; (b-d) 88 °C at three different sites; (e) crystalizing from left to right at 56.9 °C; and (f) room temperature

4.2.3. Concluding remarks

Cyclam reacted with copper(II) alkylcarboxylates, $[\text{Cu}_2(\text{C}_n\text{H}_{2n+1}\text{COO})_4]$ to form mononuclear ionic complexes of general formula $[\text{Cu}(\text{C}_{10}\text{H}_{24}\text{N}_4)(\text{H}_2\text{O})_2](\text{C}_n\text{H}_{2n+1}\text{COO})_2$ in good yields (50-80%). Except for **1** ($n = 6$), all other crystalline complexes were found to exhibit triclinic polymorphism in $P-1$ space group; **1** was spatially arrayed in monoclinic $P2_1/c$ polymorph.

Owing to the variation in the crystal polymorphism, comparative studies were done on **1** against the representative complex, **6** ($n = 15$). These two complexes showed dissimilarity in their magnetic properties: **1** exhibited an antiferromagnetic interaction between the Cu(II) metal centres, while **6** did not. Also, **1** was thermally less stable than **6**. The residue from the thermal decomposition of **1** was CuO, while that of **6** was mixture of CuO and Cu₂O. Finally, **1** was not mesogenic, while **6** was mesogenic.

4.3. Copper(II)-cyclam-arylcarboxylates

4.3.1. Structural elucidation

(a) $[\text{Cu}(p\text{-H}_2\text{NC}_6\text{H}_4\text{COO})_2(\text{C}_{10}\text{H}_{24}\text{N}_4)].2\text{H}_2\text{O}$ (**8**)

Bis(*p*-aminobenzoato)(1,4,8,11-tetraazacyclotetradecane- $\kappa^4\text{N}^1, \text{N}^4, \text{N}^8, \text{N}^{11}$)copper(II) dihydrate (**8**) was synthesized from the reaction of $[\text{Cu}_2(p\text{-H}_2\text{NC}_6\text{H}_4\text{COO})_4]$ and cyclam (mole ratio 1:2) in ethanol. It was obtained as purple needles, and the yield was 47%.

The single crystal XRD analysis showed that Cu atom is located on a special position (0, 1, 0) of the centre of inversion. The complex adopts a Jahn-Teller distorted octahedron geometry where the Cu atom is chelated by four aza-N atoms at the equatorial position of neutral cyclam [Cu–N1 = 2.0912(1) Å and Cu–N2 = 2.0111(1) Å], and axially coordinated by two *p*-H₂NC₆H₄COO[−] ligand with bond elongation [Cu–O1 = 2.5712(1) Å] (**Figure 4.38**). Two lattice H₂O molecules also mutually crystallized.

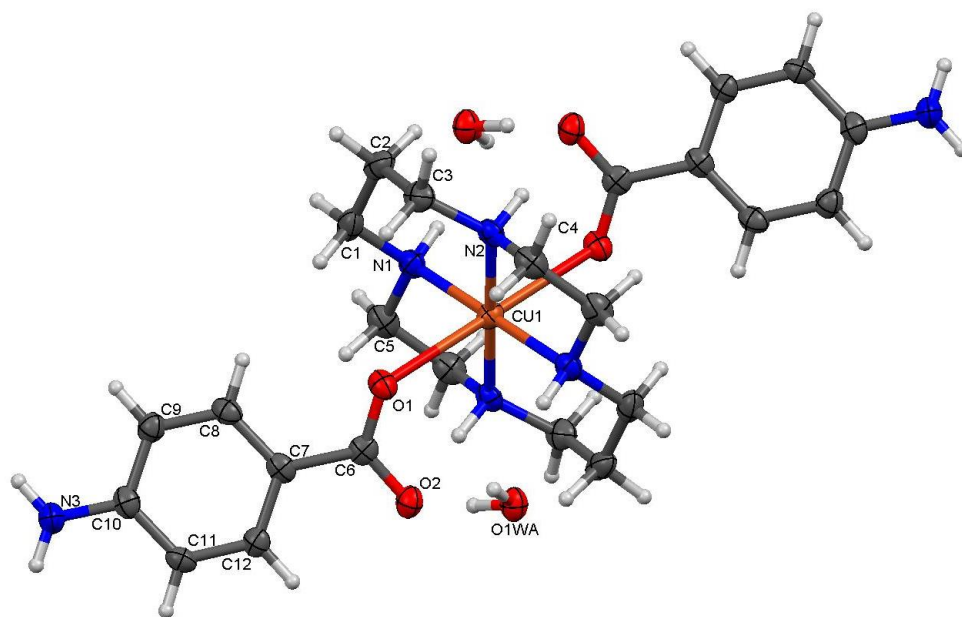


Figure 4.38 Molecular structure of **8**, showing displacement ellipsoids at 70% probability level; operator used to generate symmetry equivalent elements (unlabelled atoms): $-x, 2-y, -z$

Intramolecular N–H···O hydrogen bond was formed between cyclam and carboxylate group (*aza*-N2–H2···O2). The lattice H₂O dominate the formation of intermolecular hydrogen bonding, where it was trifurcated with *aza*-N1–H1···O1W, O1W–H···O2 and O1W–H···O1 hydrogen bonds. The terminal amine group links the macrocycles intermolecularly through N3–H3B···O2 hydrogen bond, giving an extensive chain along the *b*-axis. These present hydrogen bonding network had formed a two-dimensional layer parallel to (001) plane (**Figure 4.39**).

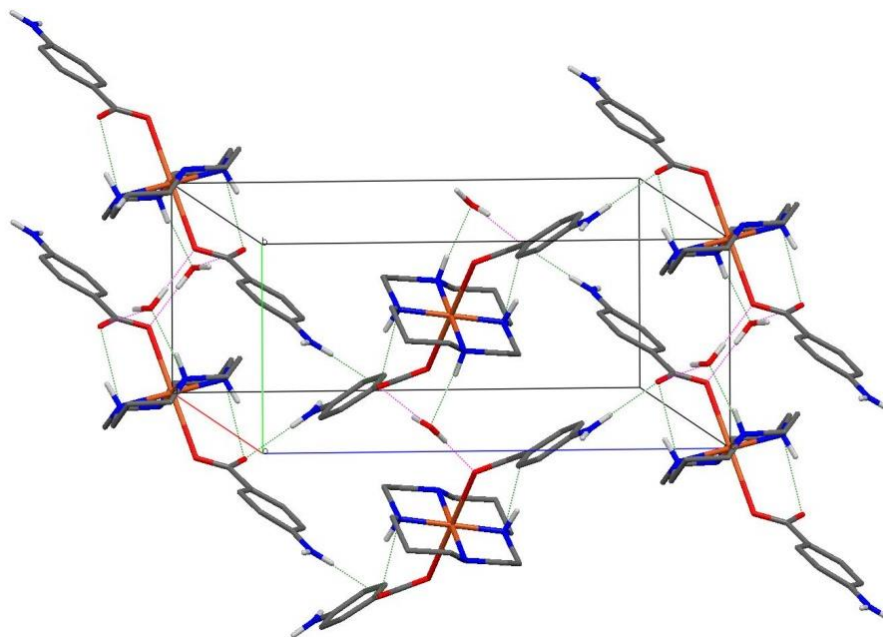


Figure 4.39 Unit cell of **8**, viewed along crystallographic *a*-axis; the crystal structure formed two dimensional networks via O–H···O and N–H···O hydrogen bond (pink and green dashed lines, respectively).

As previously found in the the copper(II)-cyclam-alkylcarboxylates analogs, the four aza-N atoms of the cyclam ring are in *R,R,S,S* chirality, and it attributes the most stable *trans*-III configuration of the macrocycle.

The FTIR spectrum of **8** (**Figure 4.40**) shows the presence of the expected functional groups and bonds (**Table 4.8**). The Δ_{COO} value ($\bar{\nu}_{\text{as,COO}} - \bar{\nu}_{\text{s,COO}}$) is 217 cm^{-1} , in agreement with the monodentate carboxylate ligand [10] found from its crystal structure.

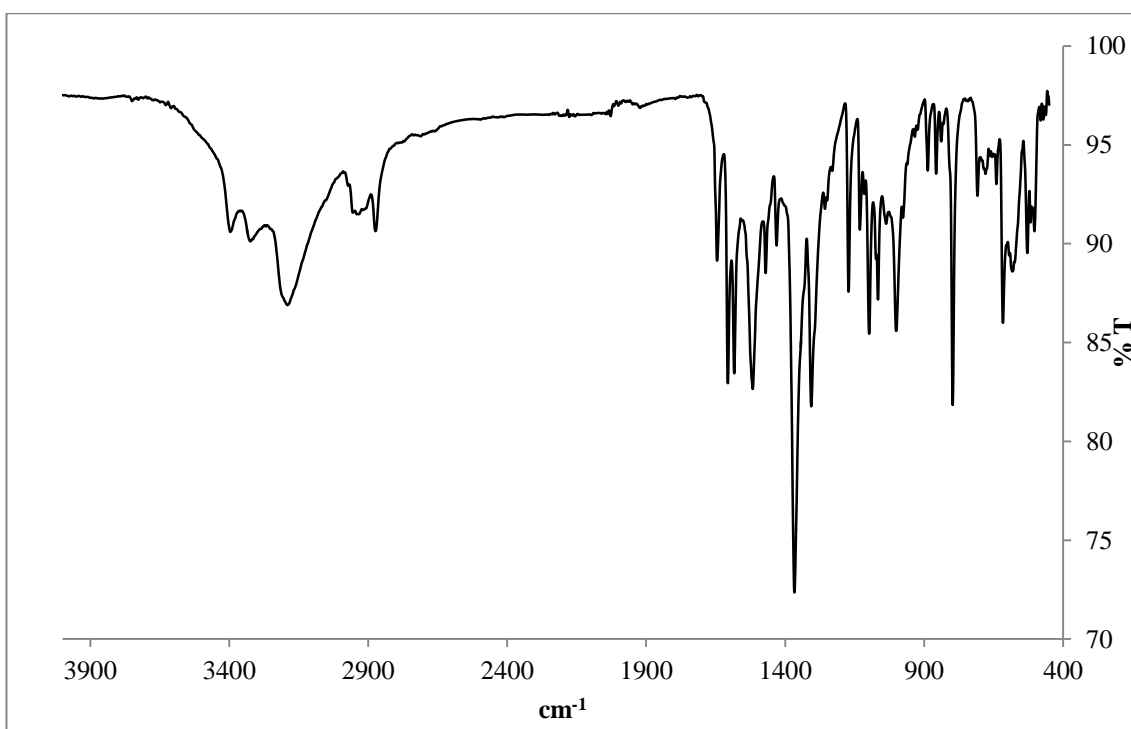


Figure 4.40 The FTIR spectrum of **8**

Table 4.8 The FTIR and assignments of **8**

Wavenumber (cm ⁻¹)	Assignment
3395, 3323	NH ₂
3192	Lattice H ₂ O
1644	C=O
1606	Aromatic C=C
1583	$\bar{\nu}_{\text{asym}} \text{COO}$
1366	$\bar{\nu}_{\text{sym}} \text{COO}$

Its electronic spectrum in acetone (**Figure 4.41**) shows a broad *d-d* band at $\lambda_{\text{max}} = 504 \text{ nm}$ ($\epsilon_{\text{max}} = 87 \text{ M}^{-1} \text{ cm}^{-1}$). The peak position suggests a square planar geometry at Cu(II) centre. The result implied that the octahedral geometry noted from the crystal structure was not maintained in solution. This is likely due to the dissociation of the

weakly $p\text{-H}_2\text{NC}_6\text{H}_4\text{COO}^-$ ligand at the axial positions, as a result of four strong Cu– N_{cyclam} equatorial bonds.

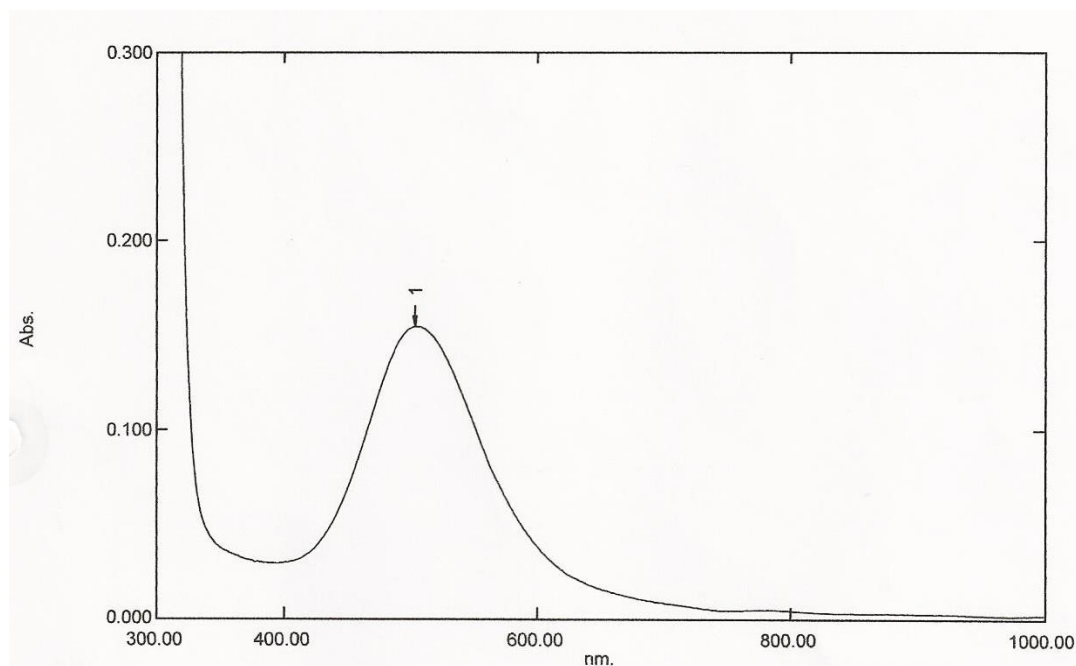


Figure 4.41 The UV-vis spectrum of **8**



(1,4,8,11-tetraazacyclotetradecane- $\kappa^4\text{N}^1, \text{N}^4, \text{N}^8, \text{N}^{11}$)bis(p -hydroxybenzoato)copper(II)

9 was obtained as purple crystals from the reaction of $[\text{Cu}_2(p\text{-HOC}_6\text{H}_4\text{COO})_4]$ and cyclam (mole ratio 1:2) in ethanol. The yield was 24%.

The single-crystal XRD result shows that the structure of **9** is similar to **8**, with an exception being the absence of lattice H_2O molecules in the crystal system (**Figure 4.42**). The complex had also exhibited similar coordination behaviour where the carboxylate groups are directly bound to the Cu atom. The Cu–N bonds at the equatorial position [Cu–N1 = 2.023(1) Å; Cu–N2 = 2.017(1) Å] and Cu– $\text{O}_{\text{carboxyl}}$ bond at the apex [Cu–O1 = 2.383(1) Å] were shorter than that of **8**.

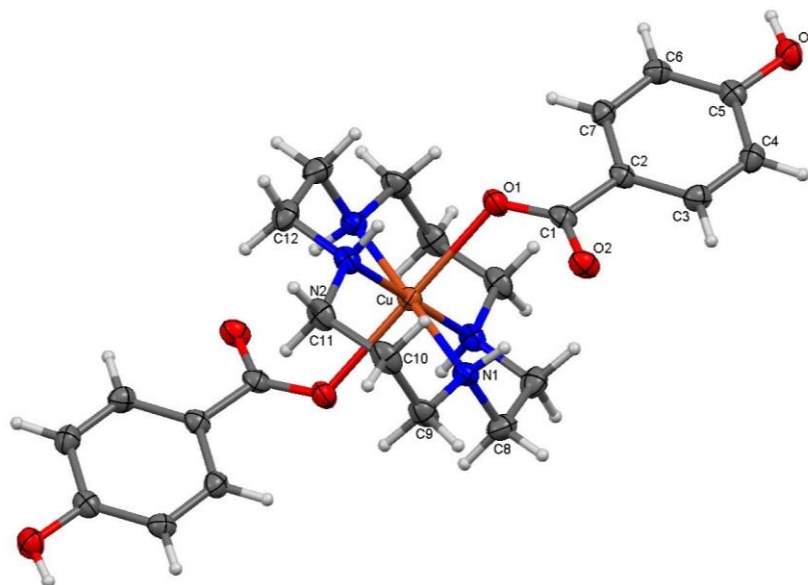


Figure 4.42 Molecular structure of **9**, showing displacement ellipsoids at 70% probability level; operator used to generate symmetry equivalent elements (unlabelled atoms): $1-x, 1-y, -z$

Similar to **8**, the *aza*-N atom formed intramolecular hydrogen bond with the *carboxyl*-O2 atom (N1–H1···O2). The intermolecular forces governed by the O–H···O hydrogen bond contributed by the terminal hydroxyl (O3–H3···O2) mediates the linkage of the macromolecules along the *b*-axis. The O2 atom is hence bifurcated and these hydrogen bond forces had resulted in the formation of a layered array parallel to (001) plane (**Figure 4.43**).

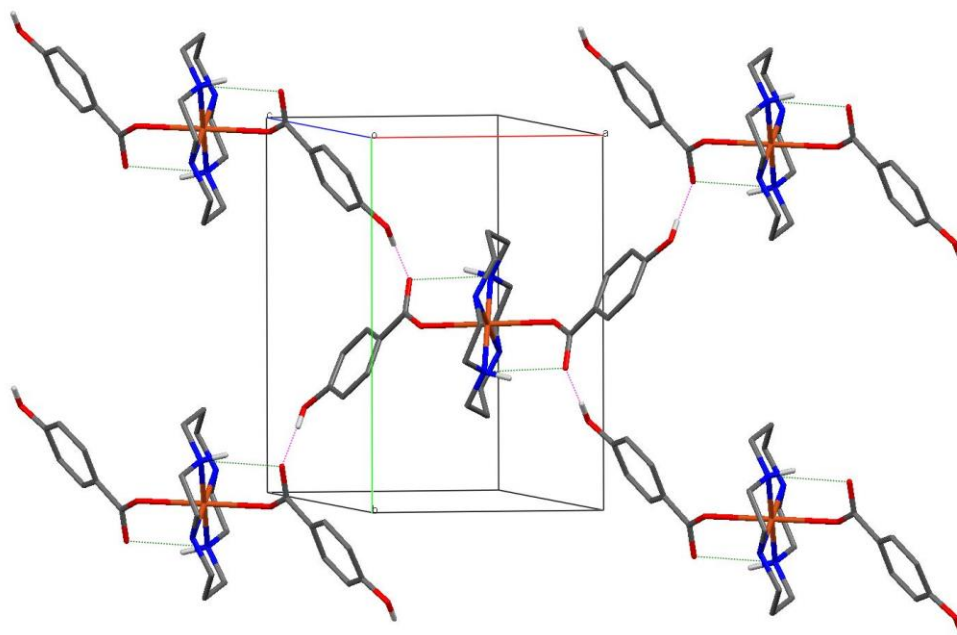


Figure 4.43 Unit cell of **9**, viewed along crystallographic *c*-axis; the crystal structure formed two dimensional networks via O–H···O and N–H···O hydrogen bond (pink and green dashed lines, respectively).

Similar to **8**, the FTIR spectrum of **9** (**Figure 4.44**) shows the presence of the expected functional groups and bonds, and the Δ_{COO} value is 216 cm^{-1} (calculated from the values of $\bar{\nu}_{\text{asym COO}} = 1586 \text{ cm}^{-1}$ and $\bar{\nu}_{\text{sym COO}} = 1370 \text{ cm}^{-1}$).

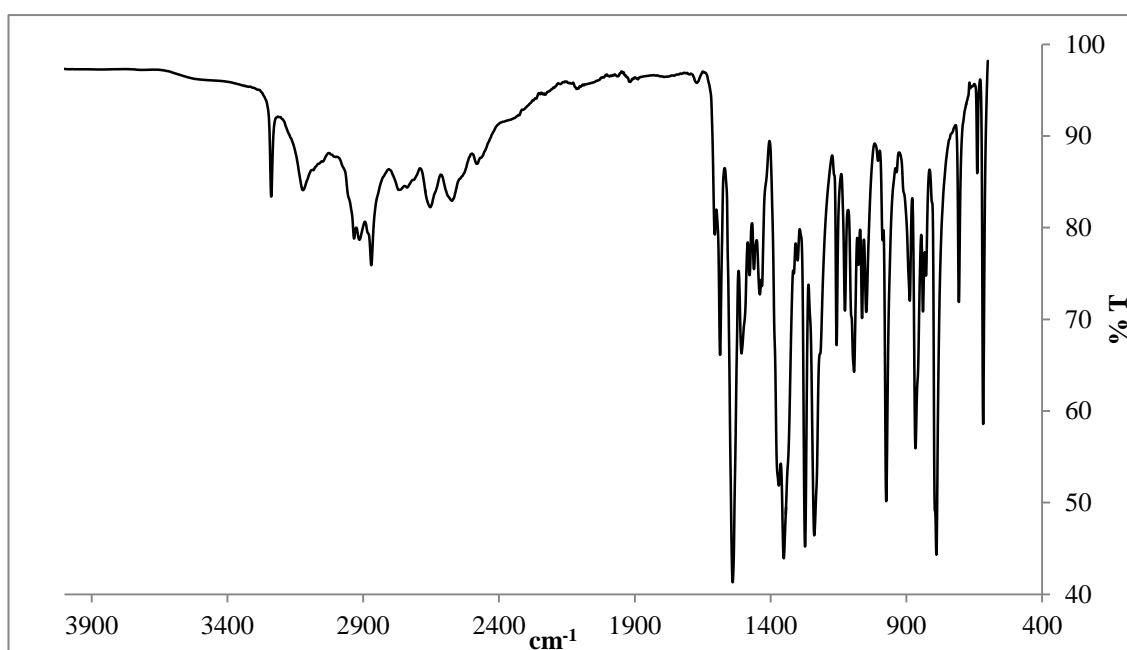


Figure 4.44 The FTIR spectrum of **9**

Its electronic spectrum in aqueous solution (**Figure 4.45**) shows a broad *d-d* band at $\lambda_{\max} = 507 \text{ nm}$ ($\epsilon_{\max} = 88 \text{ M}^{-1} \text{ cm}^{-1}$). The value is similar to that of **8** ($\lambda_{\max} = 504 \text{ nm}$; $\epsilon_{\max} = 87 \text{ M}^{-1} \text{ cm}^{-1}$), suggesting similar square planar geometry at Cu(II) in solution.

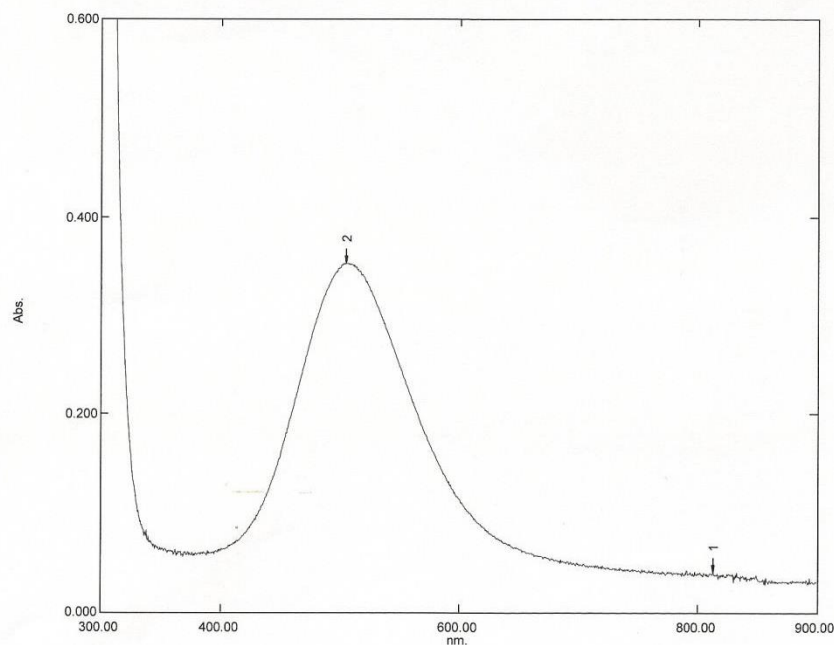
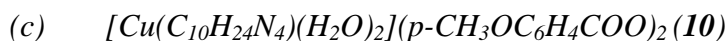


Figure 4.45 The UV-vis spectrum of **9**



Diaqua(1,4,8,11-tetraazacyclotetradecane- $\kappa^4 N^1, N^4, N^8, N^{11}$)copper(II) *p*-methoxybenzoate (**10**) was obtained from the reaction of $[\text{Cu}_2(p\text{-CH}_3\text{OC}_6\text{H}_4\text{COO})_4]$ and cyclam (mole ratio 1:2) in ethanol. The yield was 58%.

Its structure consists of a mononuclear cationic $[\text{Cu}(\text{cyclam})(\text{H}_2\text{O})_2]^{2+}$ and two *p*- $\text{CH}_3\text{OC}_6\text{H}_4\text{COO}^-$ anions (**Figure 4.46**). In contrast to the two previously described copper(II)-cyclam-arylcaboxylates, the anions of **10** do not coordinate with Cu(II) cyclam. The axial positions of the metal centre are instead occupied by H_2O molecules. Around the cyclic core environment, the equatorial bond distances are: $\text{Cu-N1} = 2.010(2) \text{ \AA}$ and $\text{Cu-N2} = 2.019 \text{ \AA}$, while the axial bond length is: $\text{Cu-O1W} = 2.535(2) \text{ \AA}$.

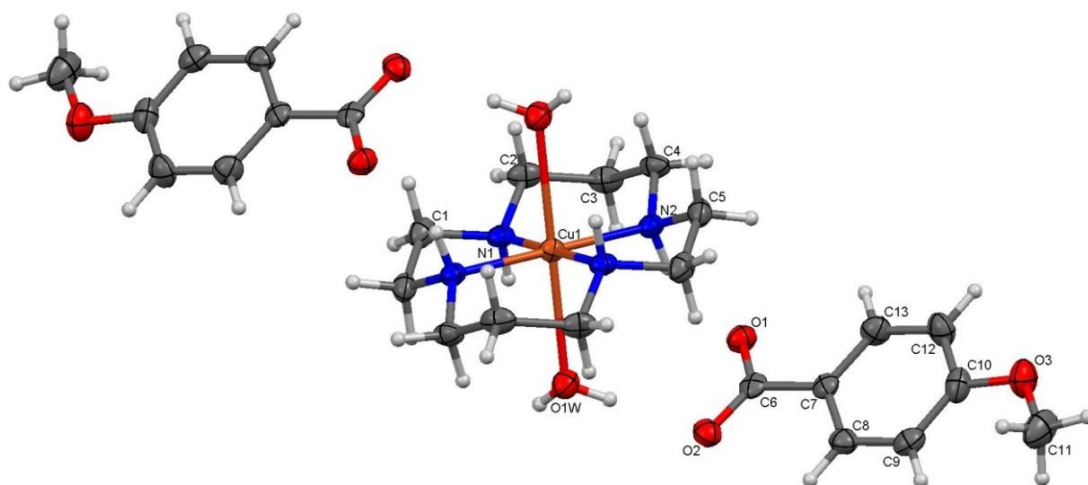


Figure 4.46 Molecular structure of **10**, showing displacement ellipsoids at 70% probability level; operator used to generate symmetry equivalent elements (unlabelled atoms): $1-x$, $1-y$, $2-z$

The *carboxyl*-O1 atom is bifurcated by being hydrogen-bonded to the axial H₂O (O1w–H1wB···O1), and participate in the N2–H2···O1 interaction formed by the N atom of the adjacent [Cu(cyclam)(H₂O)₂]²⁺. Similar hydrogen bond interactions are observed for *carboxyl*-O2 (O1w–H1wA···O2 and N1–H1···O2 respectively). These intermolecular forces lead to the formation of successive chain along the crystallographic *b*-axis (**Figure 4.47**). Unlike **9**, the terminal methoxy substituents of the aryl groups are not involved in any specific hydrogen bonding.

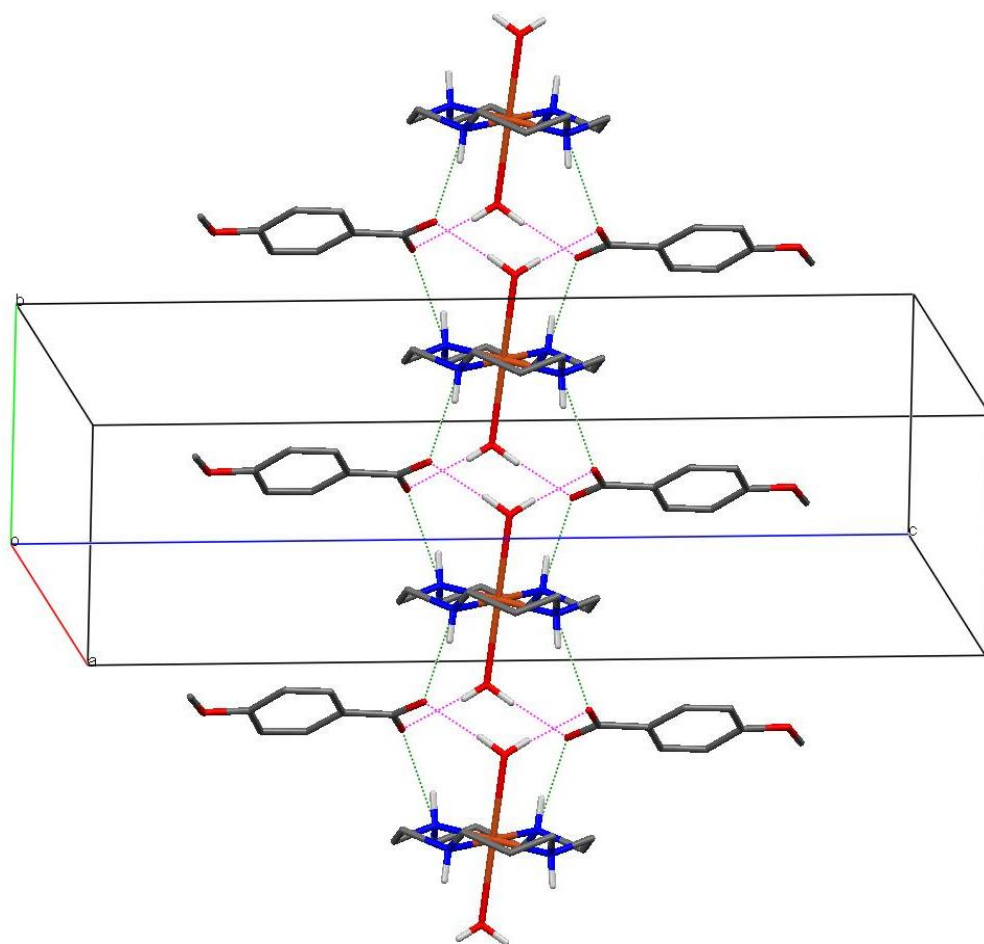


Figure 4.47 Unit cell of **10**, viewed along the *a*-axis; the O–H···O and N–H···O hydrogen bonds (pink and green dashed lines, respectively) have led to the formation of chain along the *b*-axis.

As for the above complexes, the FTIR spectrum of **10** (**Figure 4.48**) shows the presence of the expected functional groups and bonds, and the Δ_{COO} value is 225 cm^{-1} (calculated from the values of $\bar{\nu}_{\text{asym COO}} = 1593 \text{ cm}^{-1}$ and $\bar{\nu}_{\text{sym COO}} = 1368 \text{ cm}^{-1}$).

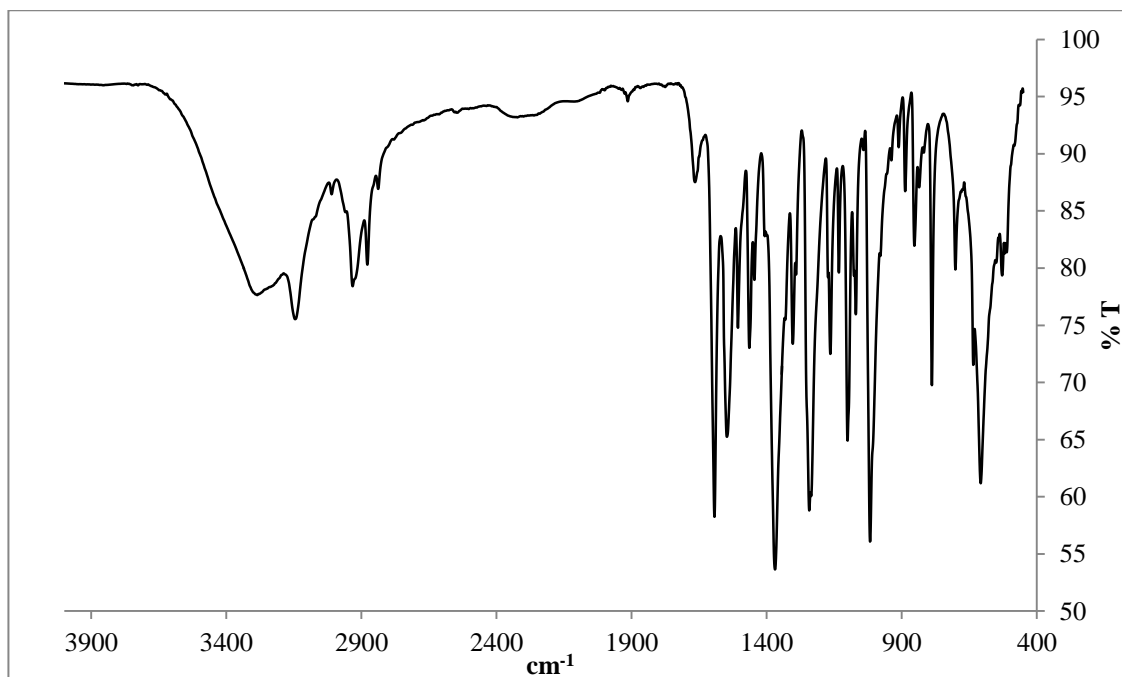


Figure 4.48 The FTIR spectrum of **10**

Its electronic spectrum in ethanol (**Figure 4.49**) and data ($\lambda_{\max} = 536 \text{ nm}$; $\epsilon_{\max} = 119 \text{ M}^{-1} \text{ cm}^{-1}$) are also similar to the above complexes, and may be similarly explained.

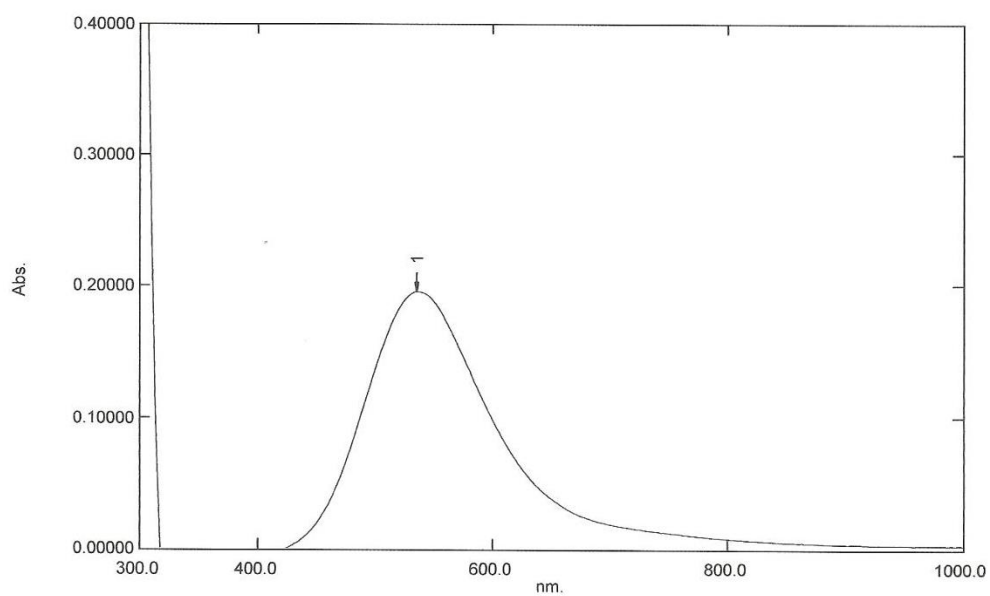
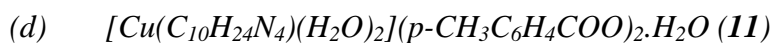


Figure 4.49 The UV-vis spectrum of **10**



Diaqua(1,4,8,11-tetraazacyclotetradecane- $\kappa^4 N^1, N^4, N^8, N^{11}$)copper(II) *p*-methylbenzoate monohydrate (**11**) was obtained from the reaction of $[Cu_2(p-CH_3C_6H_4COO)_4]$ and cyclam (mole ratio 1:2) in ethanol. The yield was 67%.

The X-ray diffraction studies show that **11** exhibits similar coordination behaviour as **10**, but in its structure, one lattice H_2O molecule had mutually crystallized (**Figure 4.50**). The Cu–N bonds at the equatorial position [Cu–N1 = 2.025(3) Å, Cu–N2 = 2.012(2) Å, Cu–N3 = 2.029(3) Å and Cu–N4 = 2.010(2) Å] and the axial Cu–O [Cu–O1w = 2.481(2) Å and Cu–O2w = 2.531(2) Å] bond distances are comparable to that of **10**.

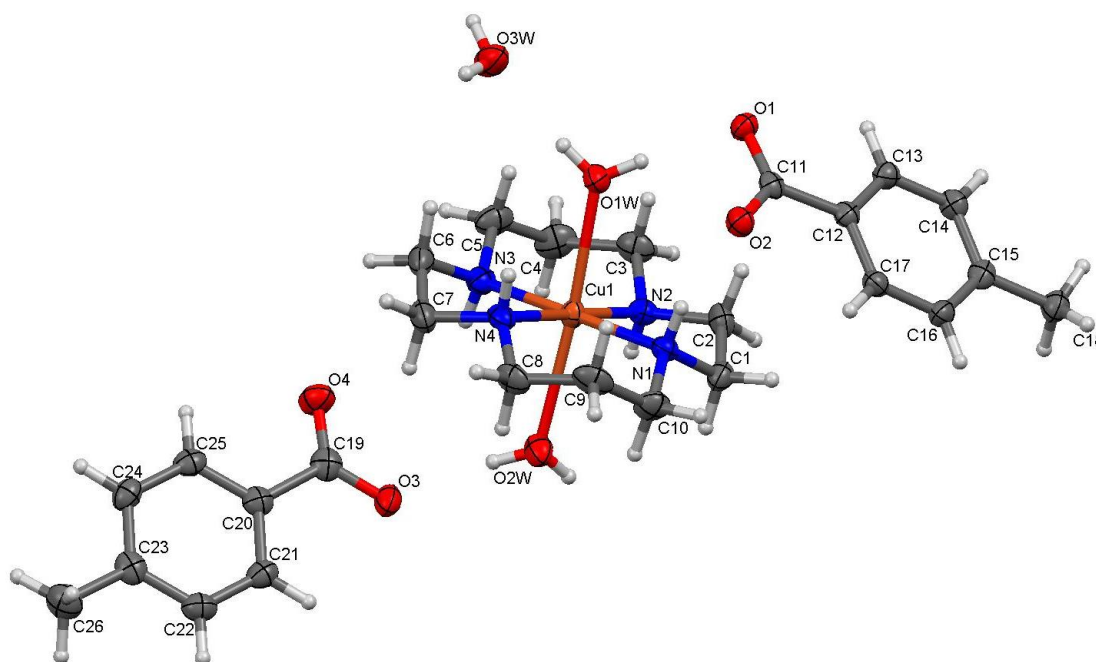


Figure 4.50 Molecular structure of **11**, showing displacement ellipsoids at 70% probability level

The O1, O2 and O3 atoms of $p-CH_3C_6H_4COO^-$ ion act as the acceptors for both O–H \cdots O (O1w–H11 \cdots O1, O2w–H22 \cdots O2 and O2w–H21 \cdots O3 respectively) and N–H \cdots O (N2–H2 \cdots O1, N1–H1 \cdots O2 and N4–H4 \cdots O3 respectively) hydrogen bonds, hence bifurcated. However, the *carboxyl*-O4 atom did not attribute such trends and

instead formed a simple hydrogen bond with the lattice H₂O molecule (O3w–H32···O4). The lattice H₂O subsequently formed another O–H···O hydrogen bond with the coordinated H₂O ligand (O1w–H12···O3w). Similar to **10**, such hydrogen bond networks had given a successive chain along the *b*-axis and the terminal methyl substituents of the aromatic ring did not have any significant interaction (**Figure 4.51**).

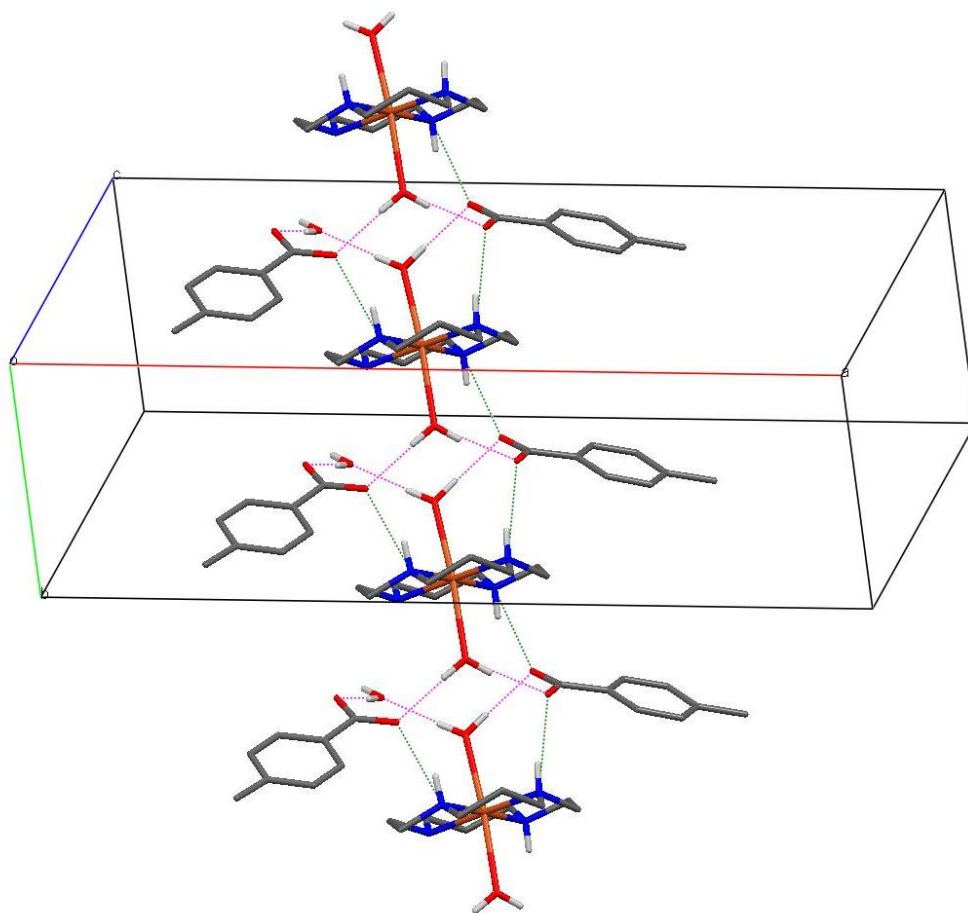


Figure 4.51 Unit cell of **11**, viewed along the *c*-axis; the O–H···O and N–H···O hydrogen bonds (pink and green dashed lines, respectively) have led to the formation chain along the *b*-axis.

Similar to the above complexes, the FTIR spectrum of **11** (**Figure 4.52**) shows the presence of the expected functional groups and bonds, and the Δ_{COO} value is 145 cm^{-1} (calculated from the values of $\bar{\nu}_{\text{asym COO}} = 1549 \text{ cm}^{-1}$ and $\bar{\nu}_{\text{sym COO}} = 1404 \text{ cm}^{-1}$).

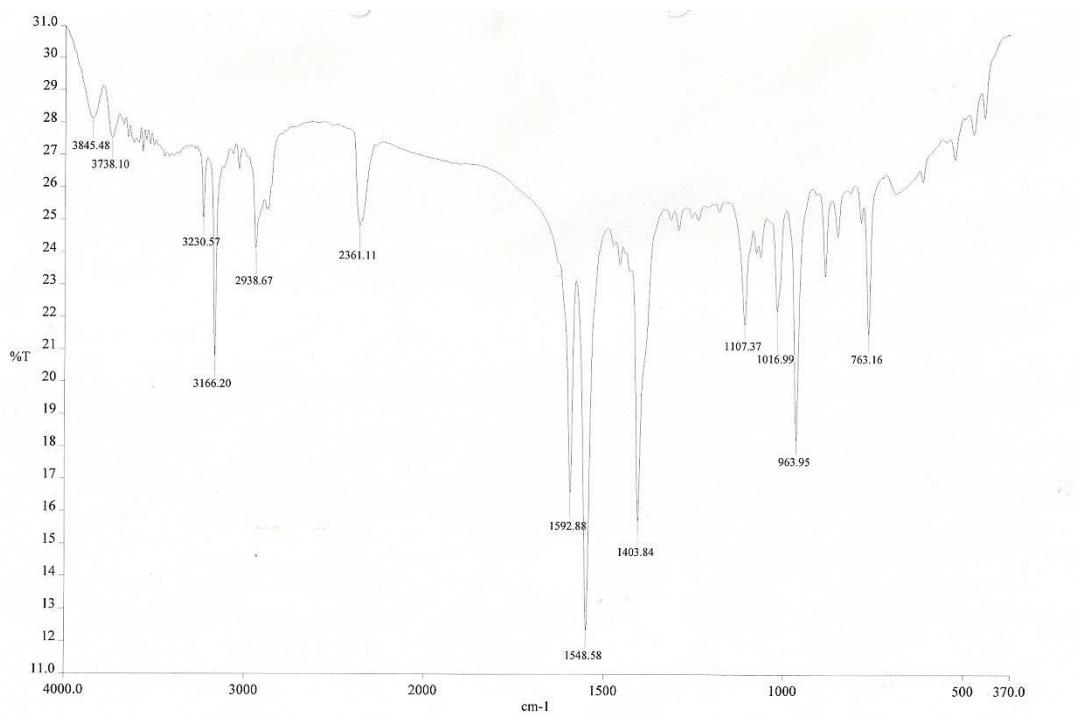


Figure 4.52 The FTIR spectrum of **11**

Its electronic spectrum in ethanol (**Figure 4.53**) and data ($\lambda_{\text{max}} = 531 \text{ nm}$; $\epsilon_{\text{max}} = 105 \text{ M}^{-1} \text{ cm}^{-1}$) are also similar to the above complexes, and may be similarly explained.

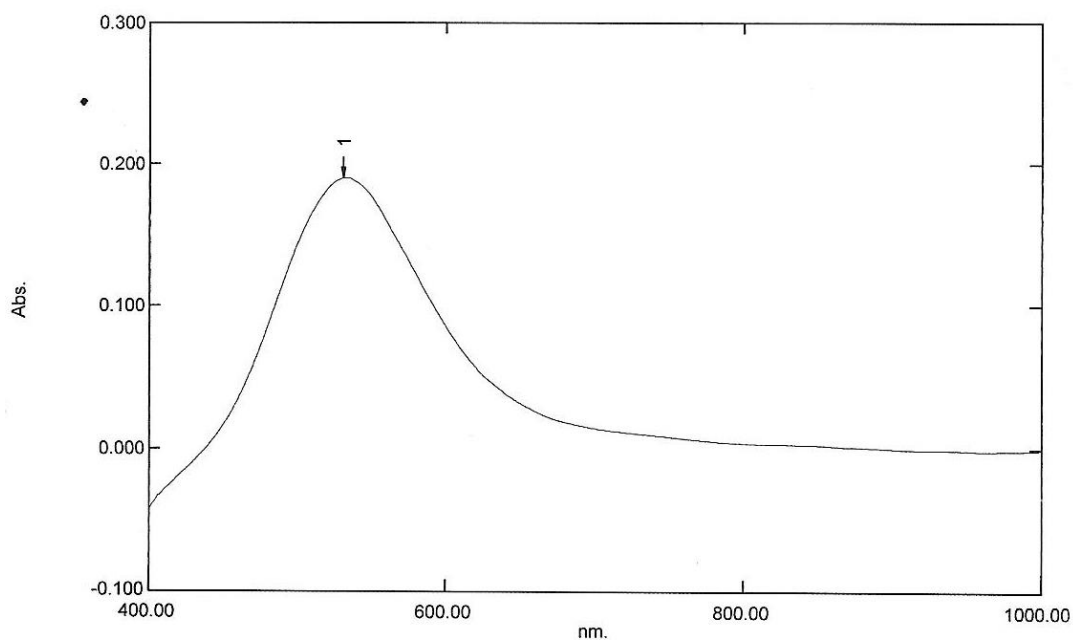
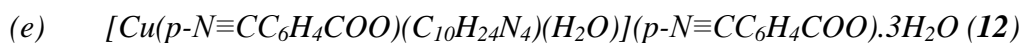


Figure 4.53 The UV-vis spectrum of **11**



Aqua(1,4,8,11-tetraazacyclotetradecane- $\kappa^4 N^1, N^4, N^8, N^{11}$)(*p*-cyanobenzoato) copper(II) *p*-cyanobenzoate trihydrate (**12**) was obtained from the reaction of $[Cu_2(p-N\equiv CC_6H_4COO)_4]$ and cyclam (mole ratio 1:2) in ethanol. The yield was 37%.

The X-ray diffraction studies show that **12** is partially ionic with one *p*- $N\equiv CC_6H_4COO$ ligand being covalently bonded to Cu atom, and other *p*- $N\equiv CC_6H_4COO$ ion remained uncoordinated. The equivalent axial position of Cu atom is occupied by the H_2O ligand. Three independent H_2O molecules were also found in the crystal lattice (**Figure 4.54**). The inter-atomic distances of the equatorial plane are $[Cu-N1 = 2.007(3) \text{ \AA}, Cu-N2 = 2.032(3) \text{ \AA}, Cu-N3 = 2.033(3) \text{ \AA}$ and $Cu-N4 = 2.021(3) \text{ \AA}]$ while the axial bond lengths are elongated as the above complexes $[Cu-O1w = 2.408(3) \text{ \AA}$ and $Cu-O1 = 2.475(3) \text{ \AA}]$.

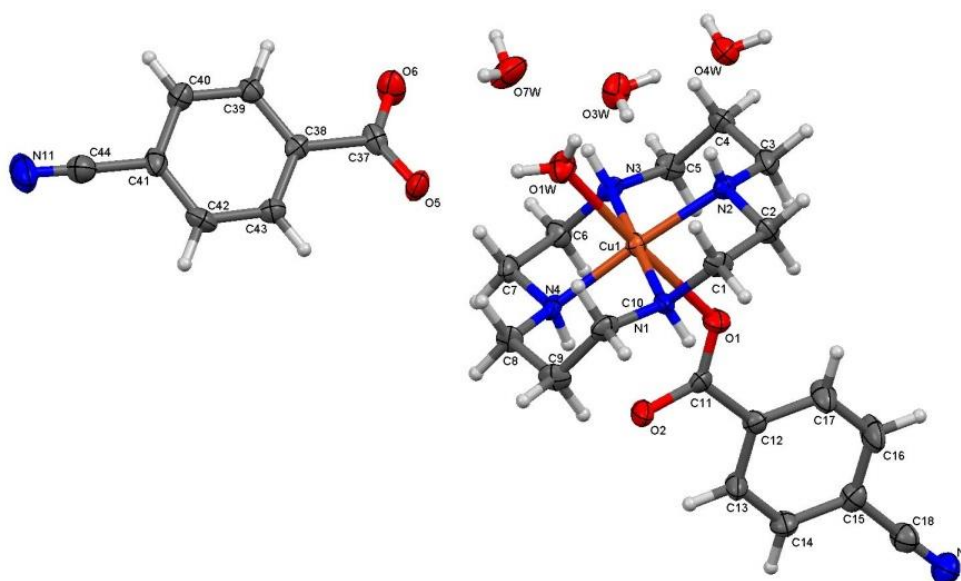


Figure 4.54 The molecular structure of **12**, showing displacement ellipsoids at 70% probability level

Similar to the above complexes, the FTIR spectrum of **12** (**Figure 4.55**) shows the presence of the expected functional groups and bonds, and the Δ_{COO} value is 206 cm^{-1} (calculated from the values of $\bar{\nu}_{\text{asym COO}} = 1594\text{ cm}^{-1}$ and $\bar{\nu}_{\text{sym COO}} = 1387\text{ cm}^{-1}$).

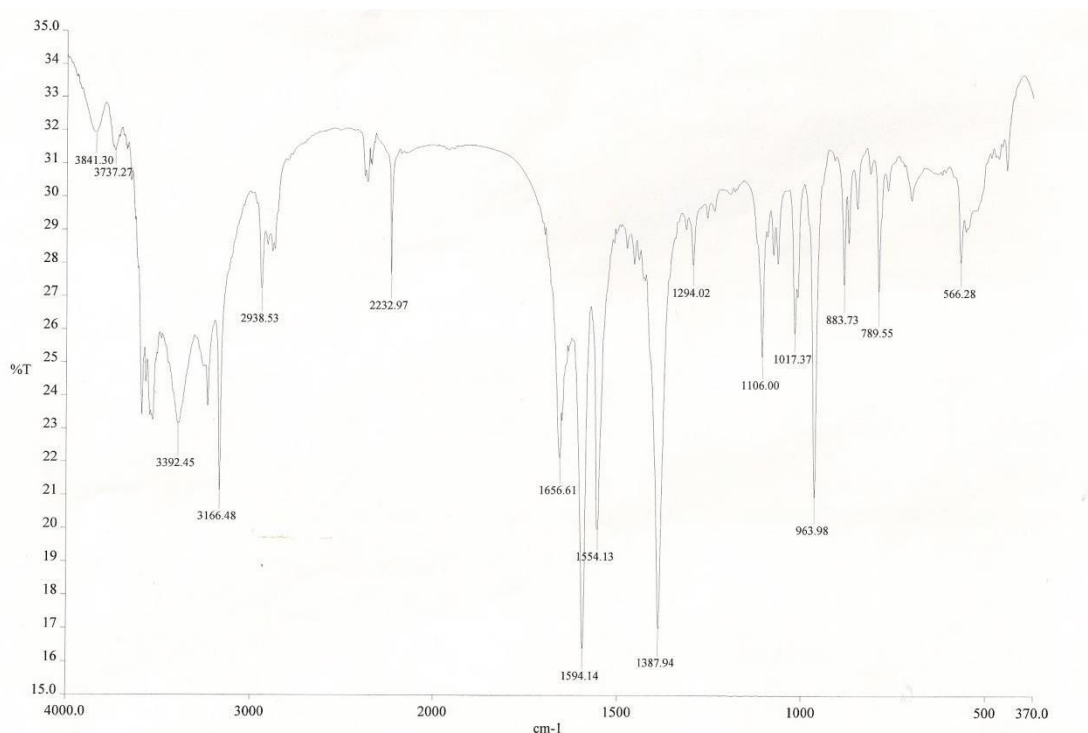


Figure 4.55 The FTIR spectrum of **12**

Its electronic spectrum in ethanol (**Figure 4.56**) shows a *d-d* band at $\lambda_{\text{max}} = 524\text{ nm}$ ($\epsilon_{\text{max}} = 137\text{ M}^{-1}\text{ cm}^{-1}$), suggesting a square planar geometry at Cu(II). The spectrum also shows two overlapping peak centered at 368 nm ($\epsilon_{\text{max}} = 125\text{ M}^{-1}\text{ cm}^{-1}$) which may be assigned to the intraligand *n-π** and *π-π** transitions.

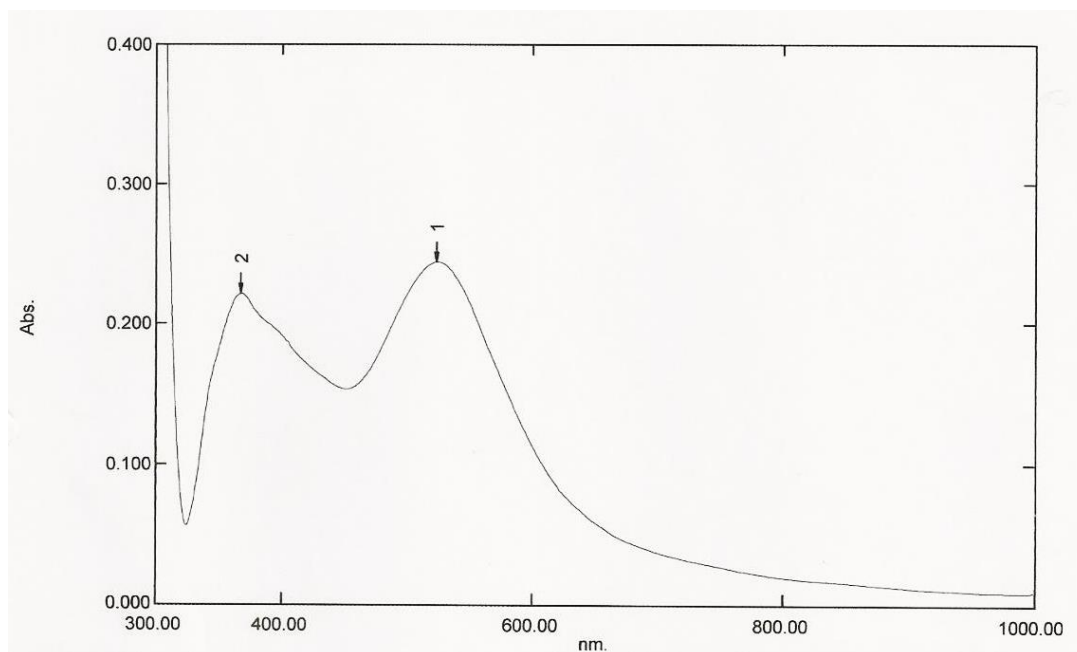
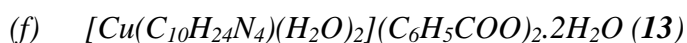


Figure 4.56 The UV-vis spectrum of **12**



Diaqua(1,4,8,11-tetraazacyclotetradecane- $\kappa^4 N^1, N^4, N^8, N^{11}$)copper(II) benzoate dihydrate (**13**) was obtained from the reaction of $[Cu_2(C_6H_5COO)_4]$ and cyclam (mole ratio 1:2) in ethanol. The yield was 53%.

The single crystal XRD showed that the coordination mode of **13** is similar to that of **10** and **11**, where the Cu atom is hexa-coordinated and the axial sites are occupied by H_2O rather than carboxylate ligands. However, in its structure, an additional pair of lattice H_2O molecule is present (**Figure 4.57**). The selected bond lengths [Cu–N1 = 2.019(2) Å, Cu–N2 = 2.031(1) Å and Cu–O1w = 2.420(1) Å] are comparable to those reported by Lindoy in 2003 [4].

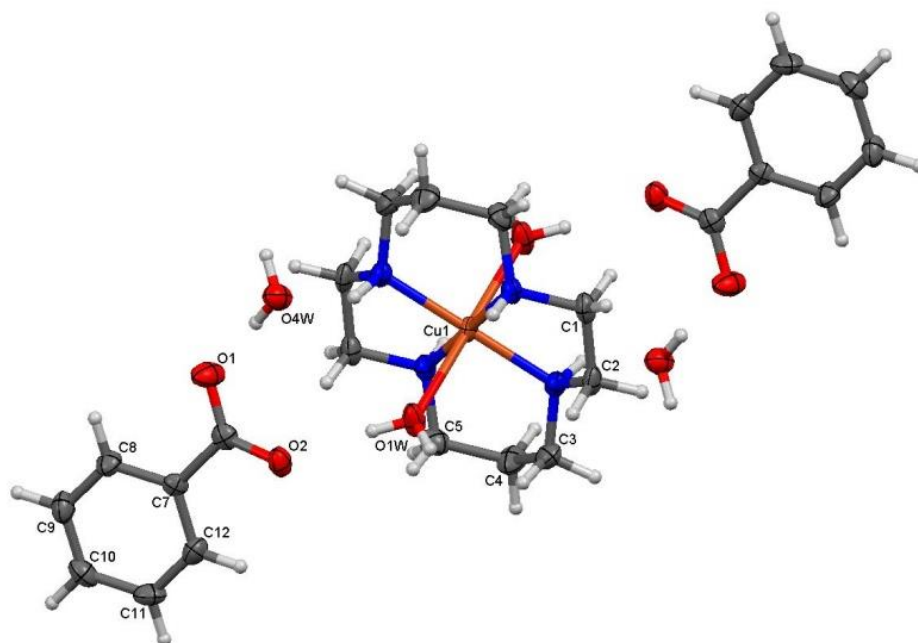


Figure 4.57 Molecular structure of **13**, showing displacement ellipsoids at 70% probability level; operator used to generate symmetry equivalent elements (unlabelled atoms): $-1-x, -1-y, -z$

Similar to the above complexes, the FTIR spectrum of **13** (**Figure 4.58**) shows the presence of the expected functional groups and bonds, and the Δ_{COO} value is 162 cm^{-1} (calculated from the values of $\bar{\nu}_{\text{asym COO}} = 1540 \text{ cm}^{-1}$ and $\bar{\nu}_{\text{sym COO}} = 1378 \text{ cm}^{-1}$).

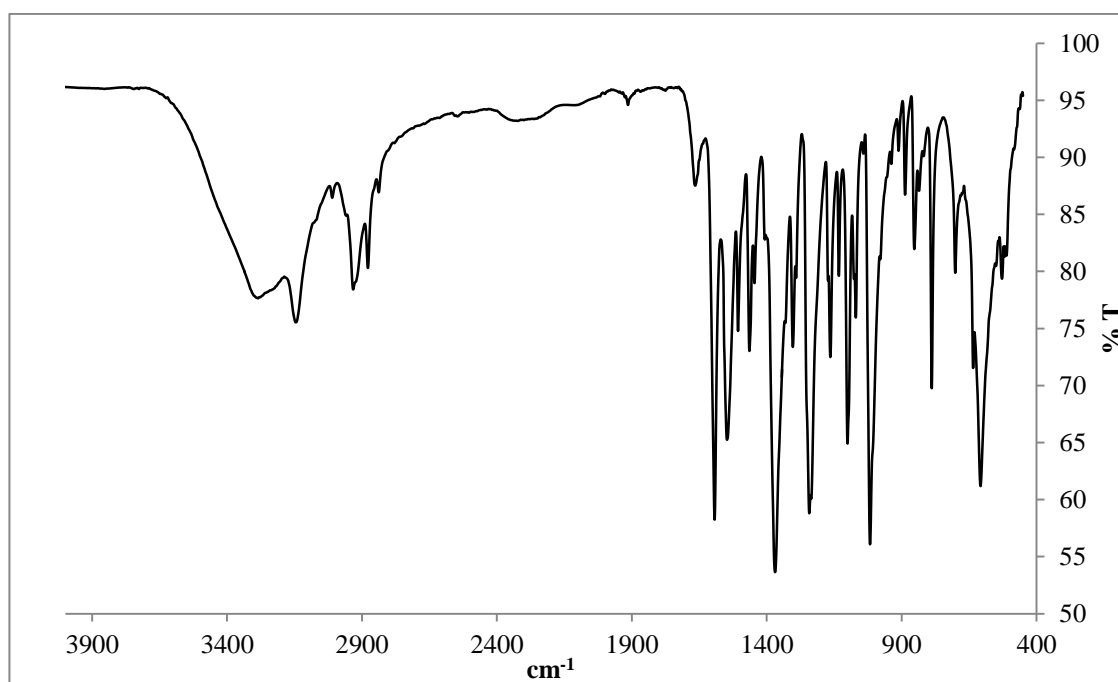


Figure 4.58 The FTIR spectrum of **13**

Its electronic spectrum in aqueous solution (**Figure 4.59**) and data ($\lambda_{\max} = 503 \text{ nm}$; $\epsilon_{\max} = 83 \text{ M}^{-1} \text{ cm}^{-1}$) are also similar to the above complexes, and may be similarly explained.

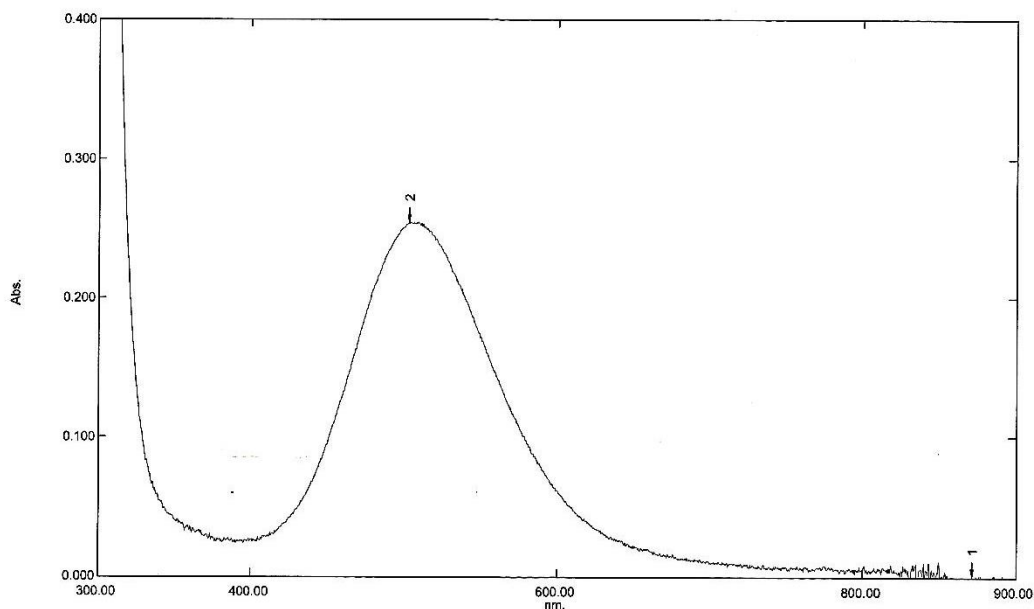


Figure 4.59 The UV-vis spectrum of **13**



Diaqua(1,4,8,11-tetraazacyclotetradecane- $\kappa^4 N^1, N^4, N^8, N^{11}$)copper(II)

pentafluorobenzoate dihydrate (**14**) was obtained from the reaction of $[Cu_2(C_6F_5COO)_4]$ and cyclam (mole ratio 1:2) in ethanol. The yield was 66%.

The single crystal XRD result showed that the structure of **14** is similar to that of **13** (**Figure 4.60**). The inter-atomic distances are also comparable [Cu–N1 = 2.015(2) Å, Cu–N2 = 2.031(2) Å and Cu–O1w = 2.485(1) Å].

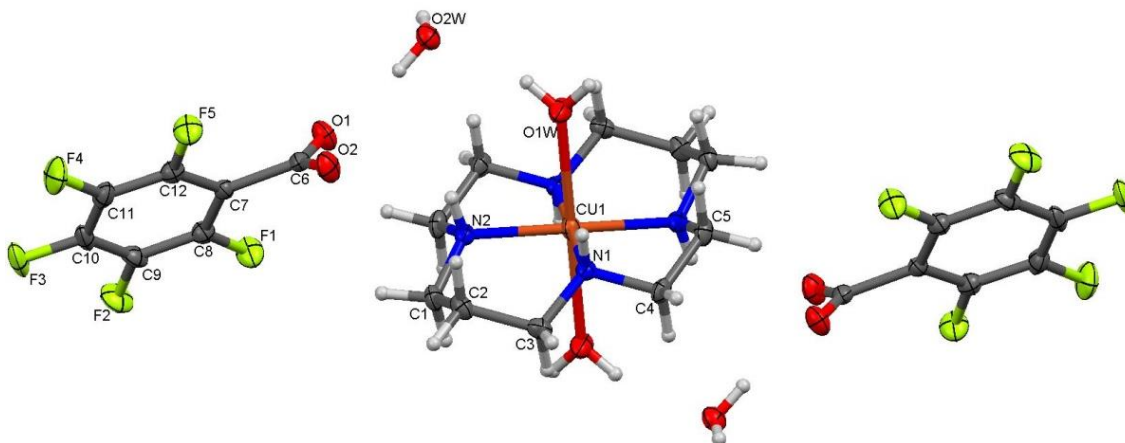


Figure 4.60 Molecular structure of **14**, showing displacement ellipsoids at 70% probability level; operator used to generate symmetry equivalent elements (unlabelled atoms): $1-x, 1-y, 1-z$

Its extensive intermolecular network is dominated by the lattice H_2O , which formed trifurcated hydrogen bonding of $\text{O2W-H}\cdots\text{O1}$, $\text{O1W-H}\cdots\text{O1}$ and $\text{N1-H}\cdots\text{O2W}$. It acts both as the donor as well as the acceptor within the respective bonds. The resulting chain is parallel to the a -axis. The coordinated H_2O ligand is bifurcated with $\text{O-H}\cdots\text{O}$ hydrogen bond ($\text{O1w-H11}\cdots\text{O2}$ and $\text{O1w-H12}\cdots\text{O2w}$); while each *carboxyl*-O atom form only single $\text{O-H}\cdots\text{O}$ hydrogen bond ($\text{O2w-H21}\cdots\text{O1}$ and $\text{O1w-H11}\cdots\text{O2}$). As anticipated from its ionic structure, no intramolecular forces were observed (**Figure 4.61**).

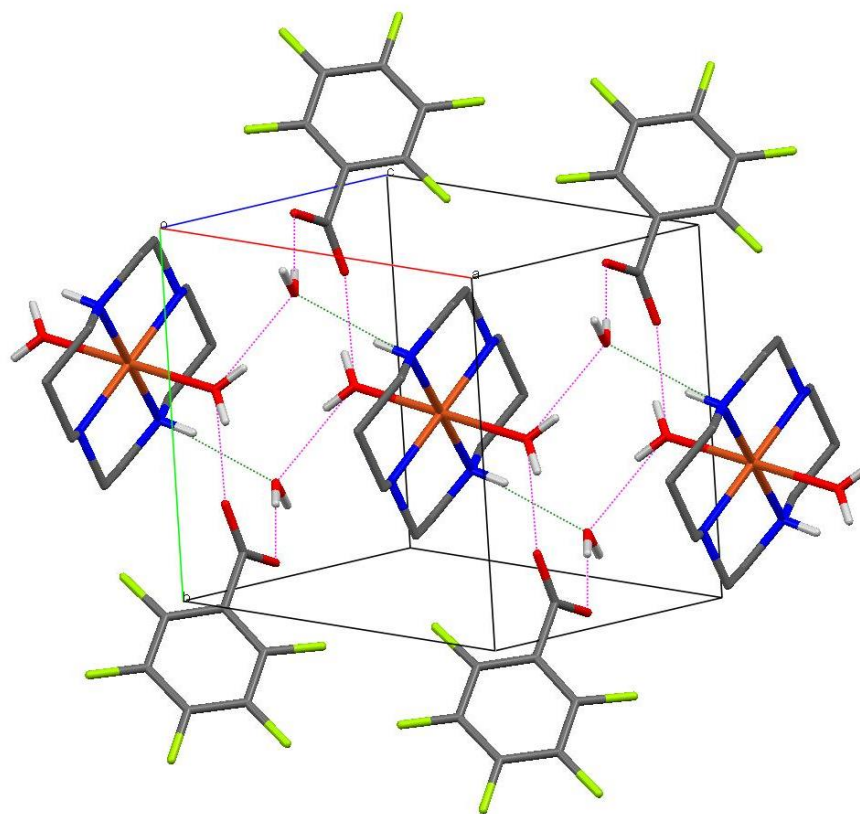


Figure 4.61 Unit cell of **14**, viewed along the *c*-axis; the O–H···O and N–H···O hydrogen bonds (pink and green dashed lines, respectively) have led to the formation chain along the *a*-axis.

Similar to the above complexes, the FTIR spectrum of **14** (**Figure 4.62**) shows the presence of the expected functional groups and bonds, and the Δ_{COO} value is 163 cm^{-1} (calculated from the values of $\bar{\nu}_{\text{asym COO}} = 1520 \text{ cm}^{-1}$ and $\bar{\nu}_{\text{sym COO}} = 1357 \text{ cm}^{-1}$).

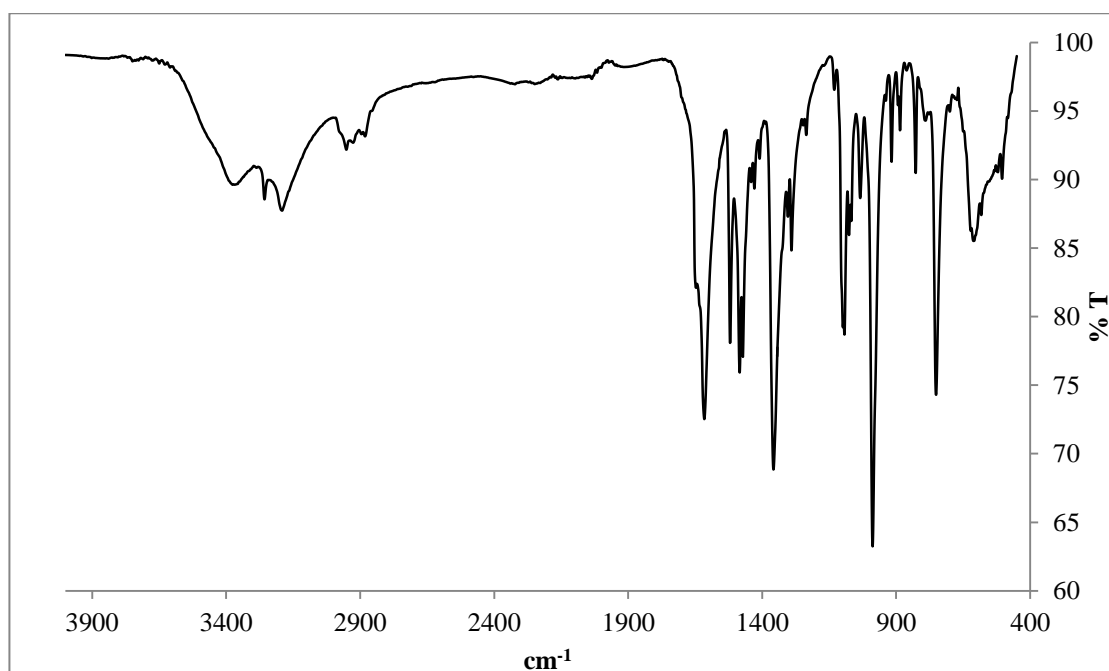


Figure 4.62 The FTIR spectrum of **14**

Its electronic spectrum in ethanol (**Figure 4.63**) and data ($\lambda_{\max} = 522 \text{ nm}$; $\epsilon_{\max} = 105 \text{ M}^{-1} \text{ cm}^{-1}$) are also similar to the above complexes, and may be similarly explained.

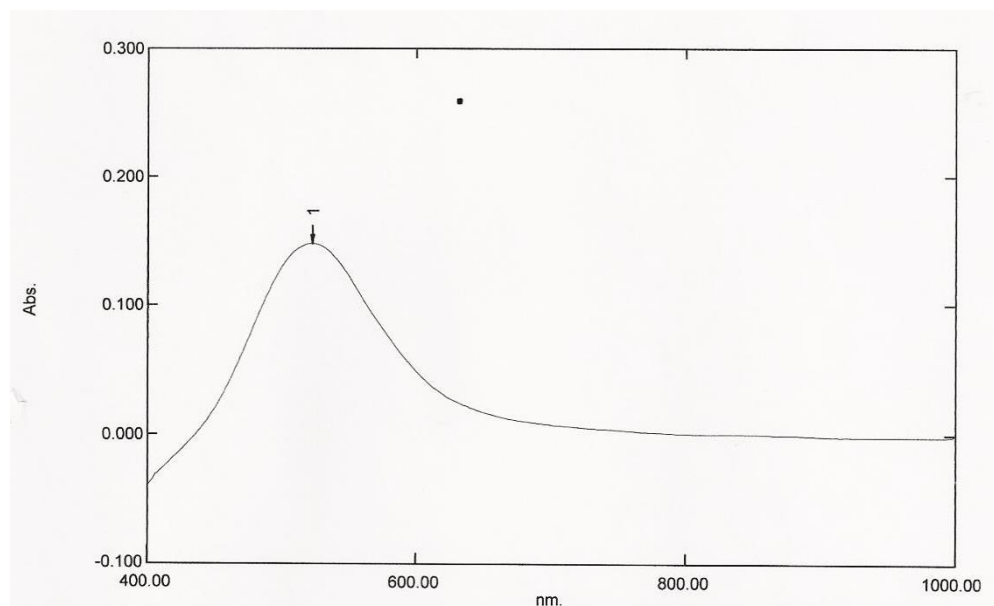


Figure 4.63 The UV-vis spectrum of **14**

The selected crystal parameters and refinement details of the above complexes were given in **Table 4.9**.

Table 4.9 Selected crystal parameters and refinement details of aromatic crystalline complexes

	8	9	10	11	12	13	14
Empirical formula	C ₂₄ H ₄₀ CuN ₆ O ₆	C ₂₄ H ₃₄ CuN ₄ O ₆	C ₂₆ H ₄₂ CuN ₄ O ₈	C ₂₆ H ₄₄ CuN ₄ O ₇	C ₂₆ H ₄₀ CuN ₆ O ₈	C ₂₄ H ₄₂ CuN ₄ O ₈	C ₂₄ H ₃₂ CuF ₁₀ N ₄ O ₈
Formula weight	572.16	538.1	602.19	588.19	628.18	578.16	758.08
Wavelength (Å)	0.71073	0.71073	0.71073	0.71073	0.71073	0.71073	0.71073
Temperature (K)	150(2)	100(2)	100(2)	100(2)	100(2)	100(2)	100(2)
Crystal system	Monoclinic	Monoclinic	Orthorhombic	Monoclinic	Monoclinic	Triclinic	Triclinic
Space group	<i>P2₁/n</i>	<i>P2₁/c</i>	<i>Pbca</i>	<i>C2/c</i>	<i>P2₁</i>	<i>P-1</i>	<i>P-1</i>
Volume (Å ³)	1324.34(10)	1194.70(3)	2836.80(17)	5594.4(8)	3034.3(3)	1372.15(13)	723.85(10)
<i>a</i> (Å)	10.4489(5)	8.2488(1)	15.5810(6)	31.925(3)	8.9981(5)	7.0632(4)	7.1976(6)
<i>b</i> (Å)	7.7841(3)	13.2976(2)	7.534(2)	7.1779(6)	34.903(2)	14.0491(8)	8.7632(7)
<i>c</i> (Å)	16.9644(8)	11.1659(2)	25.8128(9)	28.750(3)	9.8852(6)	14.1742(8)	12.1574(10)
α (°)	90.00	90.00	90.00	90.00	90.00	79.6320(10)	79.3780(10)
β (°)	106.301(4)	102.725(1)	90.00	121.8800(10)	102.2130(10)	89.8520(10)	75.4080(10)
γ (°)	90.00	90.00	90.00	90.00	90.00	82.7300(10)	80.6060(10)
<i>Z</i>	2	2	4	8	4	1	1
ρ_{calc} (g cm ⁻³)	1.435	1.496	1.410	1.397	1.375	1.399	1.739
<i>F</i> (000)	606	566	1276	2504	1324	614	387
Measured data	7782	12947	15747	26024	29427	14303	6996
Unique data	3062	2751	2501	6434	13905	4834	3306
Goodness of fit	0.938	1.07	1.02	1.008	0.946	1.028	1.057
Observed data [<i>I</i> ≥ 2.0σ(<i>I</i>)]	2225	2481	1842	4523	12456	4058	3028
Final R indices [<i>I</i> ≥ 2.0σ(<i>I</i>)]	R ₁ = 0.0467 wR ₂ = 0.1053	R ₁ = 0.024 wR ₂ = 0.065	R ₁ = 0.0354 wR ₂ = 0.0786	R ₁ = 0.0418 wR ₂ = 0.0928	R ₁ = 0.0446 wR ₂ = 0.1259	R ₁ = 0.0283 wR ₂ = 0.0661	R ₁ = 0.0373 wR ₂ = 0.1081
R indices (all data)	R ₁ = 0.0718 wR ₂ = 0.1177	R ₁ = 0.028 wR ₂ = 0.067	R ₁ = 0.0573 wR ₂ = 0.0890	R ₁ = 0.0729 wR ₂ = 0.1085	R ₁ = 0.0518 wR ₂ = 0.1325	R ₁ = 0.0376 wR ₂ = 0.0726	R ₁ = 0.0413 wR ₂ = 0.1113

4.3.2. Physical properties

The arylcarboxylate ($p\text{-XC}_6\text{H}_4\text{COO}^-$) ions showed different coordination mode in its interaction with Cu(II) centre in all complexes studied. In complexes **8** and **9** ($X = \text{NH}_2$ and OH respectively) the carboxylate ions were coordinated to the Cu(II) centre. On the other hand, complexes **10**, **11** and **13** ($X = \text{OCH}_3$, CH_3 and H respectively) exist as free ion and the apices of the Cu atom were occupied by H_2O ligand. Similar coordination mode was observed for $\text{C}_6\text{F}_5\text{COO}^-$ ion of complex **14**.

Interestingly, the $p\text{-N}\equiv\text{CC}_6\text{H}_4\text{COO}^-$ ion of complex **12** showed both coordination modes: free and coordinated. Owing to the similarities in crystallization conditions, the differences in the coordination mode may arise from the differences in the pK_a values of the starting carboxylic acid, particularly of complex **9** ($p\text{-HOC}_6\text{H}_4\text{COOH}$, $\text{pK}_a = 3.57$), **10** ($p\text{-CH}_3\text{OC}_6\text{H}_4\text{COOH}$, $\text{pK}_a = 3.47$), , and **12** ($p\text{-N}\equiv\text{CC}_6\text{H}_4\text{COOH}$, $\text{pK}_a = 3.55$) [11].

Hence, the basicity of the conjugate base increases in the following order: $p\text{-CH}_3\text{OC}_6\text{H}_4\text{COO}^- < p\text{-N}\equiv\text{CC}_6\text{H}_4\text{COO}^- < p\text{-HOC}_6\text{H}_4\text{COO}^-$. This trend nicely explains the different coordination modes of these ligands. Thus, the magnetic and thermal properties of these complexes were further studied.

(a) Magnetic studies

The experimental data and μ_{eff} values of **9**, **10** and **12** are shown in **Table 4.10**.

Table 4.10 The magnetic data for **9**, **10** and **12**

	9	10	12
$\chi_g (10^{-6} \text{ cm}^3 \text{ g}^{-1})$	1.81	1.40	1.23
$\chi_M (10^{-6} \text{ cm}^3 \text{ mol}^{-1})$	974.0	843.1	772.7
$\chi_D (10^{-6} \text{ cm}^3 \text{ mol}^{-1})$	-260.36	-331.00	-339.44
$\chi_M^{\text{corr}} (10^{-6} \text{ cm}^3 \text{ mol}^{-1})$	1234.36	1174.10	1112.1
$\chi_M^{\text{corr}} T (\text{cm}^3 \text{ K mol}^{-1})$	0.3678	0.3499	0.3314
$\mu_{\text{eff}} (\text{BM})$	1.72	1.67	1.63

It is found that the experimental values for **9**, **10** and **12** are in good agreement to the spin-only value for a mononuclear Cu(II) complex (1.73 BM), indicating no magnetic communications between the Cu(II) centres. Hence, the differences in the coordination modes of these arylcarboxylates do not affect the magnetic properties of the complexes formed.

(b) Thermal properties

The thermal properties of the complexes were studied by thermogravimetric analysis (TGA).

The TGA trace of **9** (**Figure 4.64**) shows that the complex undergoes a rapid thermal degradation beginning at 196 °C with a total mass loss of 86.0%. This corresponds to the decomposition of cyclam and two *p*-HOC₆H₄COO⁻ ligand (found 88.2%). There is a small amount of residue remaining at temperature above 538.7 °C (14.2%). This agrees well with the calculated value of 14.8%, assuming that it is made up of pure CuO.

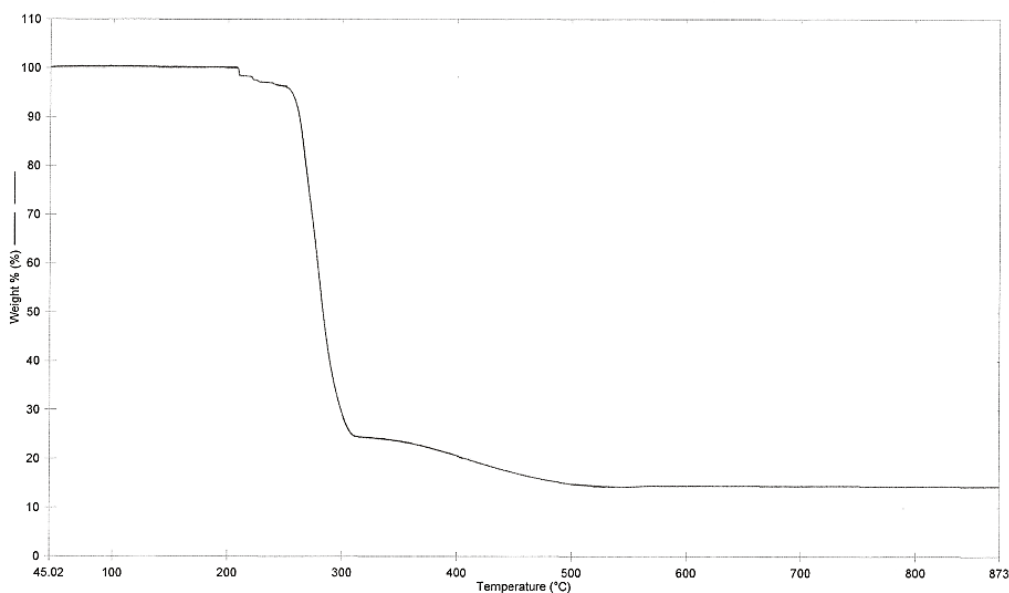


Figure 4.64 TGA trace of **9**

The TGA trace of **10** (**Figure 4.65**) shows an initial weight loss at 106.4 °C, assigned to the evaporation of the two coordinated H₂O ligand (found, 5.9%; expected, 6.0%). Similarly, the following major weight loss began at 234.5 °C corresponds to the decomposition of cyclam and two *p*-CH₃OC₆H₄COO⁻ ion (found 80.7%, expected 83.5%). The amount of CuO residue at temperature above 606.9 °C was 10.8% (expected 13.2%).

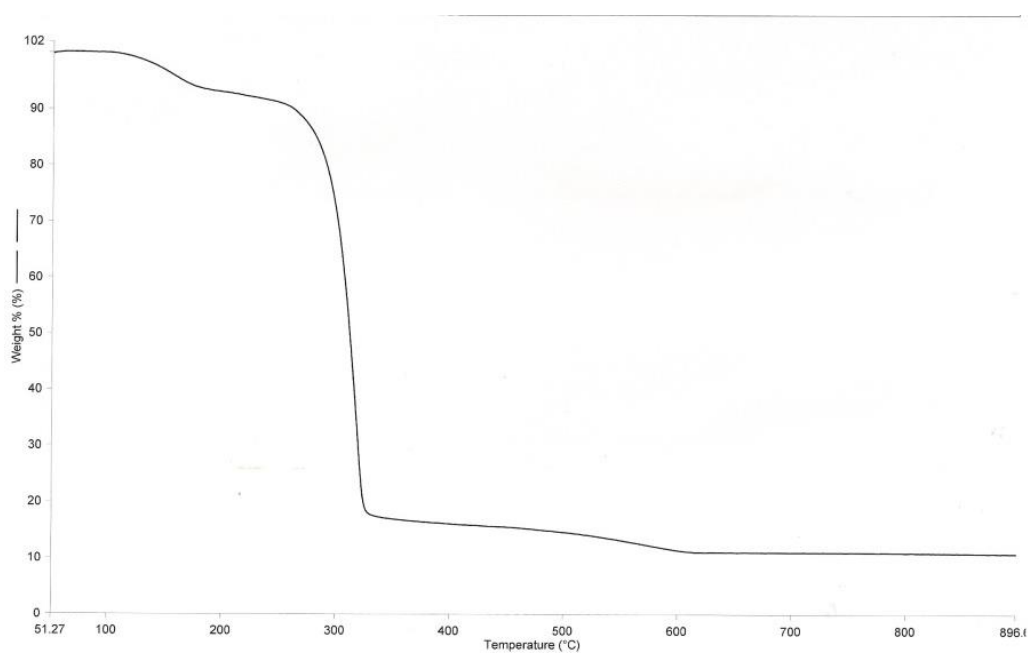


Figure 4.65 TGA trace of **10**

For complex **12**, its TGA trace (**Figure 4.66**) shows an initial first weight loss occurring at about 50 °C, corresponding to the evaporation of three uncoordinated H₂O molecules, followed by one H₂O ligand at 90.6 °C (total, 8.1%; expected, 11.5%). Similar to complexes **9** and **10**, the subsequent weight loss corresponds to the decomposition of cyclam and two *p*-N≡CC₆H₄COO⁻ moieties at 270.9 °C (found 74.7%; expected 78.4%). The amount of CuO residue at temperatures above 650 °C was 14.0% (expected 12.7%).

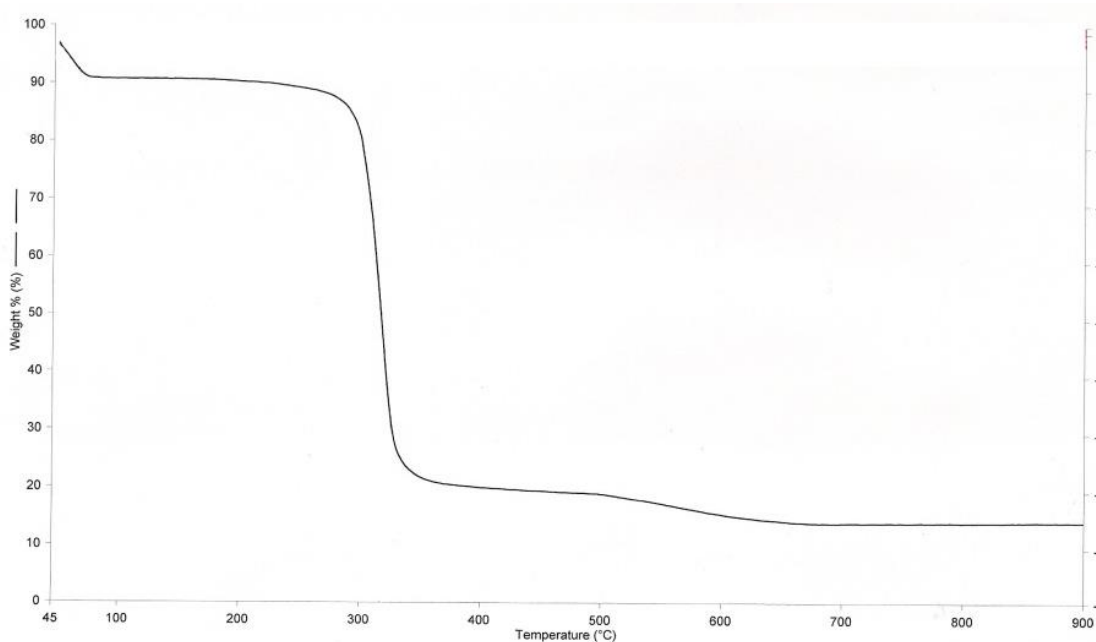


Figure 4.66 TGA trace of **12**

4.3.3. Concluding remarks

Cyclam reacted with copper(II) arylcarboxylates [Cu₂(*p*-XC₆H₄COO)₄] (X = NH₂, OH, OCH₃, CH₃, C≡N, H) and [Cu₂(C₆F₅COO)₄] to form either covalent or ionic mononuclear complexes in reasonably good yields (24 – 67%).

Complexes **8** and **9** (X = NH₂ and OH respectively) were covalent, while complexes **10**, **11**, **13** (X = OCH₃, CH₃ and H respectively) and **14** (C₆F₅) were ionic. Complex **12** with *p*-N≡CC₆H₄COO ligand was exceptionally showing both covalent and

ionic coordination modes. Thus, complexes **9**, **10** and **12** were selected for comparative magnetic and thermal studies.

The experimental μ_{eff} values obtained for **9**, **10** and **12** were 1.72, 1.67 and 1.63 BM respectively, and comparable to the spin-only value for a mononuclear Cu(II) complex (1.73 BM). This indicates no magnetic communication between the Cu(II) centres of the complexes. From that account, it is deduced that the magnetic properties of these arylcarboxylates were not influenced by the coordination mode that the complexes had formed.

The thermal stabilities were also similar to each other. Complexes **9**, **10** and **12** decomposed at 196.0 °C, 234.5 °C and 270.9 °C respectively. The residual amounts of CuO were about the same (~10 – 14%).

4.4. Molecular modelling

It is noted from the crystal structures of all complexes studied that only two complexes, $[\text{Cu}(p\text{-H}_2\text{NC}_6\text{H}_4\text{COO})_2(\text{C}_{10}\text{H}_{24}\text{N}_4)] \cdot 2\text{H}_2\text{O}$ (**8**) and $[\text{Cu}(p\text{-HOC}_6\text{H}_4\text{COO})_2(\text{C}_{10}\text{H}_{24}\text{N}_4)]$ (**9**), had their carboxylate groups covalently bonded to the Cu(II) centre. All of the other complexes, except **12**, were ionic. Complex **12** was partially ionic.

To gain further insight into this selective binding mode recognition, a molecular modelling of these complexes and selected ionic homologues, namely $[\text{Cu}(\text{C}_{10}\text{H}_{24}\text{N}_4)(\text{H}_2\text{O})_2](\text{CH}_3(\text{CH}_2)_5\text{COO})_2 \cdot 2\text{H}_2\text{O}$ (**1**) and $[\text{Cu}(\text{C}_{10}\text{H}_{24}\text{N}_4)(\text{H}_2\text{O})_2](p\text{-CH}_3\text{OC}_6\text{H}_4\text{COO})_2$ (**10**), was applied. Its main objective is to investigate the intrinsic electronic properties of the complexes that lead to the differing molecular interaction of the carboxylate group.

Computational analysis was conducted through a series of self-consistent field (SCF) theory, known as Hartree-Fock (HF) method. To determine the lowest energy conformation, geometry optimization was performed on the complexes (asymmetrical

unit) and their moieties were also calculated individually, with 6–311G(d,p) basis set used on all atoms. The convergence criterion for the SCF cycles was at its default value, 10^{-6} .

Subsequently, the wave functions for these equilibrium geometries were used to determine Mulliken charges, molecular electrostatic potential map and theoretical FTIR intensities and binding energy. The energy obtained from the calculation was in Hartree atomic unit of energy, a.u, and its expression in SI unit, kJ mol^{-1} was based on the conversion factor given in **Appendix 3**.

4.4.1. Computational results

(a) $[Cu(p\text{-H}_2\text{NC}_6\text{H}_4\text{COO})_2(\text{C}_{10}\text{H}_{24}\text{N}_4)].2\text{H}_2\text{O}$ (**1**)

Figure 4.67 depicts the optimized structure of the asymmetrical unit of **1**. The minimized energy value of the structure is -2518.70 a.u (-6.613×10^6 kJ mol^{-1}). The atoms were displayed using van der Waals radii with 65% scaling factor.

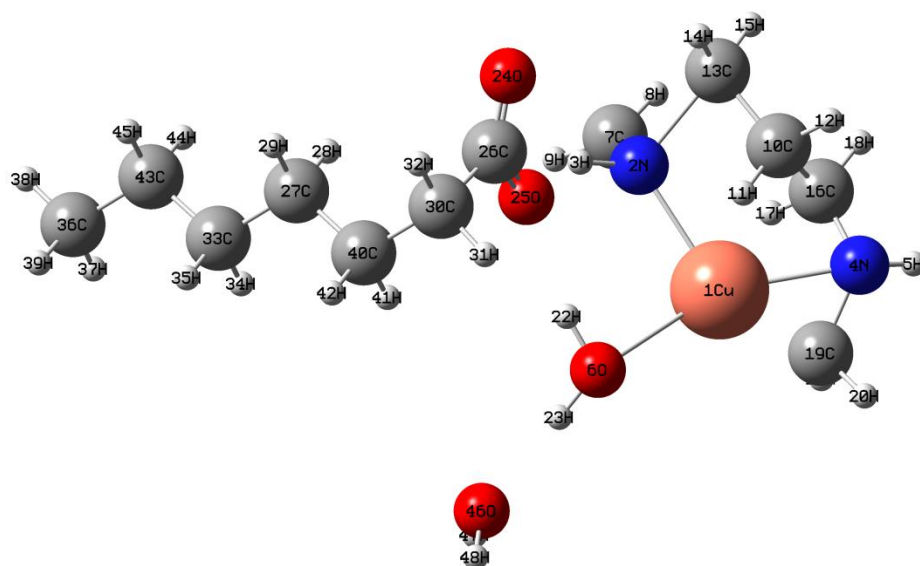


Figure 4.67 The optimized structure of **1**

Some selected geometrical parameter, specifically the predicted bond lengths, of **1** is presented in **Table 4.11**, and the values were compared with the experimental X-ray diffraction data in accordance with the atomic numbering scheme given in **Figure 4.67**.

Table 4.11 Comparison of selected theoretical and experimental bond lengths of **1**

Bond type	Bond length (Å)	
	Theoretical	Experimental
Cu ₁ -N ₂	2.153	2.018
Cu ₁ -N ₄	2.213	2.027
Cu ₁ -O ₆	2.473	2.507
N ₂ -C ₇	1.497	1.488
N ₂ -H ₃	1.064	0.911
N ₂ -C ₁₃	1.896	1.483
C ₁₃ -C ₁₀	1.528	1.515
C ₁₀ -C ₁₆	1.53	1.519
C ₁₆ -N ₄	1.362	1.474
N ₄ -C ₁₉	1.477	1.478
N ₄ -H ₅	0.998	0.909
C ₂₆ -O ₂₄	1.182	1.258
C ₂₆ -O ₂₅	1.329	1.246

The calculated FTIR intensities were also compared with the corresponding experimental intensities (**Figure 4.68**). As the HF method tends to overestimate the electron correlation and fundamental modes within a structure, scaling factor has to be used to obtain a considerably better agreement with the experimental data. Typically calculations using HF method was scaled by a factor of 0.89 [12].

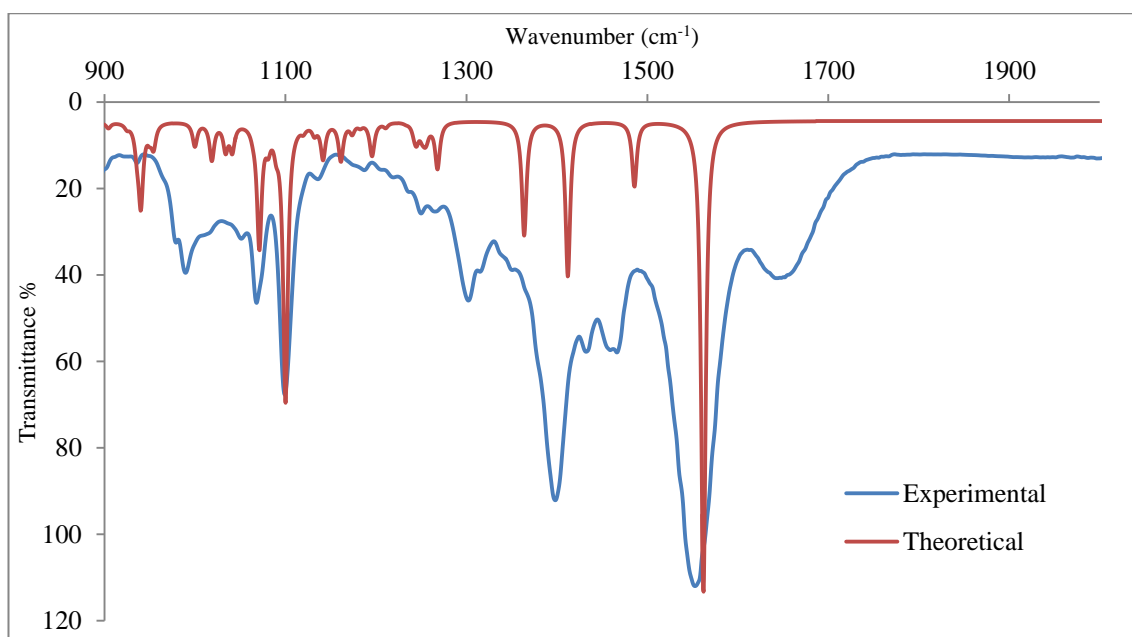


Figure 4.68 Comparison of theoretical and experimental FTIR spectra of **1**

Subsequently, the partial charge distribution or the electronegativity of each atom could be determined. It is a relative measurement of the amount of electron sharing that resulted from the electron transfer between atoms that were involved in the bonding interaction. For a given atom that has higher electronegativity, it will have a greater share of the electrons, and therefore will have a slight negative charge compared to the other atom, which will then have a slight positive charge. The charge distribution values of selected atoms of **1** were presented in **Table 4.12**. The initial elementary charge unit of energy, e , was then converted to kJ mol^{-1} (**Appendix 3**).

Table 4.12 The partial charge energy for selected atoms of **1**

Atom	Energy (kJ mol^{-1})
Cu ₁	+60.788
N ₂	-42.068
N ₄	-42.648
O ₆	-65.419
O ₄₆	-50.656
O ₂₄	-43.323
O ₂₅	-49.209
C ₂₆	+49.498

Positive energy value corresponds to a positively charged atom, and similarly, negative energy value represents a negatively charged atom. It is noted that the O_{water} atom (O_6) was bearing much lower energy compared to the O_{carboxyl} atom of the $\text{CH}_3(\text{CH}_2)_5\text{COO}^-$ ion (O_{24} and O_{25}). This may explain its favourable coordination towards Cu(II) ion rather than the carboxylate group.

Accordingly, the data could be mapped onto the surface of a constant total electron density surrounding the molecule, which will give a visualised molecular electrostatic potential surface. In the surface map, the reddish region was where the lowest electrostatic energy values were found (electron-rich) and bluish regions had the highest electrostatic energy values (electron-poor) [13]. Any colour that appeared in between the two boundaries was relatively considered as an intermediate, or neutral, as depicted in **Figure 4.69**.

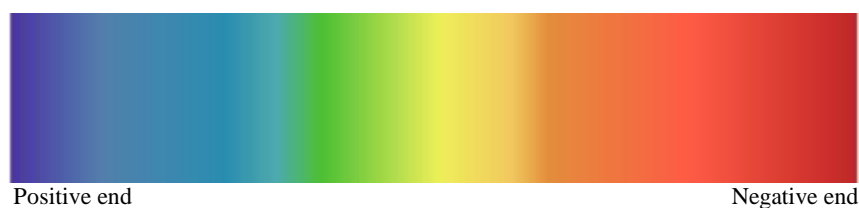


Figure 4.69 Colour scheme showing relative electrostatic charge distribution

Complex **1** had showed a uniform energy dispersion throughout its whole structure, particularly within the core region comprising Cu(II) ion and *trans*- N_4O_2 donor set (**Figure 4.70**). The hydrophobic region of the $\text{CH}_3(\text{CH}_2)_5\text{COO}^-$ ion remained neutral, and the carboxylate group showed only weak electronegativity.

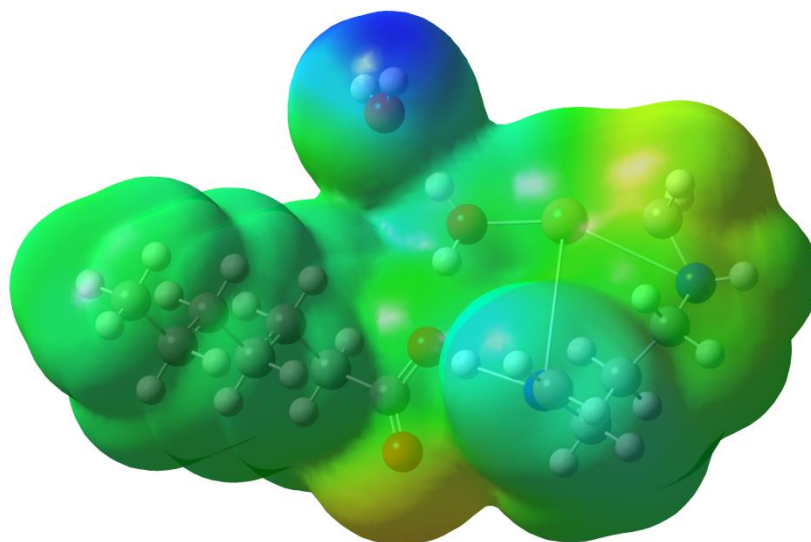


Figure 4.70 Molecular electrostatic potential map surface map of **1**

The optimized structure discussed represents complex **1** that was obtained experimentally. To understand why the Cu atom of **1** would favourably bind with H₂O rather than CH₃(CH₂)₅COO⁻, another molecular modelling that simulates the coordination of Cu atom with CH₃(CH₂)₅COO ligand (covalent) was performed. Then, the binding energy (BE) was compared. The BE was calculated from the following relationship:

$$BE = E_{\text{complex}} - E_{(\text{Cu-cyclam})} - E_{\text{CH}_3(\text{CH}_2)_5\text{COO}} - nE_{\text{H}_2\text{O}}$$

(n = number of H₂O molecules present)

For ionic complex, BE = -0.663 a.u. (-1.741 x10³ kJ mol⁻¹), while for covalent complex, BE = +12.746 a.u (+33.465 x10³ kJ mol⁻¹). The more negative value (more exothermic) indicates that the ionic complex is more stable compared to the covalent complex.

Table 4.13 Comparison of selected theoretical and experimental bond lengths of **8**

Bond type	Bond length (Å)	
	Theoretical	Experimental
Cu ₁ -N ₂	1.856	2.011
Cu ₁ -N ₄	1.888	2.019
Cu ₁ -O ₂₁	3.312	2.571
N ₂ -C ₁₈	1.412	1.475
N ₂ -H ₃	0.997	0.930
N ₂ -C ₆	1.489	1.480
C ₆ -C ₉	1.545	1.513
C ₉ -C ₁₂	1.548	1.516
C ₁₂ -N ₄	1.481	1.480
N ₄ -C ₁₅	1.467	1.486
N ₄ -H ₅	0.996	0.930
C ₂₆ -O ₂₁	1.236	1.271
C ₂₆ -O ₂₂	1.241	1.266

The calculated FTIR intensities were also compared with the corresponding experimental intensities (**Figure 4.72**).

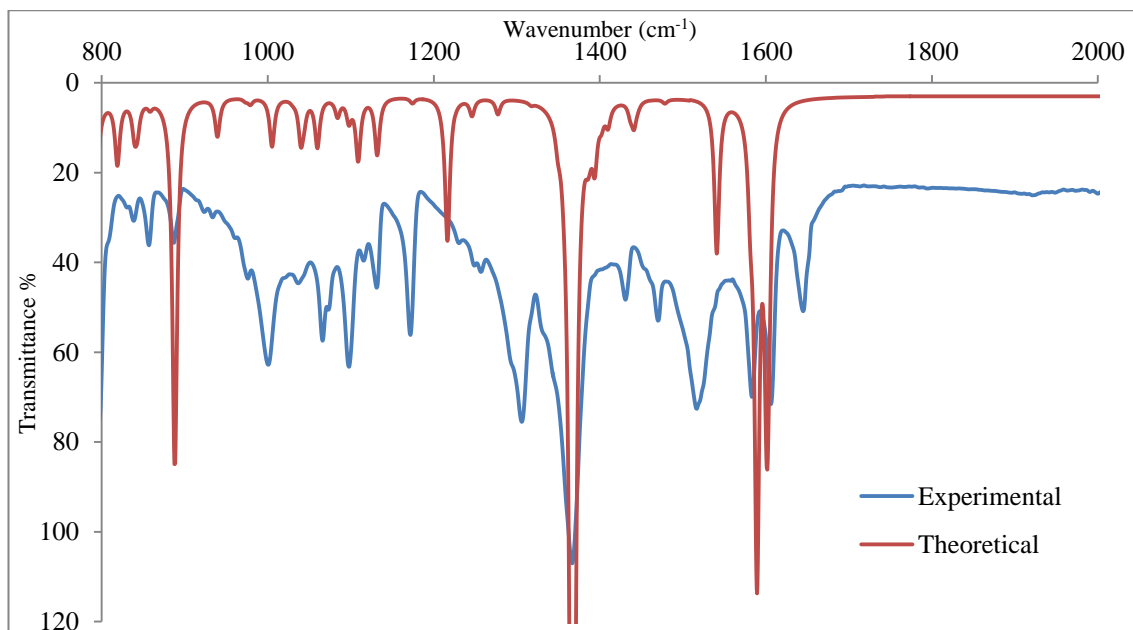


Figure 4.72 Comparison of theoretical and experimental FTIR spectra of **8**

The partial charge distribution values of the selected atoms of **8** were presented in **Table 4.14**.

Table 4.14 The partial charge energy for selected atoms of **8**

Atom	Energy (kJ mol ⁻¹)
Cu ₁	+110.788
N ₂	-60.980
N ₄	-65.516
O ₃₇	-55.770
O ₂₁	-64.261
O ₂₂	-66.673
C ₂₆	+66.191

It is noted that O_{carboxyl} atom (O₂₁ and O₂₂) of *p*-H₂NC₆H₄COO ligand were bearing much lower energy compared to O_{water} atom (O₃₇). This may explain its favourable coordination towards the Cu(II) ion rather than the water molecule.

The electrostatic potential map of **8** was also generated and shown in **Figure 4.73**. To the contrary, the polarisation effect in **8** is more pronounced. This could be seen by

the strong differences in polarisation effect, specifically between the positive region of the cyclic core centre and its counter anion.

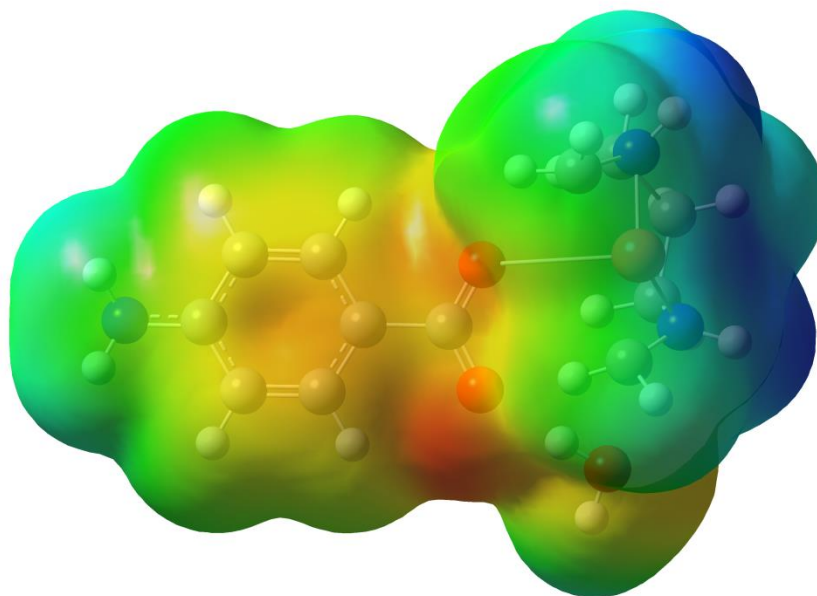


Figure 4.73 The molecular electrostatic potential surface map of **8**

The BE of this covalent compound was found to give more negative value (-0.979 a.u; -2.570×10^3 kJ mol⁻¹) than its simulated ionic state (11.807 a.u; 30.999×10^3 kJ mol⁻¹). Hence, it is deduced that the natural covalent complex is more stable and unlikely to form ionic complex.



The optimized structure of complex **9** is given in **Figure 4.74**. The minimized energy value is -2436.69 a.u (-6.398×10^6 kJ mol⁻¹). Selected bond lengths are given in **Table 4.15**.

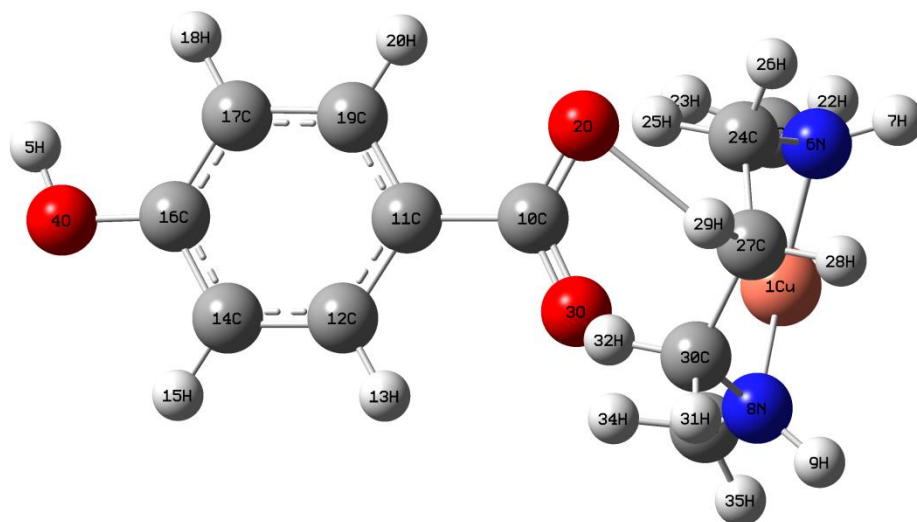


Figure 4.74 The optimized structure of **9**

Table 4.15 Comparison of selected theoretical and experimental bond length of **8**

Bond type	Bond length (Å)	
	Theoretical	Experimental
Cu ₁ -N ₆	1.859	2.023
Cu ₁ -N ₈	1.871	2.017
Cu ₁ -O ₂	2.975	2.383
N ₆ -C ₂₁	1.433	1.481
N ₆ -H ₇	0.997	0.930
N ₆ -C ₂₄	1.487	1.478
C ₂₄ -C ₂₇	1.547	1.524
C ₂₇ -C ₃₀	1.548	1.520
C ₃₀ -N ₈	1.484	1.477
N ₈ -C ₃₃	1.452	1.483
N ₈ -H ₉	0.997	0.930
C ₁₀ -O ₂	1.233	1.253
C ₁₀ -O ₃	1.241	1.276

The calculated FTIR intensities were also compared with the corresponding experimental intensities (**Figure 4.75**).

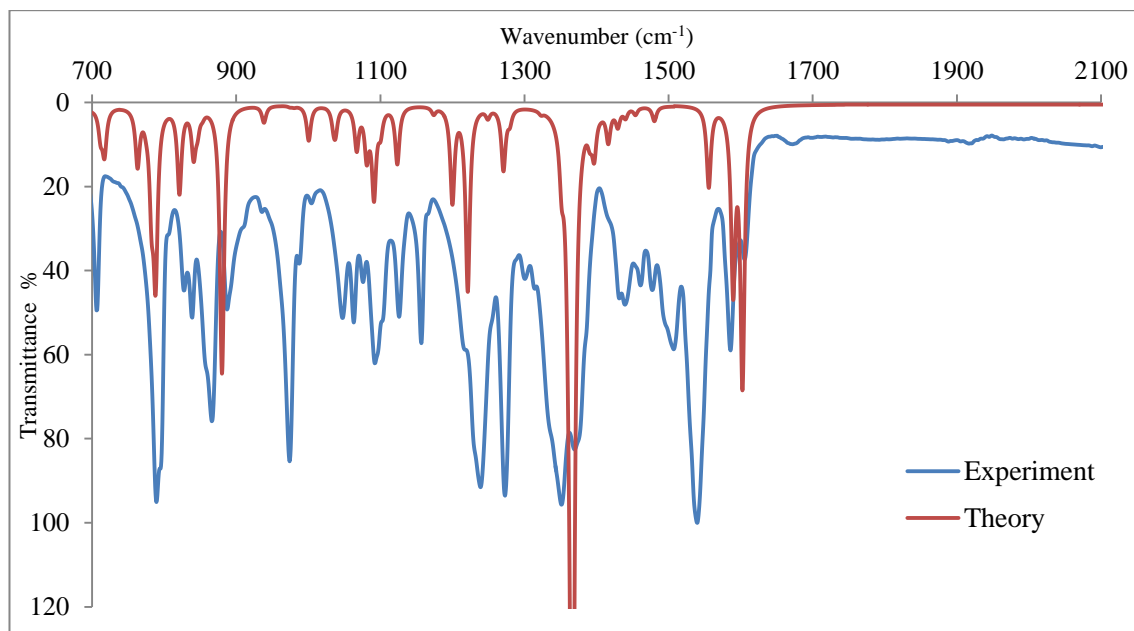


Figure 4.75 Comparison of theoretical and experimental FTIR spectra of **9**

The partial charge distribution values of selected atoms of the complex were presented in **Table 4.16**.

Table 4.16 The partial charge energy for selected atoms of **9**

Atom	Energy (kJ mol ⁻¹)
Cu ₁	+110.961
N ₆	-62.621
N ₈	-66.480
O ₂	-62.331
O ₃	-65.322
C ₁₀	+63.971

The electrostatic potential surface map of **9** was also generated and shown in **Figure 4.76**. Similar to complex **8**, the surface map of **9** shows distinct energy

polarisation, particularly between the cyclic core centre and coordinating *p*-HOC₆H₄COO ligand.

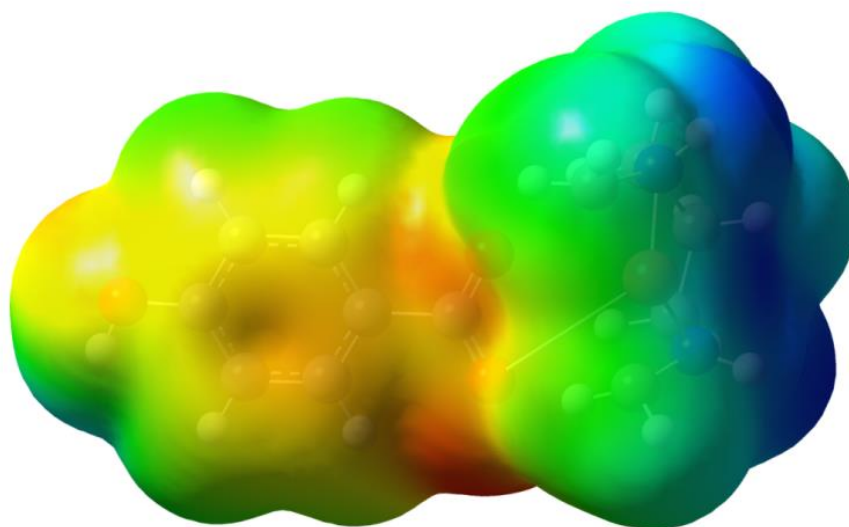
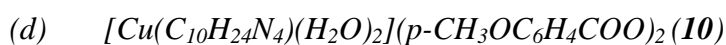


Figure 4.76 The molecular electrostatic potential surface map of **9**

The BE of this denoted covalent compound was found to give more negative value (-0.525 a.u; 1.378×10^3 kJ mol⁻¹) than its simulated ionic state (12.401 a.u; 32.559×10^3 kJ mol⁻¹). Hence, it is deduced that the natural covalent complex is more stable and unlikely to form ionic complex.



The optimized structure of complex **10** is given in **Figure 4.77**. The minimized energy value is -2551.89 a.u (-6.700×10^6 kJ mol⁻¹). Selected bond lengths are given in **Table 4.17**.

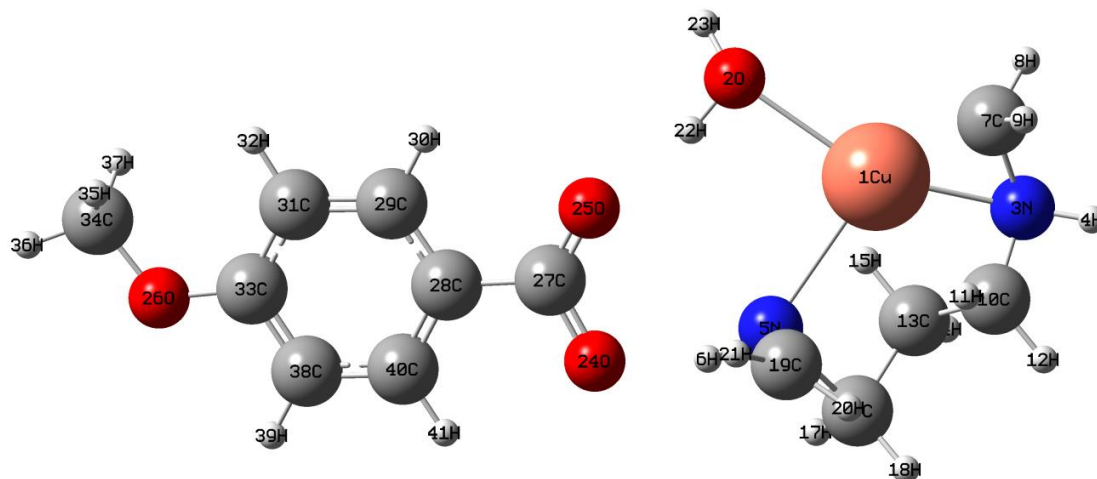


Figure 4.77 The optimized structure of **10**

Table 4.17 Comparison of selected theoretical and experimental bond lengths of **10**

Bond type	Bond length (Å)	
	Theoretical	Experimental
Cu ₁ –N ₃	2.223	2.010
Cu ₁ –N ₅	2.298	2.019
Cu ₁ –O ₂	2.424	2.535
N ₃ –C ₇	1.477	1.479
N ₃ –H ₄	0.998	0.910
N ₃ –C ₁₀	1.448	1.484
C ₁₀ –C ₁₃	1.531	1.513
C ₁₃ –C ₁₆	1.530	1.517
C ₁₆ –N ₅	1.458	1.481
N ₅ –C ₁₉	1.246	1.479
N ₅ –H ₆	0.993	0.910
C ₂₇ –O ₂₄	1.304	1.258
C ₂₇ –O ₂₅	1.199	1.266

The calculated FTIR intensities were also compared with the corresponding experimental intensities (**Figure 4.78**).

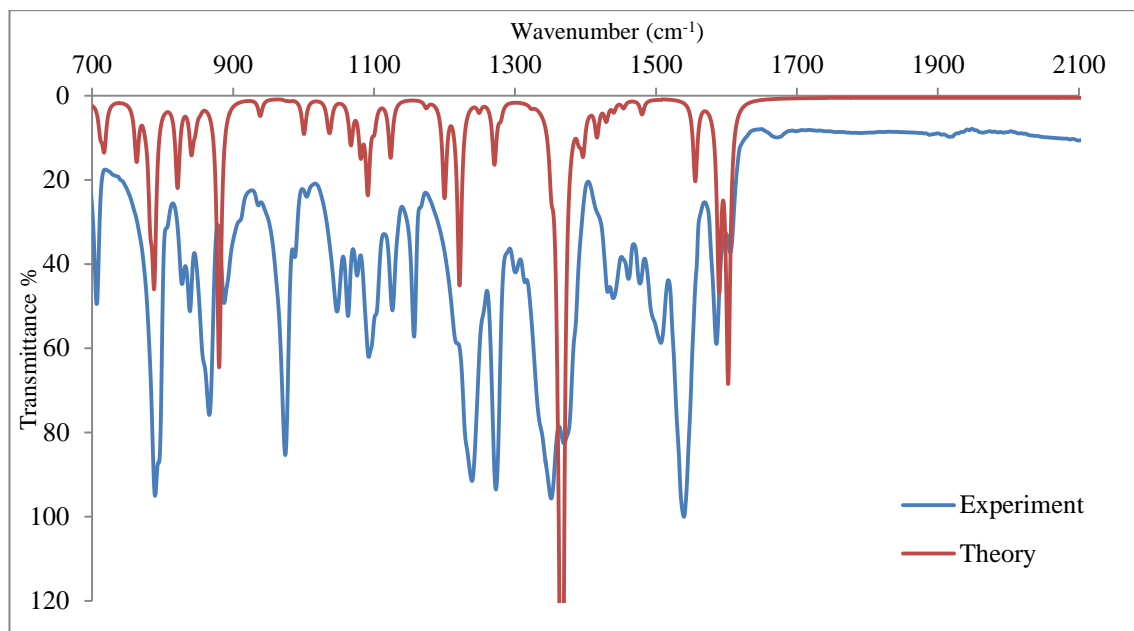


Figure 4.78 Comparison of theoretical and experimental FTIR spectra of **10**

The partial charge distribution values of the selected atoms are presented in **Table 4.18**.

Table 4.18 The partial charge energy for selected atoms of **10**

Atom	Energy (kJ mol ⁻¹)
Cu ₁	+61.559
N ₃	-42.744
N ₅	-42.551
O ₂	-62.138
O ₂₄	-42.267
O ₂₅	-54.998
C ₂₇	+68.410

The electrostatic potential surface map of **10** was generated and shown in **Figure 4.79**. The complex showed insignificant differences in terms of charge distribution and energy polarisation.

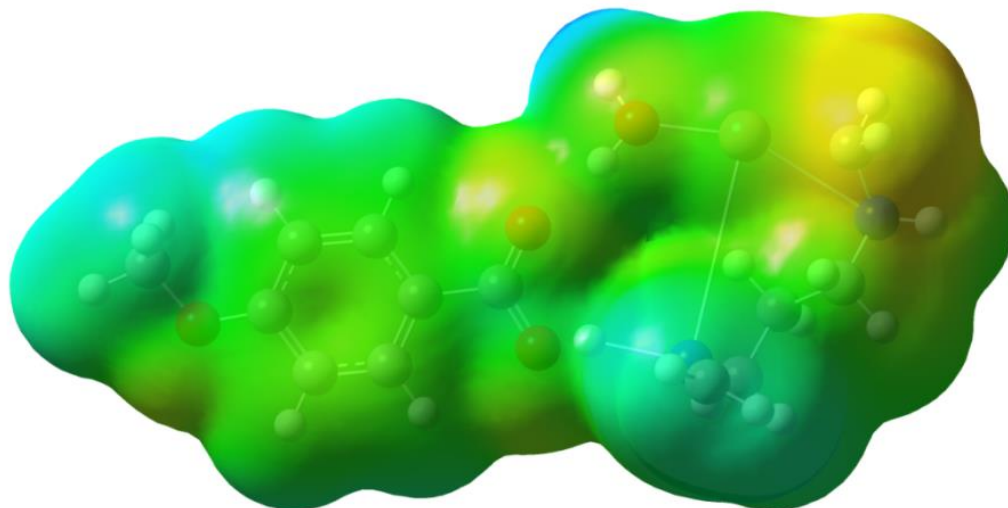


Figure 4.79 The molecular electrostatic potential surface map of **10**

The BE of this denoted ionic compound was found to give more negative value (-0.649 a.u; 1.704×10^3 kJ mol⁻¹) than its simulated covalent state (-0.178 a.u; -467.339 kJ mol⁻¹). Hence, it is deduced that the natural ionic complex is more stable and unlikely to form covalent complex.

4.4.2. Concluding remarks

The structure optimization of complexes **1**, **8**, **9** and **10** were successfully computed using SCF-HF method with 6-311G(d,p) basis set. The calculation was in good estimation as the theoretical geometric parameters and the simulated harmonic vibrational frequencies are comparable to their corresponding experimental data.

When comparing the data, some of the computed bond lengths deviate largely because the theoretical calculations were performed upon isolated molecule in vacuum, while the experimental results were obtained on solid [14]. The theoretical FTIR spectra were scaled to a factor of ~ 0.89 .

Similar trend was observed in the ionic complexes (**1** and **10**) where the energy polarisations were more uniform. This implies that the electron densities are more evenly distributed throughout the whole structure. The O_{water} ligand were found lower in energy than the competing O_{carboxyl}, thus favourably bind to the Cu(II) centre. Their binding energy was also significantly more exothermic than their simulated covalent structure.

The covalent compounds (**8** and **9**) however show a more distinct polarisations difference. The electrons were found to be heavily scattered around the cyclic core that comprised the Cu(II) ion and *trans*-N₄O₂ donor set. As the carboxylate groups contributed to the higher polarity, the Cu(II) metal centre would selectively coordinate with the anionic *p*-HOC₆H₄COO and *p*-CH₃OC₆H₄COO ligand. Their binding energies were also significantly more exothermic than their simulated ionic structures.

References

- [1] Bosnich, B., Poon, C. K., Tobe, M.L. *Inorg. Chem.* (1965) 4, 1102-1108.
- [2] Meyer, M., Dahaoui-Gindrey, V., Lecomte, C., Guillard, R., *Coord. Chem. Rev.* (1998) 178–180, 1313-1405.
- [3] Abdullah, N., Kamarazaman, Z. A., Alhakem, Y. A. Z., Abdullah, N., Ahmad Tajidi, N.S. (2011) *CCDC 858037*. Cambridge Crystallographic Data Centre.
- [4] Lindoy, L. F., Mahinay, M. S., Skelton, B., White, A. H. *J. Coord. Chem.* (2003) 56, 1203-1213.
- [5] Burrows, H. D., Ellis, H. A. *Thermochim. Acta* (1982) 52, 121-129.
- [6] Cabaniss, S. E., McVey, I. F. *Spectrochim. Acta Part A*: (1995) 51, 2385-2395.
- [7] Buyukkidan, N., Yenikaya, C., Ilkimen, H., Karahan, C., Darcan, C., Sahin, E. *Russ. J. Coord. Chem.* (2013) 39, 96-103.
- [8] Zeng, M. –H., Zhang, W. –X., Sun, X. –Z., Chen, X. –M. *Angew. Chem. Int. Ed.* (2005) 44, 3079-3082.
- [9] Pajtasova, M., Ondrusova, D., Jona, E., Mojumdar, S. C., L’Alikova, S., Bazylakova, T., Gregor, M., *J. Therm. Anal. Calorim.* (2010) 100, 769-777.
- [10] Zeleňák, V., Vargová, Z., Györyová, K.. *Spectrochim. Acta Part A*: (2007) 66, 262-272.

- [11] Hollingsworth, C. A., Seybold, P. G., Hadad, C. M. *Int. J. Quantum Chem.* (2002) 90, 1396-1403.
- [12] Udhayakala, P. Jayanthi, A., Rajendiran, T. V., Gunasekaran, S. *Int. J. ChemTech Res.* (2011) 3, 1851-1862.
- [13] Balachandran, V., Karthick, T., Perumal, S., Nataraj, A. *Spectrochim. Acta Part A:* (2012) 92, 137-147.
- [14] Morales-Roque, J., Carrillo-Cardenas, M., Jayanthi, N., Cruz, J., Pandiyan, T. *J. Mol. Struc-THEOCHEM* (2009) 910, 74-79.